이학박사 학위논문

자기 조립된 나노 또는 마이크로 크기의 구조체 형성과 조절, 그리고 응용에 대한 연구

Studies on Fabrication and Control of Self-assembled Nano- and Micro-architectures and Their Applications

2017 년 8 월

서울대학교 대학원

화학부 유기화학전공

장 동 학

Abstract

Studies on Fabrication and Control of Self-assembled Nano- and Micro-architectures and Their Applications

Donghak Jang

Major in Organic Chemistry

Department of Chemistry

The Graduate School

Seoul National University

Amphiphiles can self-assemble into various nano- and micro-supramolecular architectures. A self-assembly of amphiphiles can transform into another assemblies due to changes of molecular structure and external environment. Also, properties of the supramolecular architectures can be controlled through changing molecular structure and external environment. In this study, we investigated self-assembly of amphiphiles, controlled self-assembling process and developed various supramolecular architectures and functional materials.

In **part I**, we investigated the influence of molecular structure, external environment and additive on changes in self-assemblies and formation of supramolecular architectures. It was found that development of various supramolecular architectures can be achieved by controlling self-assembly.

A three-component system consisting of terephthaloylbisalanine (TBA), dodecylamine (DA) and metal cation was introduced to obtain structural diversity of supra-amphiphiles. The supra-amphiphiles by hydrogen-bonded complex between TBA and DA can self-assemble into nano- and micro-supramolecular architectures. As the ratio of TBA increased from 0.5 to 2.0, self-assemblies of the TBA_xDA_y changed from ribbon-like structures to rod-, tube- and fiber-like structures through self-assembling process of monoclinic, column and lamellar subunits. In addition, the flat-ribbon structures of self-assembly of *rac*-$TBA_{1.0}DA_{2.0}$ changed into helical-ribbon structures through changing chirality of TBA to "*L*" conformation. Through an addition of Zn^{2+}, Cd^{2+} and Co^{2+} having different coordination geometry, the TBA_xDA_y supra-amphiphiles could self-assemble into cylindrical micelle, tube and bilayer structures. We demonstrated that various self-assembled nano- and micro-architectures can be obtained by controlling each component of two- or three-component system.

It was found that amphiphiles undergo different self-assembling process depending on chemical structures and conformational changes. A distinctive supramolecular architecture could be obtained by controlling external condition. Amphiphilic compounds, EG_nA, have varying geometry depending on solvent polarity. EG_nA, which consists of two *N*-dodecylbenzamide linked by ethylene glycol oligomer, has hairpin-like conformation through hydrogen bonding interactions between two amide moieties. In nonpolar solvent, the

volume ratio of the hydrophilic head to hydrophobic tail increased due to strong hydrogen bonding interactions and geometry of the ethylene glycol oligomer. EG_4A and EG_6A with higher volume ratio self-assembled into cylindrical micelles, but EG_5A with equal volume ratio self-assembled into bilayer ribbon-like structures. On the other hand, in polar solvent, distortion of the ethylene glycol oligomer was weakened by the weak hydrogen bonding interactions. Therefore, short-length EG_4A self-assembled into fiber structures, while EG_5A and EG_6A transformed into ribbon-like structures. We demonstrated that controlling hydrogen-bonding interactions of amphiphiles through changes in solvent polarity could lead to the changes from cylindrical micelle to bilayer structure.

Furthermore, it is possible to control morphology of self-assemblies through co-assembly between two amphiphiles in a different geometry. NDI•Car with conical geometry self-assembled into a micro-sized micelle due to higher volume ratio of hydrophilic head. On the other hand, NDI•OAc with flat geometry transformed into a nano-sized ribbon structure through self-assembly. The volume ratio of hydrophilic head and hydrophobic tail can be adjusted by mixing the conical NDI•Car and flat NDI•OAc. It will allow the control of co-assemblies through changes in the volume ratio. In fact, the micelle structure of NDI•Car gradually transformed into the ribbon-like structure with increasing NDI•OAc mixing ratio. Particularly, when the ratio of NDI•Car and NDI•OAc is between 1:1 and 1:9, the mixtures co-assembled into nano-sized tubular structures. It was found to control structural change of supramolecular architectures through co-assembly of two or more amphiphiles in a different geometry.

In **part II**, we demonstrated addition of various additives led to changes

in self-assembled supramolecular architectures. Also, it was shown that surface of the supramolecular architecture could be modified using functional compounds through non-covalent interactions.

We would like to modify the surface of self-assemblies into functional materials through host-guest interactions. Dipicolylamine(dpa)-metal complexes on the surface of self-assemblies will be able to develop a functional materials through host-guest interactions with phosphate derivatives. To incorporate dpa group on the surface of self-assemblies, amphiphilic 2-(dipicolylamino)ethyldodecanoyl amide (lipid-**1**) was synthesized. First, structural changes of self-assemblies of lipid-**1** were induced by the difference in binding affinity and geometry of metal cations and anions. The micelle structure of Co(II)-**1** shown structural changes into vesicular structures when binding with pyrophosphate. In the case of Cd(II)-**1** assemblies, vesicle fusion was observed by binding with pyrophosphate. However, the addition of phosphate and acetate anion could not be lead to changes of the self-assemblies due to geometry and weak binding affinity to anion. Based on these results, surface of the self-assemblies of Zn(II)-**1** could be modified with functional phosphate derivatives without significant structural changes. After adding the fluorescent phosphate derivative, FMN (flavin mono-nucleotide), to Zn(II)-**1** vesicle, confocal microscope analysis confirmed that surface of the vesicle was stained with fluorescence from FMN. We demonstrated that the surface of self-assemblies can be modified with functional materials through host-guest interactions between dpa-Zn(II) complexes and phosphate derivatives.

In **part III**, we demonstrated that a small molecule can be detected and distinguished through controlling self-assembly. We developed two reaction-

based low molecular weight gelators (LMWGs) and investigated whether the reaction-based LMWGs selectively discriminate the analytes.

In order to increase selectivity to anion in polar solvent, a functional group which selectively reacts with anion was introduced into the LMWG system. In this study, F^- responsive LMWG **1** was designed by introducing *tert*-butyldimethylsilyl (TBDMS) group into 7-hydroxycoumarin derivative. It was confirmed that LMWG **1**, which has no gelation property, turned into gel by adding F^- in aqueous media. Particularly, partial cleavage of TBDMS by F^- shown fluorescence as well as sol to gel transition. Since the TBDMS moiety was only cleaved by F^-, LMWG **1** will have no gelation property by adding other anions. LMWG **1** did not show self-assembled gel formation by addition of various anions including other halogen anions. In contrast to hydrogen bonding based LMWGs, we demonstrated that reaction based LMWG has high selectivity to F^- even in aqueous media.

It is difficult to discriminate Hcy from Cys due to chemical and structural similarities. It is possible that small structural changes in amphiphiles can be induced into different self-assemblies. Therefore, we developed LMWG which can discriminate Hcy from Cys through reaction-based gelation process. Hcy responsive LMWG, CHO-1, can be developed by introducing aldehyde group into 7-hydroxycoumarin derivative. Unlike CHO-1, which has no gelation property, 6-membered cyclic adduct of CHO-1 and Hcy showed gel formation with fluorescence emission in aqueous media. However, 5-membered cyclic adduct of CHO-1 and Cys showed no gelation property in same condition. Due to the difference in geometry of CHO-1•Hcy and CHO-1•Cys, it self-assembled into different sized network-fiber architectures. As a result, selective gel formation was observed only by addition of Hcy. Gelation

property of other biothiols and amino acids was also evaluated to confirm the selectivity to Hcy. As in the case of Cys, no results of gel formation were shown by other molecules. The selective gel formation between CHO-1 and Hcy was successfully able to discriminate Hcy from Cys and other biothiols. Reaction-based LMWG will be effective in distinguishing other compounds that have similar structural and chemical properties.

Keywords: Self-assembly, Three-components system, LMWGs, Organogel, Hydrogel, Naphthalene diimide, Homocystein (Hcy), Cysteine (Cys), Fluoride, Dipicolylamino-Zn(II) complex (dpa-Zn(II)), Surface modification, Chemodosimeter, Sol to gel transition.

Student Number: 2003-20495.

Contents

Part I

Fabrication and Control of Self-assembled

Supramolecular Architectures

Background

1. Introduction to Self-assembly of Amphiphiles

Self-assembly is described as pre-designed compounds in system spontaneously and reversibly organized into well-defined high order structures.[1] The pre-designed low or high molecular weight compounds interact with each other by various non-covalent interactions such as hydrogen bonding, van der Waals force, π-π stacking, electrostatic interaction, metal-ligand interaction, and etc.[2] The self-assembling process is driven by non-covalent interactions and controlled by the balance of attraction and repulsive non-covalent interactions within and between the compounds. This balance of competing forces is determined by the molecular design and the preparation method used (**Figure 1**). The pre-designed compounds are able to self-assemble into an aggregate, whose novel structures and properties are determined by nature and the positioning of the compounds.

The most comprehensive demonstration of a self-assembly is found in nature. It is exhibited in the formation of cell membrane, double helical and triple helical DNA and secondary, tertial and quaternary structure proteins. The formation of amyloid fibers which is responsible for neurodegenerative diseases is also related in self-assembling process. To achieve such high levels of organization, information must be built into the smallest building blocks, such as phospholipids, nucleotides and amino acids. These building units contain this information in the form of chirality, hydrogen-bonding capacity, steric demands, electrostatic, properties, hydrophilic or hydrophobic characters, and metal ion binding capabilities. These examples found in nature have inspired many supramolecular chemists to design molecular building

blocks that are able to self-assemble into various architectures.

A controlled self-assembling process provides several benefits in fabricating highly ordered architectures. These include a highly convergent synthetic protocol based on the simultaneous assembly of the pre-determined building blocks, whose preparation requires significantly fewer steps than the comparable covalent synthesis. An inherent defect-free assembly, as the equilibria between the constituents and the final products contribute to the self-rearrangement of the components within the assembled structure and thus to the self-correction of defects.

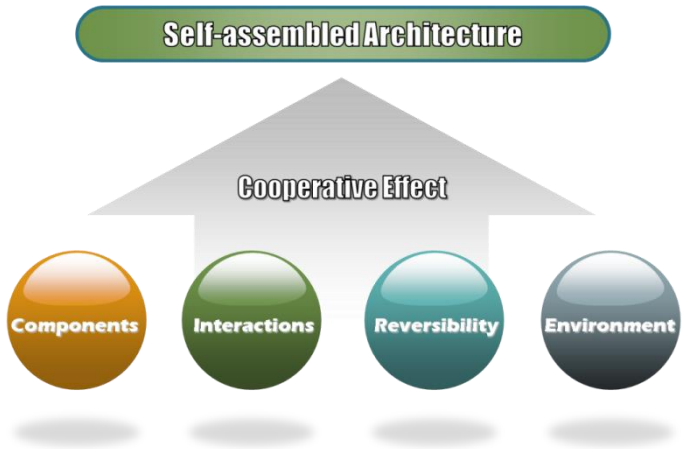

Figure 1. Schematic representation of self-assembling process to fabricate nano- and micro-supramolecular structures.

Amphiphiles are compounds possessing both hydrophilic and hydrophobic component. Self-assembling process of the amphiphiles provides unique and new opportunities for designing novel materials for advanced applications in nanotechnology. A hydrophilic head group of amphiphiles preferentially immerges in the polar environment, while the hydrophobic tail group preferentially resides in the nonpolar environment. These arranged

amphiphilic compounds self-assemble into diverse supramolecular architectures.

Despite the weakness of the forces involved in the self-assembly of amphiphiles, the relevant number of these soft interactions will produce an overall effect that is strong enough to hold other amphiphile molecules together as well as to ensure their stability in solution. Moreover, the weakness of the involved interactions makes the structure more flexible, enabling the system to withstand minor perturbation while preserving the reversibility of the self-assembled structure.

The assembly of the amphiphilic molecules holds great advantages to the fabrication of various well-defined soft-material such as micelles, reversed micelles, lyotropic mesophases, monolayers, and vesicles.[3] The structure and the property of the assemblies are closely connected to features of solvent, structure of the amphiphile, and additive. In particular, the relative volume fraction of hydrophilic head and hydrophobic tail in the amphiphiles is an important factor in determining the morphology of supramolecular architectures (**Figure 2**).[3b, 4] It has been proposed that self-assembled aggregates of amphiphiles can be predicted by the packing parameter, $P=v/(a_0 \times l_c)$, where v is volume of the hydrophobic tail, a_0 is the hydrophilic head surface area at the critical micelle concentration (cmc) and l_c is the amphiphile length.

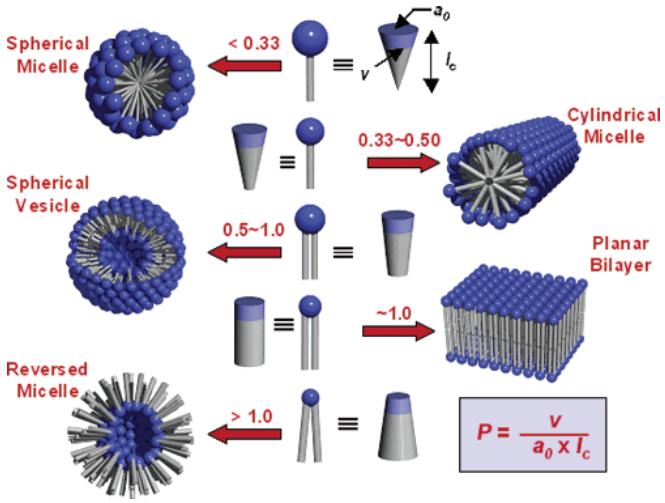

Figure 2. Various self-assembled morphologies with varying critical packing parameter (*P*) of each lipid.

For the purpose of self-assemblies with different function, we can design amphiphiles with varying topologies. The diverse topologies are one of the reasons why amphiphiles are widely chosen to fabricate functional materials. Despite the long history of amphiphiles, they still continue to attract scientists, inspiring them to design new type of amphiphiles. We will discuss and summarize recent efforts on how to design and prepare diversified amphiphiles to satisfy different requirements. It is hoped that the study on the self-assembly of amphiphiles can enrich the field of molecular engineering of functional supramolecular systems and provide new avenues for the construction of self-assembling soft materials and functional surfaces using rational design.

2. Current Developments of Supramolecular Chemistry with Amphiphiles

Amphiphiles play a variety of roles in personal care and household

detergency including cleansing, foam formation, conditioning and viscosity control which is combined with safety and mildness in use. The presence of water-soluble groups such as sulphate or ammonium allows for the solubility in polar solvents. These polar groups can be classified into neutral (non-ionic), anionic (negatively charged), cationic (positively charged) and zwitterionic (both positive and negative charge) feature (**Figure 3**). Although amphiphiles usually consist of one hydrophilic polar head group, recently dimeric amphiphile containing two hydrophobic tails and two polar head groups linked together with a short spacer have drawn considerable interest from industrial and academic researchers. This relatively new type of amphiphile, known as gemini amphiphile, offers several interesting physicochemical properties, such as lowering surface tension and very low critical micelle concentration.

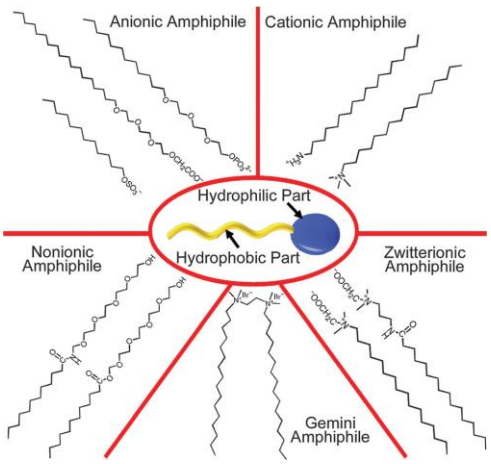

Figure 3. Typical example of low molecular weight amphiphiles

Amphiphilicity was formerly based upon the solubility of the molecules in water. However, this definition cannot now be considered accurate as amphiphilicity can be extended to various media, including organic solvent.

That is, even some compounds bearing both fluorocarbon and hydrocarbon chains can form bilayer-like assemblies in an appropriate hydrocarbon solvent. The fluorocarbon group has a low affinity for hydrocarbon solvent and hence is solvophobic, while in contrast, hydrocarbon region are solvophilic. These two terms, solvophilic and solvophobic, are often used as alternative for hydrophilic and hydrophobic when non-aqueous solvent is used as surrounding media. If there is an appropriate structural balance between the solvophilic and solvophobic part, then assembly structure similar to those involving hydrophobic–hydrophilic amphiphile can be formed (**Figure 4**).

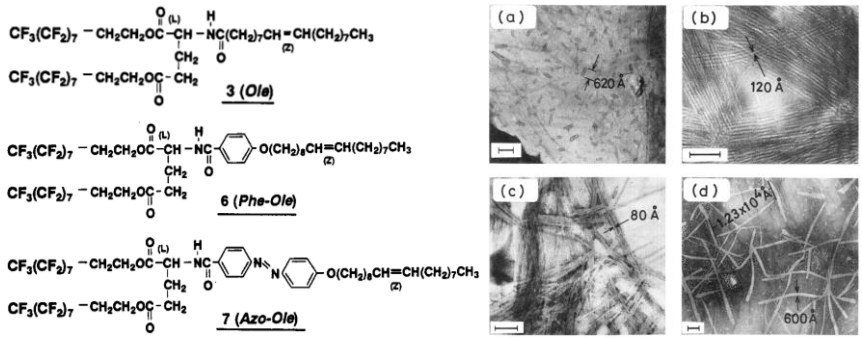

Figure 4. Molecular structures and TEM images of amphiphiles. (a) Vesicle-like and (b) aligned rods oval aggregates of **3** (Ole) in chlorocyclohexane and benzene, respectively. (c) Stacked tube-like aggregate of **6** (Phe-Ole) and (d) tape-like aggregate of **7** (Azo-Ole) in chlorocyclohexane.

Another extension of amphiphilicity obviates the necessity of intrinsically amphiphilic molecule in the formation of amphiphile assemblies. Requirements of amphiphilicity can be satisfied by different types of molecules in admixture (e.g. one solvophilic and one solvophobic) that can form amphiphilic units through some specific supramolecular interactions. For example, when a cyanuric acid derivative containing a hydrophilic region

is mixed with a melamine derivative containing hydrophobic tails, assembly similar to lipid bilayer is formed through complementary hydrogen bonding (**Figure 5**).

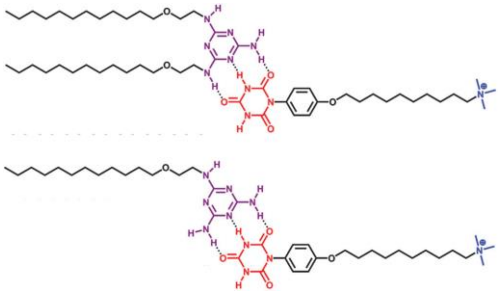

Figure 5. Double chain and single chain supramolecular amphiphiles based on hydrogen bonding between cyanuric acid and melamine derivative.

Amphiphilic assemblies are not limited to purely organic structure. The sophisticated amphiphile design allows us to prepare organic–inorganic hybrid assembly. For example, amphiphiles with alkoxysilane heads have been used to form hybrid assembly. At the surface of these assemblies, cross-linked silanol groups form an inorganic silica-like structure. This structure is known as a cerasome as it has both a ceramic-like surface and a liposome-like cell structure (**Figure 6**). The cerasome is mechanically stable and can be further assembled into a multi-cellular form without causing the vesicular structure to collapse.

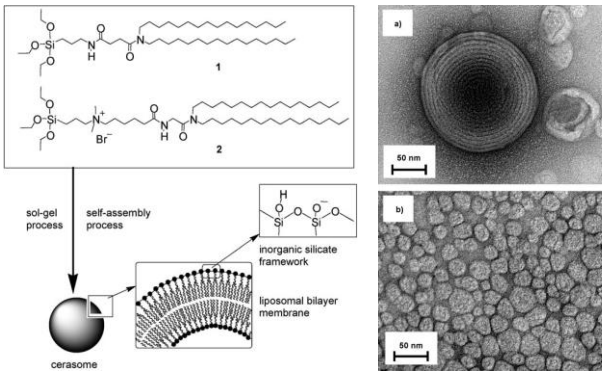

Figure 6. Molecular structures and schematic representation of the cerasome. TEM image of the cerasome from **2** prepared by a) vortex mixing and followed by b) ultra-sonication.

We will focus on the use of low molecular weight single component amphiphiles, block-copolymer amphiphiles and supra-amphiphiles for self-assembly at different levels of complexity.

2.1. Low Molecular Weight Single Component Amphiphiles

2.1.1. Bio-inspired Peptide Amphiphiles

Of the different biomolecular components, proteins have the largest number of distinct interactions, internally and with other molecules, and hence form the greatest variety of functional nano-structures. Unlike other biomolecular components, proteins combine a diverse structure with intricate, precise, and diverse patterns of surface chemistry. It is because of this that peptides are of particular interest for the generation of functional nano-structures using standard organic synthesis procedures.

Self-assembling peptides have been designed to form different structured aggregates such as nano-fiber, nano-vesicle, nano-belt, and nano-tube.[5] They consist of a structural and functional hydrophilic peptide conjugated to a structural hydrophobic element (**Figure 7**). The hydrophobic unit is often a lipid or alkyl chain, or less commonly, a polymer or polypeptide.[6] The coupling of a peptide to a hydrophobic unit yields an amphiphile and it is a relatively simple way of inducing supramolecular structure in aqueous solution. They mostly have well defined critical aggregation concentrations (CAC)[7] and can self-assemble in aqueous solution or at interfaces into form

well-ordered nano-structures, including peptide bilayers, nano-tubes, nano-rods, nano-vesicles and micelles.[8]

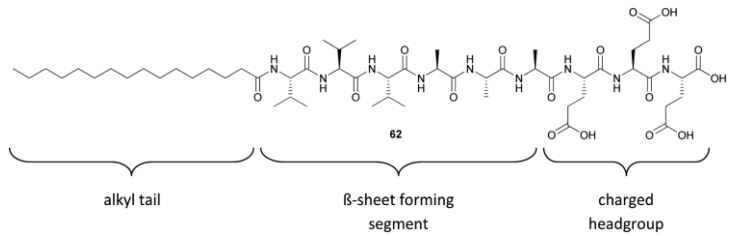

Figure 7. Molecular structure of a peptide amphiphile. The molecule is composed of three segments, the alkyl tail, the β-sheet forming peptide sequence, and the charged peptide head group.

In general, the hydrophobic element induces aggregation of the peptide amphiphiles (PAs) in an aqueous solution, while the hydrophilic peptide block displays an ordered pattern of chemical functionality at the interface of the self-assembled structure. However, as with the molecular components of a cell, or the different motifs in a protein, the different section of PA cannot function independently of one another, they each modify the structure of the other. The balance of many small forces determines the overall morphology, size, and functionality of the structures, and a deeper understanding of these factors is important for guiding future research, and for customizing PAs for specific applications.

The Stupp group reports the use of self-assembly to prepare a nano-structured composite with PAs.[9] The synthesized PA consisted of an alkyl tail with 16 carbon atoms and ionic peptide. Three features were engineered into the peptide region of the PA (**Figure 8**). They incorporated a four consecutive cysteine amino acid, phosphoserine residue, and Arg-Gly-Asp (RGD) sequence into the peptide sequence for covalent capture[10](2), formation of

hydroxyapatite(4), and adhesion of cells onto the surface[11](5), respectively.

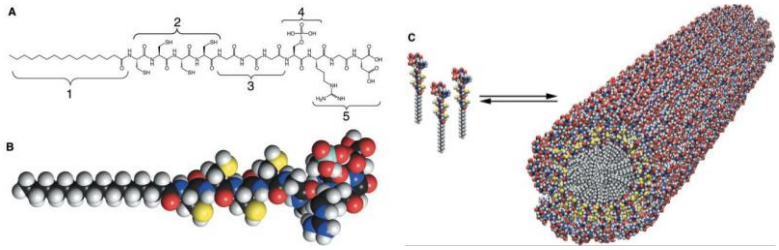

Figure 8. (**A**) Chemical structure and (B) molecular model of the peptide amphiphile, showing the overall concical shape. (C) Schematic showing the self-assembly of PA molecules into a cylindrical micelle. 1**:** Hydrophobic long alkyl tail. 2**:** Polymerizing the self-assembled structure. 3**:** Flexible linker. 4**:** Inducing mineralization of hydroxyapatite. 5**:** Cell adhesion ligand RGD. C (black); H (white); O (red); N (blue); P (cyan); S (yellow).

At pH 8, the PA was found to be soluble in excess of 50 mg/ml in water. However, upon acidification of the solution below pH 4, the material rapidly becomes insoluble. Solutions more concentrated than 2.5 mg/ml form birefringent gels in water that are self-supporting upon inversion of the container. When TEM was used with the positive stain uranyl acetate, which preferentially stains acidic groups[12], it revealed increased electron density at the periphery of the fibers. Additionally, gels that were stained, embedded in epoxy resin, and sectioned for TEM, showed fibers in cross section where donut-shaped patterns were observed, indicating that only the outer portion of the fiber was stained (**Figure 9D**). These two positive-staining experiments indicate that the hydrophobic alkyl tails pack on the inside of the fiber and the acidic moieties of the peptide are displayed on the surface of the fiber.

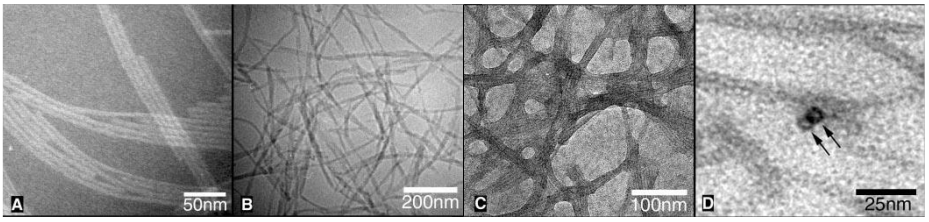

Figure 9. (A) Negative stained TEM and (B) cryo-TEM of the nano-fibers before covalent capture. (C) Positive stained TEM of nano-fibers after oxidative cross-linking and (D) their high-resolution TEM. Two fibers are observed in cross section (arrows).

Liskamp group[13] showed that the aggregation behavior of an amylin (20-29) peptide sequence can be significantly altered by alkylating to NH sulfonamide moiety. Alkylation of the NH of the sulfonamide moiety with the shortest alcohols completely prevented aggregation and secondary structure formation. However, alkylation with longer alkyl chains induced a self-assembling process and showed the formation of various aggregates (**Figure 10**). For example, the *N*-methylate or *N*-ethylate PA only show clear solution and turned into a translucent gel without forming significant self-assembled aggregates. However, when longer alkyl chain is incorporated into PAs, they show different self-assembling behavior. Depending on the size of the alkyl group, different morphologies of the aggregates were observed, e.g. lamellar sheets, twisted fibers, helical ribbons etc. By increasing the length of the alkyl tail further, driving force of self-assembly was changed from peptide-driven (hydrogen bond, hydrophobic side chain-side chain interaction) to lipid-driven (van der Waals interaction).

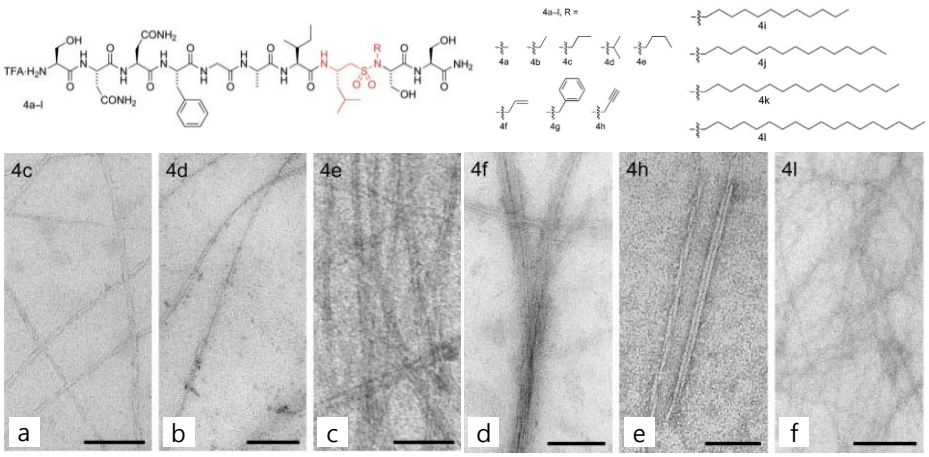

Figure 10. Structures and TEM images of amylin derivatives 4a-4l.

Hartgerink group studied the role of hydrogen bonding and amphiphilic packing in self-assembly of peptide amphiphiles (**Figure 11**).[14] The peptide consists of a 7 glycine linker region which connects the hydrophobic tail to the functional cell adhesion sequence. A headgroup of the synthesized PAs always contains the "ERGDS" (Glu-Arg-Gly-Asp-Ser) motif as an example of a bioactive adhesion sequence (RGDS), as well as glutamic acid, to help control nano-fiber formation by changing the pH or by adding multivalent cations. To study the influence of the hydrogen bonding and conformation of the amino acids in the linker region, four different series of PAs were prepared. By selectively *N*-methylating an amino acid, hydrogen bonding can specifically be controlled and interrupted. The introduction of each subsequent methylated glycine residue lowers the storage modulus, and the methylation of three glycine residues results in a weak gel formation. It was indicated that the hydrogen bonding at these sites may be disrupted while the macroscopic physical behavior is maintained. The blocking of one hydrogen bond next to the hydrophobic core prevents the gel formation. When one *N*-

methylated glycine group incorporated into glycine linker in PA, it self-assembled into gel for PAs **13**, **14** and **2** and precipitate for PA **9**-**12**. Together, these observations demonstrate that (a) blocking of the hydrogen bond at locations 5-7 reduces the strength of the resulting gel but does not eliminate it, even when all three positions are blocked, and (b) blocking even a single hydrogen bond in location 1-4 eliminates gel formation. The mechanical behavior of the hydrogels demonstrates that the interior region of the PA molecule plays an important role in defining the macroscopic physical properties of the self-assembled material.

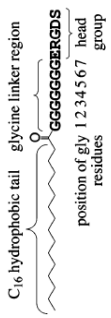

PA	Glycine Position 1	2	3	4	5	6	7	nanostructure	rheology
1	G	G	G	G	G	G	G	F	Gel
2	G	G	G	G	G	G	^{NMe}G	F	Gel
3	G	G	G	G	G	^{NMe}G	^{NMe}G	F	Gel
4	G	G	G	G	^{NMe}G	^{NMe}G	^{NMe}G	F	wGel
5	G	G	G	^{NMe}G	^{NMe}G	^{NMe}G	^{NMe}G	–	–
6	G	G	^{NMe}G	^{NMe}G	^{NMe}G	^{NMe}G	^{NMe}G	–	–
7	G	^{NMe}G	^{NMe}G	^{NMe}G	^{NMe}G	^{NMe}G	^{NMe}G	–	–
8	^{NMe}G	^{NMe}G	^{NMe}G	^{NMe}G	^{NMe}G	^{NMe}G	^{NMe}G	–	–
9	^{NMe}G	G	G	G	G	G	G	F	–
10	G	^{NMe}G	G	G	G	G	G	F	–
11	G	G	^{NMe}G	G	G	G	G	F	–
12	G	G	G	^{NMe}G	G	G	G	F	–
13	G	G	G	G	^{NMe}G	G	G	F	Gel
14	G	G	G	G	G	^{NMe}G	G	F	Gel
15	^{NMe}G	^{NMe}G	G	G	G	G	G	–	–
16	^{NMe}G	^{NMe}G	^{NMe}G	G	G	G	G	–	–
17	^{NMe}G	^{NMe}G	^{NMe}G	^{NMe}G	G	G	G	–	–
18	^{NMe}G	^{NMe}G	^{NMe}G	^{NMe}G	^{NMe}G	G	G	–	–
19	^{NMe}G	^{NMe}G	^{NMe}G	^{NMe}G	^{NMe}G	^{NMe}G	G	–	–

Figure 11. Molecular structure of PA and self-assembly behaviors of *N*-methylated PAs **1**-**19**.

Tovar group report a new class of peptide amphiphiles which bear internal π-conjugated segments that can be manipulated and self-assembled into 1D nano-structure.[15] They prepared biothiophene bearing an Fmoc-protected amine and a free carboxylic acid and incorporated β-sheet forming peptide motifs to yield PA **2**. With PA **2**, environmental conditions that promoted carboxylate charge screen (e.g. HCl or $CaCl_2$) initiated self-assembly resulting in the macroscopic formation of self-supporting gels suggestive of entangled 1D structure (**Figure 12**). The IR spectra for **2**

displayed characteristic β-sheet amide I bands accompanied by minor random-coil contributions. Circular dichroism (CD) of assembled **2** had intense absorptions only associated with the π-conjugated unit. The bi-signate CD response crossing over at 320 nm is classic signature for exciton coupled chromophores in chiral environments. The natural propensities for β-sheet to adopt macromolecular twists would also dictate twisted H-aggregates.[16] These objects are consistent with coiled tape-like or even more complex fibrillar structure.

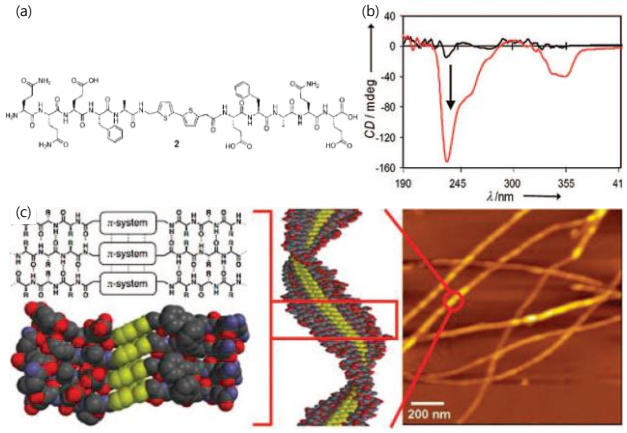

Figure 12. (a) Molecular structure of self-assembling peptide **2**. (b) CD of **2** in basic (dissolved, black traces) and acidic (assembled, red traces) aqueous solution. (c) Energy minimized illustration of β-sheets and π-stacks as line drawing and space-filling models (left), the helical twist sense along a model aggregate (middle) and tapping-mode AFM images of self-assembled aggregates of **2**.

2.1.2. Amphiphiles with Carbohydrate Headgroup

Carbohydrate-mediated cell–cell recognition is important in a variety of biological processes, including the infectivity of pathogens, immune response and reproduction.[17] Since each binding event of a carbohydrate-mediated

system involves weak interactions (hydrogen bonding), the receptors involved must establish multiple interactions to achieve high selectivity.[18] It is this multivalent binding process that provides a unique advantage for oligosaccharide-mediated recognition over other recognition strategies involving biomolecules such as proteins or nucleic acids. Hence, many studies focus on incorporating carbohydrate group into amphiphilic molecule.[19]

Shimizu group has demonstrated that long chain phenyl glucoside formed twist nano-fiber, helical ribbon, and nano-tubular structures.[20] The self-assembly of a series of long chain pheny glucosides amphiphile **1-4** varying in number of cis-double bonds in the lipophilic part (**Figure 13**). The self-assembly of **1-4** occurred rapidly under mild conditions. For example, 30 min of vortexing at 100 ℃ and 5 hrs of room-temperature incubation were sufficient to ensure the formation of stable supramolecular assemblies in aqueous solutions for **2-4**. However, **1** was insoluble in water and only formed a typical nano-fiber structure in a mixture of water and methanol (1:1 v/v). Amphiphile **2** shows the twist fiber structure, whereas **3** shows the left-handed coiled tube (less than 5%), and the helical ribbon structures as the major morphology, showing the influence of double bonds on the final morphology of the self-assembled structures. On the other hand, amphiphile **4** possessing three cis double bonds in the lipophilic region displays the helical ribbon morphology and nano-tubular structure as the major morphology. The relatively strong intermolecular hydrogen bonding interaction of a glucopyranoside moiety of **3** and **4** provided a highly ordered chiral packing structure which lead to the formation of the nano-tubular structure.

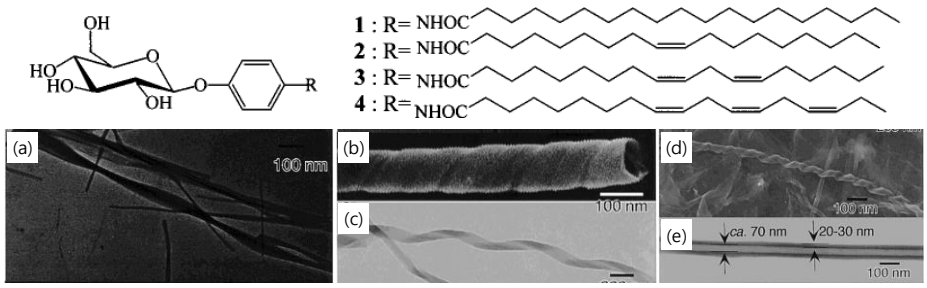

Figure 13. Molecular structure of glucoside amphiphiles. EF-TEM and SEM images of the self-assembled (a) **2**, (b and c) **3**, and (d and e) **4**.

2.1.3. Self-assembling Behaviors of Bola-amphiphile

Bola-amphiphilic molecules contain two functional head groups and their hydrophobic chain linker (**Figure 14**).[21] Since they exhibit unique hierarchically self-assembled structures at both interfaces, including air/water, liquid/solid, and in solutions, the synthesis and application of bola-amphiphilic molecules has been extensively studied. In the last two decades, various synthetic methods have been developed to produce functional bola-amphiphiles that mimick their natural counterparts. More attention has been given to studies of their hierarchally organized structures and applications in various fields, including drug delivery, gene delivery, electronics, medical imaging, etc.

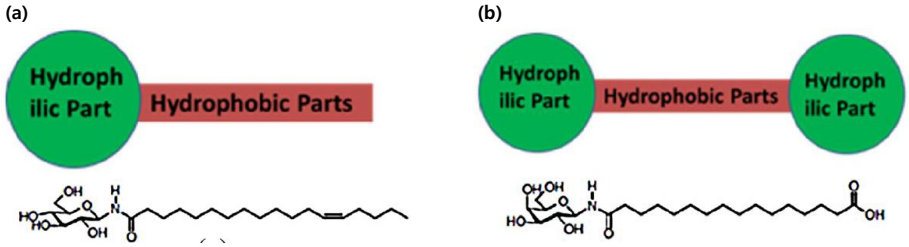

Figure 14. A schematic drawing and molecular structures of (a) conventional amphiphilic molecule and (b) defined bola-amphiphiles.

Shimizu group have found that asymmetrical 1-glucosamide bola-amphiphile **1**(n) with even-numbered oligomethylene chains self-assemble in water to form nanotubes and three types of micro-tubes.[22] The asymmetric bola-amphiphile, *ω*-[*N*-β-D-glucopyranosylcarbamoyl]alkanoic acids, with even-numbered oligomethylene chains self-assembled in water to form lipid nano- and micro-tubes (**Figure 15**). The nano-tubes encapsulated the staining reagent phosphotungstate, which revealed them to be hollow cylinders up to several hundred micrometers long with 30-43 nm outer diameters and 14-29 nm inner diameters. The membrane stacking periodicity was compared using powder X-ray diffraction analysis. They found that the nanotubes consist of a asymmetrical monolayer lipid membrane (MLM) in which the molecules are packed in a parallel fashion. This suggests that the inner surface of the nano-tubes is covered with carboxylic head-groups and the outer surface with 1-glucosamide head-groups. The micro-tubes had three types of molecular arrangements. The first type was a symmetrical MLM, in which the molecules were packed in an antiparallal fashion. The other two types had asymmetrical MLM stacking with head to head and head to tail motifs. Increasing the number of oligomethylene spacers stabilized the asymmetrical MLM structure in both the nano- and micro-tubes.

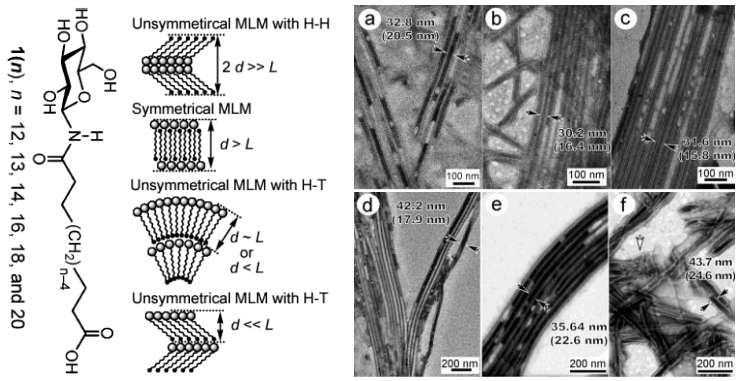

Figure 15. Molecular structures of asymmetric bola-amphiphile **1**(n) and

schematic illustration of monolayer lipid membranes (MLMs) formed from asymmetric bola-amphiphile. TEM images of nano-tubes formed from (a) **1**(12), (b) **1**(14), (c) **1**(16), (d) **1**(18), (e) **1**(20) and (f) the sodium salt of **1**(18).

2.1.4. Self-assembling Behaviors of Gemini Amphiphiles

A conventional amphiphile has a single hydrocarbon tail connected to an ionic or polar head-group. In contrast, a gemini amphiphile contains two hydrophilic head-groups linked by a spacer and two hydrophobic tails (**Figure 16**). The two closer hydrophobic chains give gemini amphiphiles a more compact molecular packing configuration that induces sensitively low surface tension. This class of amphiphile exhibits intriguing property such as sub-micellar aggregation or formation of thread-like micelles. Moreover they generally has a critical micelle concentration (CMC) that is up to two orders of magnitude lower than the CMCs of corresponding single chain surfactants and good solubilization properties.[23]

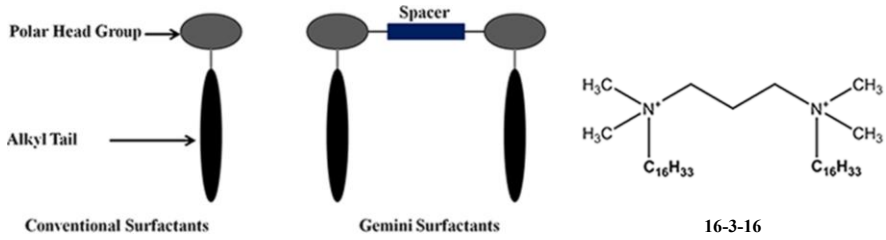

Figure 16. Structural schematic of conventional and gemini amphiphiles. Chemical structure of 16-3-16 gemini amphiphile

MacKintosh group demonstrate cationic gemini amphiphiles having chiral counterions such as *L*-tartrate form gels, in both water and some organic solvents.[24] They found that the pure 16-2-16 *L*-tartrate consistently forms twisted ribbons of the same handedness, whilst the *D*-tartrate form

ribbon of opposite handedness (**Figure 17**). However, these enantiomers do not undergo a lateral phase separation into helices with opposite chirality when mixed in arbitrary proportions. Instead, they mix homogeneously and form helices with a continuous variation of twist period and width. An increase of the enantiomeric excess causes a decrease of the twist pitch from infinity to 200 nm. On increasing the enantiomeric excess, a decrease of the mean width of the ribbons from ~400 nm to 40 nm is observed, and their period and width seem to become more regular. On addition of the sodium *L*-tartrate, a helix of 16-2-16 *L*-tartrate twists even further. The decrease of the pitch and width eventually reaches a limit at ~3 equiv. of added salt, presumably as the cationic bilayers become saturated with chiral anions. Thus tuning the geometrical parameter of these helices can be performed using very simple means.

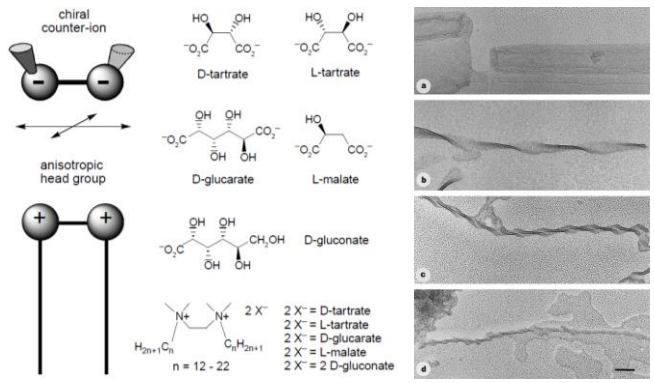

Figure 17. Cationic gemini amphiphiles with chiral counterions. TEM images of the ribbon from a) racemate, b) *L*-tartrate excess, c) pure *L* and d) pure *L* in the presence of 1 equiv. of *L*-tartrate.

Bassani group show that a cationic gemini amphiphile with an azobenzene spacer can reversibly change its conformation.[25] The structure of 16-azo-16 is based on the use of a photoactive azobenzene chromophore as a

rigid scaffold to connect two cationic alkylammonium amphiphiles (**Figure 18**). The aqueous solution, 16-azo-16 spontaneously forms vesicles upon sonication and gentle heating, shown by optical microscopy and cryo-TEM. The vesicles remained unchanged under and after irradiation of the sample, and their integrity was further confirmed by TEM. These results indicate that *E*, *Z* isomerization is insufficient to including a morphology change of the 16-azo-16 vesicles.

Vesicles formed from a mixture of 16-azo-16 and CTAB (10:1) are similar in shape to vesicles from pure gemini amphiphile. However, upon irradiation the vesicles rapidly deform and rupture to transform into much smaller birefringent objects. It is likely that the vesicles are transformed into a mixture of micelles and small crystallity. The vesicles do not spontaneously re-form after irradiation is halted, despite the reversible nature of the *E*, *Z* isomerization. The light-induced collapse of the vesicles to the destabilization of the lamellar structure occurs due to a change in the surface curvature induced by *E*, *Z* isomerization.

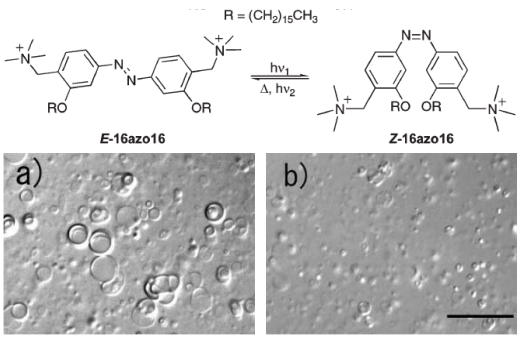

Figure 18. Molecular structure of gemini amphiphile and their photo-isomerization mechanism. DIC optical microscopic images of vesicles formed from a 10:1 mixture of 16-azo-16 and CTAB (a) before and (b) after irradiation.

2.2. Block Copolymer Based Amphiphiles

Most of today`s materials require additional processing or modification steps in order to obtain the properties that make them suitable for a particular application. As an alternative to these traditional fabrication pathways, routes that use the self-assembly of low molecular weight oligomeric or polymeric building blocks are becoming increasingly popular.[26] By designing these building blocks in such a way that they contain all the necessary information to direct their self-assembly into functional materials, additional processing or modification steps could become superfluous.

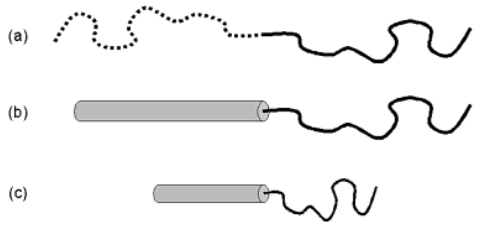

Figure 19. Schematic representation of the different types of block copolymers. (a) coil-coil diblock copolymers, (b) rod-coil diblock copolymers and (total molecular weight >20000 g/mol) and (c) rod-coil diblock oligomers (total molecular weight <20000 g/mol).

Whereas it is difficult to organize low molecular weight building blocks into periodic macroscopic assemblies, macromolecules can be assembled into a large variety of ordered morphologies covering several length-scales. We focus on block copolymer type building blocks and discuss their potential for the development of self-assembled materials. Three different classes of block copolymer type architectures will be distinguished: a) coil-coil diblock

copolymers, b) rod-coil diblock copolymers, and c) rod-coil diblock oligomers (**Figure 19**). These polymers consist of two or more chemically different polymers covalently connected. Due to thermodynamic incompatibility and chain connectivity, the phase separation between two (or more) blocks occurs only in ten nanometer ranges.

Coil-coil diblock copolymers, block copolymers comprised of two flexible, chemically incompatible and dissimilar blocks (e.g., poly(styrene)-*b*-poly(isoprene)) can microphase separate into a variety of morphologies. A self-assembly process of these copolymers is driven by an unfavorable mixing enthalpy and a small mixing entropy, while the covalent bond connecting the blocks prevents macroscopic phase separation. Li et. al. have developed a hierarchical process that combines linear triblock copolymers into concentric globular subunits.[27] The triblcok copolymer consists of polystyrene (PS), poly(methylacrylate) (PMA) and poly(acrylic acid) (PAA) with norborenyl functional group (**Figure 20**). Placement of the polymerizable norbornenyl unit at the polystyrene chain terminus was carried out so that the polymerization into a molecular brush would present hydrophobic materials to the inner region of the final supramolecularly assembled structures. When transitioned from DMF into water, the nano-structures from the triblock molecular brush copolymer and linear copolymer amphiphiles exhibited different morphologies. As shown in the TEM images, the linear amphiphilic macromolecules presented globular nano-scopic morphologies, while the molecular brushes exhibited cylindrical morphologies. The diameter of the cylinders was close to globules, suggesting that the core-shell micellar arrangement of PS-*b*-PMA-*b*-PAA polymer side chains in the molecular brushes was similar to that of the polymers. The rigid polynorbornen

backbone in the molecular brush limited the conformational freedom of the triblock copolymer grafted side chains, providing opportunities for unidirectional interactions between individual molecular brushes. On the other hand, the linear amphiphilic triblock copolymer requires multi-molecular interactions to remain as stable dispersions in water.

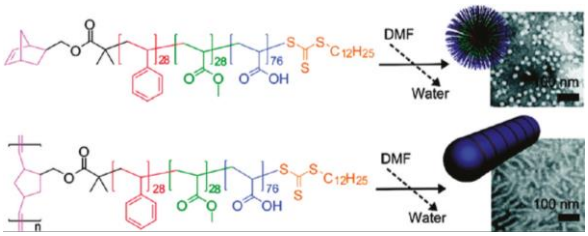

Figure 20. Molecular structure and self-assembly of molecular brushes, having triblock PS-*b*-PMA-*b*-PAA side chain, and linear amphiphilic PS-*b*-PMA-*b*-PAA triblock copolymer. TEM images of the nanostructures self-assembled from linear triblock copolymers and molecular brushes.

Replacing one of the blocks of a coil-coil diblock copolymer by a stiff, rigid or semi-flexible segment results in a rod-coil type diblock copolymer. In this case, the self-assembly is no longer solely determined by phase-separation, but is also affected by several other processes. One of the phenomena competing with phase-separation during the self-assembly of rod-coil diblock copolymer is the aggregation of the rigid segments into crystalline domains. In addition, the introduction of a rigid segment results in a disparity of stiffness between the constituent blocks. Chen group report the synthesis and self-assembled morphologies of a series of new rod-coil copolymers, poly[2,7-(9,9-dihexylfluorene)]-*b*-poly(4-vinylprydine) (PF-*b*-P4VP).[28] They found that the microphase separation varied from lamellar to cylindrical and then to spherical, depending on the length of P4VP block

(**Figure 21**). TEM images, obtained using RuO_4 to stain the PF blocks, shows stripped cluster distributed in homogeneous matrix.

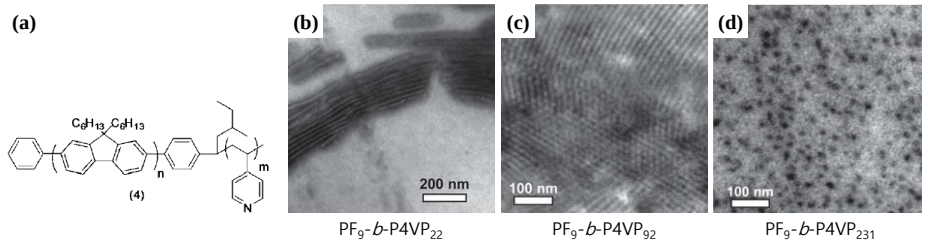

Figure 21. (a) Schematic of PF-*b*-P4VP. TEM images of (b) PF_9-*b*-$P4VP_{22}$, (c) PF_9-*b*-$P4VP_{92}$ and (d) PF_9-*b*-$P4VP_{231}$.

Self-assembly of block oligomer toward well-defined architecture has been one of the major research areas of materials science and nano and biochemistry due to its tremendous potential to produce materials with specific functions. Of the variety of self-assembling block molecules, rod-coil have particularly stimulated researcher's interest because of their unique organizing power by employing conformationally distinct blocks, that is, rigid rods and flexible coils. Any such efforts have demonstrated that a variety of assembled morphologies, such as spheres, vesicles, cylinders, twisted ribbons, barrels and toroids form in solution states.[29]

Cho group designed a series of amphiphilic rod-coils labeled with a pyrenyl moiety.[30] The rod-coil amphiphiles self-assembled into anisotropic rod-like shape in water (**Figure 22**). The TEM image of rod-coil **1** display fibrillar aggregates with lengths of up to several hundred nanometers, while the aggregates formed by rod-coil **2** were shown to be mostly truncated fibers with less than 100 nm in length. However, morphology of the more sterically bulky rod-coil **3** displays the re-entering elongated fibrillar aggregates with lengths of up to several hundred nanometers. Similar to the morphological

change in **1** and **2**, **4** was shown to shorten the lengths of the cylindrical fibers. The aggregates of **1** and **2** were self-assembled from antiparallel rod packing with the phenylene rod and pyrenyl groups facing each other. On the other hand, the **3** and **4** were self-assembled into aggregates by interdigitated rod packing between pyrenyl groups in rod segment.

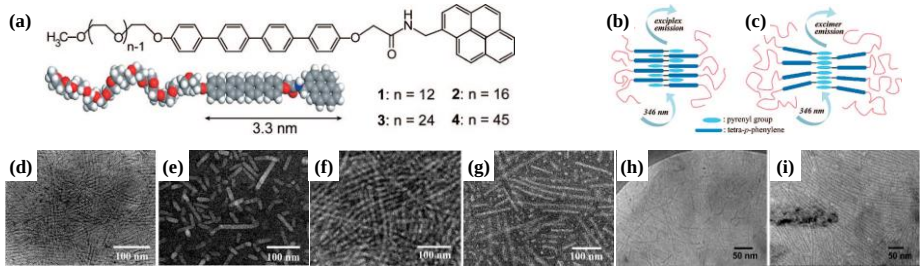

Figure 22. (a) Molecular structures of rod-coil **1**-**4**. (b) Schematic representation of (b) the antiparallel rod packing of **1** and **2**, and (c) the interdigitated rod packing of **3** and **4**. TEM images of self-assembled cylindrical fibers by (d) **1**, (e, h) **2**, (f, i) **3**, and (g) **4**.

2.3. Multi-component Supra-amphiphiles

In contrast to conventional amphiphiles based on covalent bonds, a new field of supra-amphiphiles has emerged that refer to amphiphiles constructed on the basis of non-covalent interactions or dynamic covalent bonds (**Figure 23**).[31] The supra-amphiphiles can be realized by employing suitable non-covalent interactions including hydrogen bonding, host-guest recognition, electrostatic forces, metal coordination and π-π stacking interaction. In supra-amphiphiles, hydrophilic headgroup and hydrophobic tail can be attached by non-covalent synthesis, greatly reducing the need for tedious chemical synthesis. The building block of supra-amphiphiles can be either small

molecules or polymers. The dynamic nature of the non-covalent interactions facilitates the introduction of functional moieties into supra-amphiphiles, leading to the fabrication of molecular assemblies that are responsive to environmental stimulus. It is hoped that the study on self-assembly of supra-amphiphiles can enrich the field of molecular engineering of functional supramolecular systems and provide new avenues for the construction of self-assembling soft materials.

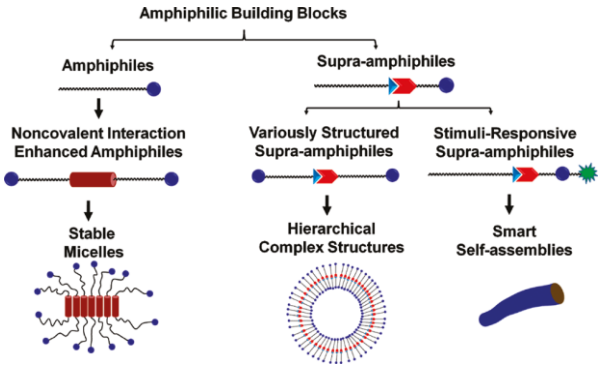

Figure 23. Diversified building blocks for self-assembly: Toward fabrication of functional soft materials and surfaces.

2.3.1 Charge-transfer Amphiphiles

Charge-transfer complex is formed by the weak association of two molecules or molecular subgroups, one of which acts as an electron donor and the other as an electron accept. Due to their easy preparation, it is possible to obtain nanoscale materials based on one-dimensional charge-transfer complex by self-assembly in aqueous solution. Many researchers developed “supra-amphiphile” for the fabrication of self-assembled materials on the basis of the water-soluble charge-transfer complexes.[32]

Zhang group show the charge-transfer supra-amphiphile consist of electron rich 1-[11-oxo-11-(pyren-1-ylmethoxy)-undecyl]pyridium bromide

(PYR) and electron deficient ethane-1,2-diyl bis(3,5-dinitrobenzoate) (DNB).[35a] PYR and DNB can initially co-assemble into a supramolecular complex driven by a charge-transfer interaction between the pyrenyl group in PYR and dinitrobenzene group in DNB. In this way, the amphiphilicity and the shape of the building units can be altered, further influencing the self-assembly behavior in aqueous media (**Figure 24**). While PYR itself self-assembled into rods, complex between PYR and DNB, sphere-like aggregates were observed, drastically different from the rod-like structures constructed by PYR alone.

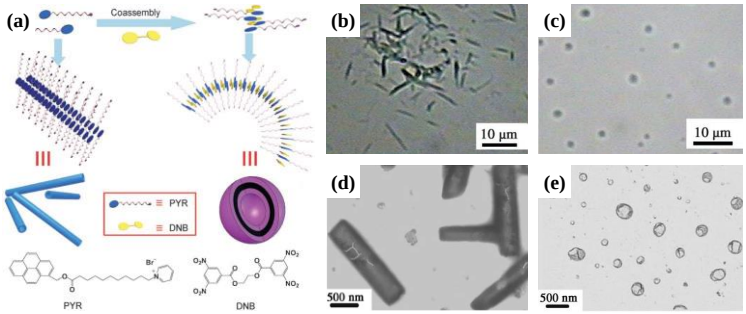

Figure 24. (a) Schematic representation of the transformation from tubes to vesicles, and the molecular structure of PYR and DNB. Optical and TEM images of (b, d) PYR aggregates and (c, e) PYR-DNB aggregates.

2.3.2 Metal-ligand Coordinated Amphiphiles

Metal-ligand coordination is another driving force for fabricating supra-amphiphiles.[33] This non-covalent bond is stronger than most intermolecular interactions. However, its reversibility makes it function as a type of supramolecular bond interaction that can be employed in the construction of complex self-assembled amphiphiles nano-structures. In the same manner, if the metal-ligand coordination is ruptured, the self-assembled aggregates are simultaneously disassembled.

De Cola group present a straightforward one-pot synthetic strategy presenting a amphiphilic platinum(II) complex with particular photophysical properties owing to aggregate formation.[34] The coordination of an alkyl pyridine (**3**) ancillary moiety to 2,6-bis(tetrazolyl)pyridine (**1**) complex allowed to enhance the solubility and self-assemble into bright nano-fibers (**Figure 25**). The soluble alkyl chain attached to the insoluble chromophore, **1**, render this complex a amphiphile. Dissolving the complex in $CHCl_3$ and diffusing *n*-hexane into the colorless non-emissive solution affords a self-assembled yellow gel that appears highly luminescent. A close inspection with SEM revealed fibers that are responsible for the structure of the emissive soft material. TEM analysis showed the interlocking nature of the nano-fibers. Self-assembly of the platinum(II) complex yielded entangled nanofibers and aggregation-induced emission.

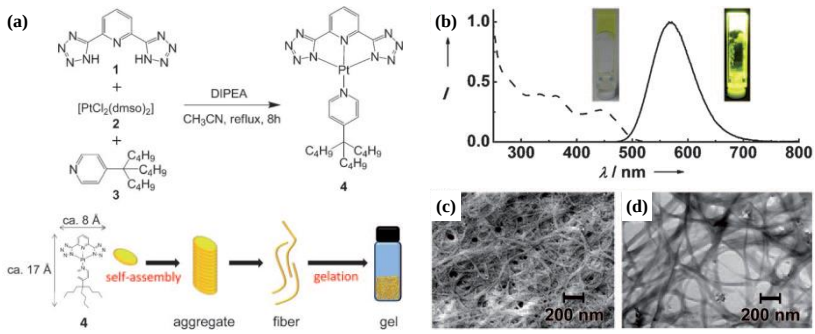

Figure 25. (a) Schematic representation of self-assembly process of platinum(II) complex **4** and its molecular structure. (b) Emission (solid line, λ_{ex}=420nm) and excitation (dash line, λ_{em}=580nm) spectra of the self-assembled gel. (c) SEM and (d) TEM image of the gel.

2.3.3 Amphiphiles Based on Host-guest Recognition

The amphiphiles based on host-guest interaction provide a flexible

platform for the development of various nano-materials. From the variety of synthetic organic molecules used as molecular receptors to construct supra-amphiphiles distinctive properties have been obtained by introducing macrocyclic hosts into the supramolecular systems. The typical example is the inclusion complex of β-Cyclodextrin (β-CD) and fatty acid or fatty alcohol, referred to as non-covalent supra-amphiphiles.[35] A combination of the dynamic/reversible nature of host-guest interactions with the new topological features and various functions to building blocks provides a versatile strategy for preparation of nano-structured functional soft materials. This respect is of paramount importance and results in the ability to undergo dynamic switching of structure, morophology and functions in response to various guest molecules.

Kim group demonstrate a construction of a series of functional nano-tubes by the cooperative self-assembly of dendrons and CDs.[36] Various functional groups were introduced onto the tube surface by utilizing CDs in the self-assembly process. The Pyrene attached dendron **1** and self-organized into vesicles in aqueous solution. Upon addition of CDs into the solution, the CD-pyrene complexation occurs through host-guest recognition. This supra-amphiphile transforms the self-assembled structures from vesicle to the CD-covered nanotubes (**Figure 26**). According to TEM analysis, introducing functionality to CDs has no influence on morphology of self-assembly of the CD-dendron complex. Considering the TEM and AFM analysis, the wall must be associated with the unilamellar bilayer of dendron **1** with the focal pyrene moiety. They can fabricate various functional nanotubes through the use of C-6 modified CDs.

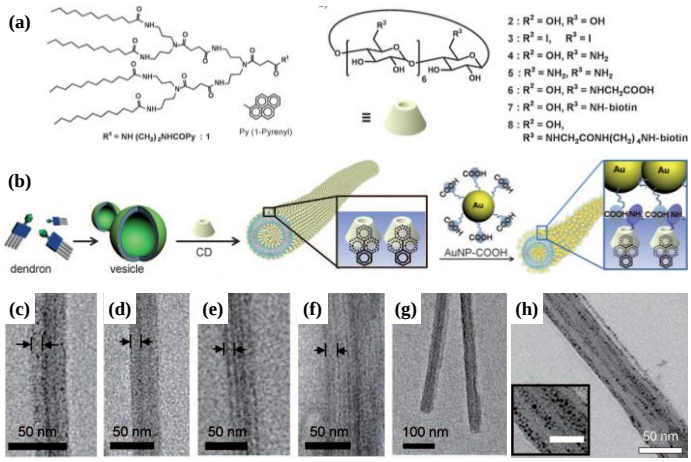

Figure 26. (a) Chemical structure of dendron **1** and CDs (b) Schematic description of the self-assembly process for the preparation of functional Den-CD-NTs. TEM images of (c) Den-iodo-CD-NT, (d) Den-per-NH_2-CO-NT, (e) Den-mono-NH_2-CD-NTs, (f) Den-COOH-CD-NT, (g) Den-biotin-C4-CD-NT and (h) AuNP-COOH/Den-mono-NH_2-CD-NT.

2.3.4 Hydrogen Bonding Supra-amphiphiles

The use of complementary hydrogen bonding for fabricating supra-amphiphiles dates back to the early work of Kunitake et. al. who employed substituted melamines as hydrogen acceptor and isocyanuric acid derivatives as hydrogen donor.[37] Through the combination with hydrogen acceptor, the amphiphilicity of amphiphilic hydrogen donor can be changed greatly as the hydrophobic segment was elongated. For example, by changing the alkyl chain length of the hydrogen acceptors, the supra-amphiphiles could self-assemble into different aggregates. The concept of hydrogen bonding based supra-amphiphiles could fabricate various nano- and micro-materials.

Park group reported an aromatic organogelator, 1-cyano-trans-1,2-bis-(3',5'-bis(trifluoromethyl)biphenyl)ethylene (CN-TFMBE), which formed

highly fluorescent organogel.[38] To add specific functional properties to CN-TFMBE, they modified the organogelator to the pyridine containing trifluoromethyl based cyanostilbene (CN-TFBMPPE).[39] It is unlikely to have sufficient self-assembling capability. However, complex of CN-TFMBPPE and 3,5-trifluoromethylbenzoic acid via complementary hydrogen bonding has a successful self-assembling capability and formed a translucent gel with fluorescence (**Figure 27**). To improve gel stability as well as to induce chirality, tartaric acid was employed as a chiral hydrogen bonding donor. When the CN-TFMBPPE and *L*-tartaric acid was mixed with 2:1 molar ratio, a transparent and highly fluorescent organogel promptly formed. According to SEM image, the CN-TFMBPPE-L-TA gel has a different morphology, sponge-like nano-fibers, to that 3,5-bistrifluoromethylbenzoic acid complex, nano-ribbon. Intermolecular hydrogen-bonding interaction between tartaric acid is induced these different self-assembly behavior. Furthermore, the intermolecular interaction also induced chirality transcription in self-assembly process. The resulting organogel shows formation of chiral aggregates and their chirality could be controlled by changing another chiral tartaric acid.

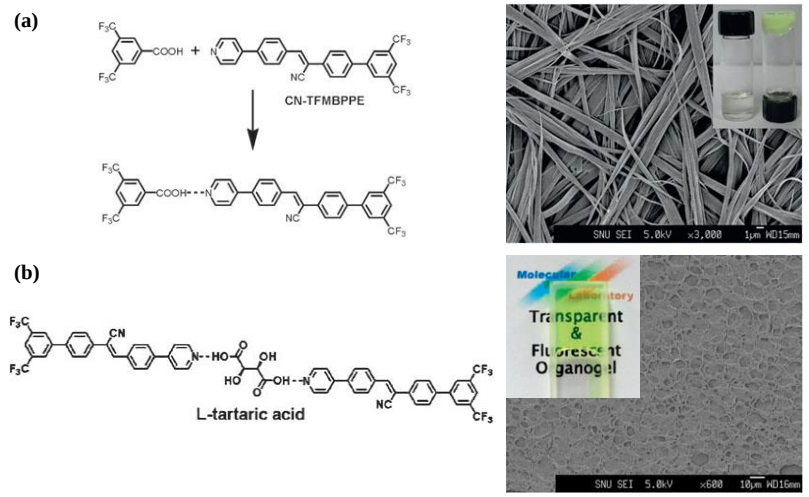

Figure 27. Schematic representation, SEM and Optical image of hydrogen

bonded complex between (a) CN-TFMBPPE and 3,5-bistrifluoromethyl-benzoic acid and (b) CN-TFMBPPE and L-tartaric acid.

3. References and Notes

1 (a) Tecila, P; Dixon, R. P.; Slobodkin, G.; Alavi, D. S. *J. Am. Chem. Soc.* **1990**, *122*, 9408. (b) Whitesides, G. M.; Mathias, J. P.; Seto, C. T. *Science*, **1991**, *254*, 1312. (c) Fujita, M.; Ogura, K. *Bull. Chem. Soc. Jpn.* **1996**, *69*, 1471.

2 (a) Whitesides, G. M.; Grzybowski, B. A. *Science*, **2002**, *295*, 2418. (b) Lehn, J. M. *Supramolecular Chemistry Concepts and Perspectives*, Wiley-VCH, Weinheim, **1995**. (c) Ringsdorf, H.; Simon, J. *Nature*, **1994**, *371*, 284.

3 (a) Isrealachvili, J. N.; Mitchell, D. J.; Ninham, B. W. *J. Chem. Soc. Faraday Trans. 2*, **1976**, *72*, 1525. (b) Israelachvili J. N. *Intermolecular and Surface Forces*, Academic Press, New York, **1985**.

4 Lim, Y.-b.; Moon, K.-S.; Lee, M. *J. Mater. Chem.* **2008**, *18*, 2909.

5 Childers, W. S.; Ni, R.; Metha, A. K.; Lynn, D. G. *Curr. Opin. Chem. Biol.* **2009**, *13*, 652.

6 Cavalli, S.; Albericio, F.; Kros, A. *Chem. Soc. Rev.* **2010**, *39*, 241.

7 (a) Khoe, U.; Yang, Y.; Zhang, S. *Marcomol. Biosci.* **2008**, *8*, 1060. (b) Nagai, A.; Nagai, H; Qu, H.; Zhang, S. *J. Nanosci. Nanotechnol.* **2007**, *7*, 2246. (c) Yang, S. J.; Zhang, S. *Supramol. Chem.* **2006**, *18*, 389. (d) Khoe, U.; Yang, Y.; Zhang, S. *Langmuir*, **2009**, *25*, 4111.

8 (a) Xu, H.; Wang, J.; Han, S.; Wang, J.; Yu, D.; Zhang, H.; Xia, D.; Zhao, X.; Waigh, T. A.; Lu, J. R. *Langmuir*, **2009**, *25*, 4115. (b) von-Maltzahn, G.; Vauthey, S.; Santoso, S.; Zhang, S. *Langmuir*, **2003**, *19*, 4332. (c) Santoso, S.; Hwang, W.; Hartman, H.; Zhang, S. *Nano Lett.* **2002**, *2*, 687. (d) Vauthey, S.; Santoso, S.; Gong, H.; Watson, N.; Zhang, S. *Proc. Natl. Acad. Sci. U. S. A.* **2002**, *99*, 5355. (e) Zhao, X.; Pan, F.; Perumal, S.; Xu, H.; Lu, J. R.; Webster, J. R. P. *Soft Matter*, **2009**, *5*, 1630.

9 Hartgerink, J. D.; Beniash, E.,; Stupp, S. I. *Science*, **2001**, *294*, 1684.

10 (a) Jack, D. Y.; King, D. S.; Chmielewski, J.; Singh, S.; Schultz, P. G. *J. Am. Chem. Soc.* **1991**, *113*, 9391. (b) Clark, T. D.; Kobayashi, K.; Ghadiri, M. R. *Chem. Eur. J.* **1999**, *5*, 782. (c) Won, Y.-Y.; Davis, H. T.; Bates, F. S. *Science*, **1999**, *283*, 960; (d) Zubarev, E. R.; Pralle, M. U.; Li, L.; Stupp, S. I. *Science*, **1999**, *283*, 523. (e) Archer, E. A.; Goldberg, N. T.; Lynch, V. *J. Am. Chem. Soc.* **2000**, *122*, 5006.

11 Pierschbacher, M. D.; Ruoslahti, E. *Nature*, **1984**, *309*, 30.

12 Harris, J. R. *Electron Micoscopy in Biology*, A Practical Approach, Oxford Univ. Press, New York, **1991**, p. 32 and p. 206.

13 Elgersma, R. C.; Meijneke, T.; de Jong, R.; Brouwer, A. J.; Posthuma, G.; Rijkers, D. T. S.; Liskamp, R. M. J. *Org. Biomol. Chem.* **2006**, *4*, 3587.

14 Paramonov, S. E.; Jun, H.-W.; Hartgerink, J. D. *J. Am. Chem. Soc.* **2006**, *128*, 7291.

15 Diegelmann, S. R.; Gorham, J. M.; Tovar, J. D. *J. Am. Chem. Soc.* **2008**, *130*, 13840.

16 (a) Cornil, J.; dos Santos, D. A.; Crispin, X.; Silbey, R.; Bredas, J. L. *J. Am. Chem. Soc.* **1998**, *120*, 1289. (b) Schenning, A.; Jonkheijm, P.; Peeters, E.; Meijer, E. W. *J. Am. Chem. Soc.* **2001**, *123*, 409.

17 (a) Dwek, R. A. *Chem. Rev.* **1996**, *96*, 683. (b) Larsen, K.; Thygesen, M. B.; Guillaumie, F.; Willats, W. G. T.; Jensen, K. J. *Carbohydr. Res*, **2006**, *341*, 1209. (c) Arnold, J. N.; Wormald, M. R.; Sim, R. B.; Rudd, P. M.; Dwek, R. A. *Annu. Rev. Immunol.* **2007**, *25*, 21.

18 Mammen, M.; Choi, S. K.; Whitesides, G. M. *Angew. Chem. Int. Ed.* **1998**, *37*, 2755.

19 (a) Fuhrhop, J.-H.; Helfrich, W. *Chem. Rev.* **1993**, *93*, 1565. (b) Fuhrhop, J.-H.; Schnieder, P.; Boekema, E.; Helfrich, W. *J. Am. Chem. Soc.* **1988**, *110*, 2861. (c) Boettcher, C.; Schade, B.; Fuhrhop, J.-H. *Langmuir*, **2001**, *17*, 873.

20 Jung, J. H.; John, G.; Yoshida, K.; Shimizu, T. *J. Am. Chem. Soc.* **2002**, *124*, 10674.

21 (a) Fuhrhop, J.-H.; Mathieu, J. *Angew. Chem. Int. Ed.* **1984**, *23*, 100. (b)

Fuhrhop. J.-H.; Wang, T. *Chem. Rev.* **2004**, *104*, 2901. (c) Escamilla, G. H.; Newkome, G. R. *Angew. Chem. Int. Ed.* **1994**, *33*, 1937.

22 Masuda, M.; Shimizu, T. *Langmuir*, **2004**, *20*, 5969.

23 Camesano, T. A.; Nagarajan, R. *Colloids and Surfaces A: Physicochemical and Engineering Aspects*, **2000**, *167*, 165.

24 Oda, R.; Huc, I.; Schmutz, M.; Candau, S. J.; Mackintosh, F. C. *Nature*, **1999**, *399*, 566.

25 Faure, D.; Gravier, J.; Labrot, T.; Desbat, B.; Oda, R.; Bassani, D. M. *Chem. Commun.* **2005**, 1167

26 Lehn, J.-M. *Supramolecular Chemistry - Concepts and Perspectives*, VCH, Weinheim, 1995.

27 Li, Z.; Ma, J.; Lee, N. S.; Wooley, K. L. *J. Am. Chem. Soc.* **2011**, *133*, 1228.

28 Sun, H.-S.; Lee, C.-H.; Lai, C.-S.; Chen, H.-L.; Tung, S.-H. *Soft Matter,* **2011**, *7*, 4198.

29 (a) Jenekhe, S. A.; Chen, X. L. *Science*, **1999**, *283*, 372. (b) Kilbinger, A. F. M.; Schenning, A. P. H. J.; Goldoni, F.; Feast, W. J.; Meijer, E. W. *J. Am. Chem. Soc.* **2000**, *122*, 1820. (c) Tu, Y.; Wan, X.; Zhang, D.; Zhou, Q.; Wu, C. *J. Am. Chem. Soc.* **2000**, *122*, 10201. (d) Wang, H.; Wang, H. H.; Urban, V. S.; Littrell, K. C.; Thiyagarajan, P.; Yu, L. *J. Am. Chem. Soc.* **2000**, *122*, 6855. (e) Zubarev, E. R.; Pralle, M. U.; Sone, E. D.; Stupp, S. I. *J. Am. Chem. Soc.* **2001**, *123*, 4105. (f) Yang, W.-Y.; Ahn, J.-H.; Yoo, Y.-S.; Oh, N.-K.; Lee, M. *Nat. Mater.* **2005**, *4*, 399. (g) Schleuss, T. W.; Abbel, R.; Gross, M.; Schollmeyer, D.; Frey, H.; Maskos, M.; Berger, R.; Killbinger, A. F. M. *Angew. Chem. Int. Ed.* **2006**, *45*, 2969. (h) Xu, J.; Zubarev, E. R. *Angew. Chem. Int. Ed.* **2004**, *43*, 5491.

30 Han, K.-H.; Lee, E.; Kim, J. S.; Cho, B.-K. *J. Am. Chem. Soc.* **2008**, *130*, 13858.

31 (a) Zhang, X.; Wang, C. *Chem. Soc. Rev.* **2011**, *40*, 94. (b) Zhang, X.; Wang, C.; Wang, Z. Q. *Small*, **2011**, *7*, 1379. (c) Jeon, Y. J.; Bharadwaj, P. K.; Choi, S.; Lee, J. W.; Kim, K. *Angew. Chem. Int. Ed.* **2002**, *41*, 4474. (d) Versluis, F.; Tomatsu, I.; Kehr, S.; Fregonese, C.; Tepper, A. W. J. W.; Stuart,

M. C. A.; Ravoo, B. J.; Koning, R. I.; Kros, A. *J. Am. Chem. Soc.* **2009**, *131*, 13186.

32 (a) Wang, C.; Yin, S.; Chen, S.; Xu, H.; Wang, Z.; Zhang, X. *Angew. Chem. Int. Ed.* **2008**, *47*, 9049. (b) Wang, C.; Guo, Y.; Wang, Y.; Xu, H.; Wang, R.; Zhang, X. *Angew. Chem. Int. Ed.* **2009**, *48*, 8962. (c) Jeon, Y. J.; Bharadwaj, P. K.; Choi, S.; Lee, J. W.; Kim, K. *Angew. Chem. Int. Ed.* **2002**, *41*, 4474.

33 (a) Moughton, A. O.; O'Reilly, R. K. *J. Am. Chem. Soc.* **2008**, *130*, 8714. (b) Song, B.; Wu, G. L.; Wang, Z. Q.; Zhang, X.; Smet, M.; Dehaen, W. *Langmuir*, **2009**, *25*, 13306. (c) Shirakawa, M.; Fujita, N.; Tani, T.; Kaneko, K.; Ojima, M.; Fujii, A.; Ozaki, M.; Shinkai, S. *Chem. Eur. J.* **2007**, *13*, 4155. (d) Zhang, J.-J.; Lu, W.; Sun, R. W.-Y.; Che, C.-M. *Angew. Chem. Int. Ed.* **2012**, *51*, 4882. (e) Zhang, J.; Song, Y.-F.; Cronin, L.; Liu, T. *J. Am. Chem. Soc.* **2008**, *130*, 14408.

34 Strassert, C. A.; Chien, C.-H.; Lopez, M. D. G.; Kourkoulos, D.; Hertel, D.; Meerholz, K.; De Cola, L. *Angew. Chem. Int. Ed.* **2011**, *50*, 946.

35 (a) Bojinova, T.; Coppel, Y.; Viguerie, N. L.; Milius, A.; Lattes, I. R.; Lattes, A. *Langmuir*, **2003**, *19*, 5233. (b) Falvey, P.; Lim, C. W.; Darcy, R.; Revermann, T.; Karst, U.; Giesbers, M.; Marcelis, A. T. M.; Lazar, A.; Colemen, A. W.; Reinhoudt, D. N.; Ravoo, B. J. *Chem. Eur. J.* **2005**, *11*, 1171. (c) Wang, Y. P.; Ma, N.; Wang, Z. Q.; Zhang, X. *Angew. Chem. Int. Ed.* **2007**, *46*, 2823.

36 Park, C.; Im, M. S.; Lee, S.; Lim, J.; Kim. C. *Angew. Chem. Int. Ed.* **2008**, *47*, 9922.

37 Kimizuka, N.; Kawasaki, T.; Kunitake, T. *J. Am. Chem. Soc.* **1993**, *115*, 4387.

38 An, B.-K.; Lee, D.-S.; Lee, J.-S.; Park, S.-Y.; Song, H.-S.; Park, S. Y. *J. Am. Chem. Soc.* **2004**, *126*, 10232.

39 Seo, J.; Chung, J. W.; Jo, E.-H.; Park, S. Y. *Chem. Commun.* **2008**, 2794.

Section 1.
Fabrication of Nano- and Micro-superstructures using Multi-component System

1.1. Introduction

Amphiphilic molecules self-assemble into various types of nano- or micro-structures such as micelles, vesicles, fibers, tubules, rods, and helices in aqueous environment.[1] Amphiphilic molecules derived from peptides,[2] carbohydrates,[3] metal complexes,[4] steroids,[5] and dendrimers[6] have been successfully utilized to fabricate a wide variety of self-assembled structures. Morphological changes in nano- or micro-structures depend on solvent polarity and the structural changes and relative fractions of the hydrophilic and hydrophobic groups. These self-assembled superstructures are not only essential parts of biological systems, such as cell membranes, they can also be applied to functional materials for molecular probes, carriers, or optoelectronic devices.[7]

The use of multi-component amphiphilic systems, as well as single-molecule amphiphilic systems, has also been attempted for nano- or micro-structure fabrication.[8] Recently, we reported examples of a two-component

gelator system, in which a variety of organogels were produced by the self-assembly of two organogelators, 3,5-bis(dodecanoylamino)benzoic acid and aromatic amines, in nonaromatic hydrocarbon solvents, through hydrogen bonding, aromatic stacking, and van der Waals interactions.[8d] We found that the shape and size of the aromatic amine have a significant effect on the gel properties as well as their superstructures. The most important feature of the two-component systems is that the morphology can be easily modulated by changing the molar ratio of each component or one of the two components. In addition, physical and optoelectronic properties of the self-assembled structures also can be easily modulated by modifying the polar head groups.

Incorporating metal ion into the organic nano-structures is a good method of generating novel organic nano-structures and expanding their applications. The different coordination geometry of transition metal ions induce different shape of coordination complexes, which result in a wide variety of superstructures.[9] Since metal-ligand interactions are known to spontaneously induce cross-linking between building blocks, a variety of superstructures can be constructed. In addition, metal-embedded organic superstructures can be used as templates for the fabrication of inorganic nano-structures, and provide the advantage of introducing various new functions.[10] Herein, we report a simple method to control the morphology of organic nano- or micro-superstructures by altering the ratio of the two organic components and incorporating various metal ions into the complex.

As shown in **scheme 1**, the basic building blocks used in this study are composed of terephthaloylbisalanine (H_2TBA), having symmetric terminal carboxylic acid groups, and dodecylamine (DA).[11] The charged hydrogen-bonded complexes (abbreviated as TBA_xDA_y) between H_2TBA and DA act as

amphiphiles in water: The TBA−ammonium complex acts as the hydrophilic head component and the dodecyl group of DA acts as the hydrophobic tail component. Therefore, TBA_xDA_y can self-assemble into various superstructures in an aqueous solvent. *L*-H_2TBA and *rac*-H_2TBA were prepared to see if chirality would exert any effect on the morphology of the superstructures. Another relevant point is that the carboxylate groups in TBA can bind, not only to ammonium ions, but also to metal ions. The incorporation of metal ion is accompanied by structural changes in the supramolecular structure formed by the aggregation of the basic building blocks, resulting in new nano- or micro-superstructures. Moreover, the resulting supramolecular structures can be easily tuned by changing the ratio of DA to H_2TBA, the chirality of H_2TBA, and incorporating metal ions.

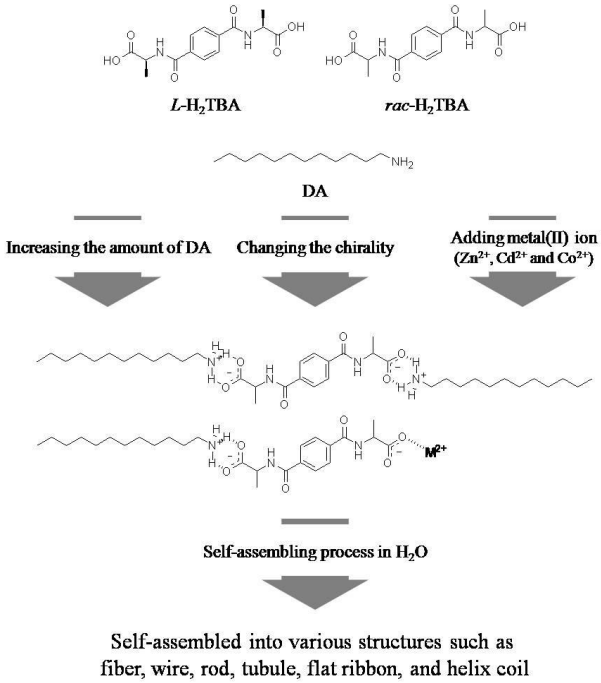

Scheme 1. Chemical structures of *L*-H_2TBA, *rac*-H_2TBA, and DA, and schematic representation of fabrication of various self-assembled structures using two- and three-component amphiphiles

1.2. Results and Discussion

The gelation behaviors of the complexes of TBA_xDA_y were tested in deionized water. MeOH solution of H_2TBA and DA in various ratios was concentrated and the resulting white solids were suspended in deionized water and heated to give rise to a colorless solution, which was then cooled to room temperature. Upon standing at room temperature, the clear solution turned into an opaque solution or gel. The mixing ratio and gel properties are listed in **table 1**. The 1:2 mixtures of *L*- or *rac*-H_2TBA and DA ($TBA_{1.0}DA_{2.0}$) became an opaque gel within 10 min. In the case of the 1:1 mixture of *L*- or *rac*-H_2TBA and DA ($TBA_{1.0}DA_{1.0}$), precipitates were formed after 20 min. While *rac*-$TBA_{1.0}DA_{1.5}$ turned into an opaque gel after 1 hr, *L*-$TBA_{1.0}DA_{1.5}$ remained in solution. Both $TBA_{1.5}DA_{1.0}$ and $TBA_{2.0}DA_{1.0}$ became opaque gels within 1 day.

Incorporation of metal ions into TBA_xDA_y was accomplished by suspending the white solid from the H_2TBA−DA mixtures in deionized water containing 1 equiv. of metal ions. The suspension was heated until clear, followed by cooling to room temperature. The mixing ratio and gel properties are listed in **table 1**. Upon incubation at room temperature, Cd(II) and Co(II) complex of *rac*-$TBA_{1.0}DA_{1.0}$ and *rac*-$TBA_{1.0}DA_{1.5}$ turned into opaque gels within 3 mins, but the corresponding Zn(II) complexes were not soluble in water, even after heating. In the cases of the Zn(II), Cd(II), and Co(II) complex of *L*-$TBA_{1.0}DA_{1.0}$, opaque gels were formed within 1 day. In contrast, Zn(II), Cd(II), and Co(II) complex of *L*-$TBA_{1.0}DA_{1.5}$ immediately formed insoluble solids upon heating.

Table 1. Mixing ratio and gel property of two- and three-component system.

Composition	Morphology	Composition	Morphology
L-$TBA_{1.0}DA_{2.0}$	G [a]	*rac*-$TBA_{1.0}DA_{2.0}$	G
L-$TBA_{1.0}DA_{1.5}$	S [b]	*rac*-$TBA_{1.0}DA_{1.5}$	G
L-$TBA_{1.0}DA_{1.0}$	P [c]	*rac*-$TBA_{1.0}DA_{1.0}$	P
L-$TBA_{1.5}DA_{1.0}$	G	*rac*-$TBA_{1.5}DA_{1.0}$	G
L-$TBA_{2.0}DA_{1.0}$	G	*rac*-$TBA_{2.0}DA_{1.0}$	G
L-$TBA_{1.0}DA_{1.0}$Zn(II)	G	*rac*-$TBA_{1.0}DA_{1.0}$Zn(II)	NS [d]
L-$TBA_{1.0}DA_{1.0}$Cd(II)	G	*rac*-$TBA_{1.0}DA_{1.0}$Cd(II)	G
L-$TBA_{1.0}DA_{1.0}$Co(II)	G	*rac*-$TBA_{1.0}DA_{1.0}$Co(II)	G
L-$TBA_{1.0}DA_{1.5}$Zn(II)	P	*rac*-$TBA_{1.0}DA_{1.5}$Zn(II)	NS
L-$TBA_{1.0}DA_{1.5}$Cd(II)	P	*rac*-$TBA_{1.0}DA_{1.5}$Cd(II)	G
L-$TBA_{1.0}DA_{1.5}$Co(II)	P	*rac*-$TBA_{1.0}DA_{1.5}$Co(II)	G

[a] G = Gel, [b] S = Clear Solution, [c] P = Precipitate, [d] NS = Not Soluble.

To confirm the self-assembled superstructures of TBA_xDA_y, scanning electron microscopy (SEM) and energy filtering-transmission electron microscopy (EF-TEM) images were obersved. According to the EM images, the self-assembled superstructures of $TBA_{1.0}DA_{2.0}$ were significantly changed by the chirality of H_2TBA. Right-handed micro-helical-ribbon structures were formed in *L*-$TBA_{1.0}DA_{2.0}$, in which the helical pitch was 2−3 μm (**Figure 1a**). However, in the case of *rac*-$TBA_{1.0}DA_{2.0}$, flat ribbon-like structures were observed (**Figure 1b**). In the case of helicity-inducing ligands, racemic ligands usually induced an equal amount of right-handed and left-handed helical structures.[12] However, our results are well matched with Fuhrhop's and Oda's, in which the resulting superstructure lost helicity, when using racemic ligands instead of chiral ligands.[8b,8c]

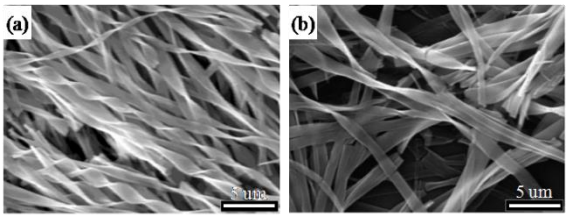

Figure 1. SEM images of (a) *L*-$TBA_{1.0}DA_{2.0}$ and (b) *rac*-$TBA_{1.0}DA_{2.0}$.

Changing the mixing ratio also dramatically changed the superstructures of the TBA_xDA_y assemblies. Nano-tubules with a diameter of approximately 500 nm were observed in *rac*-$TBA_{1.0}DA_{1.5}$. SEM images revealed a hollow, rectangular shape at the edge (**Figure 2a, b**). We were able to capture the hollow shape of *rac*-$TBA_{1.0}DA_{1.5}$ with EF-TEM (**Figure 8**). While *L*-$TBA_{1.0}DA_{1.0}$ showed entangled fibrous structures, *rac*-$TBA_{1.0}DA_{1.0}$ showed wire structures (**Figure 2c, d**). However, TBA enriched TBA_xDA_y, such as $TBA_{1.5}DA_{1.0}$ and $TBA_{2.0}DA_{1.0}$, self-assembled into wire-like superstructures (**Figure 9**).

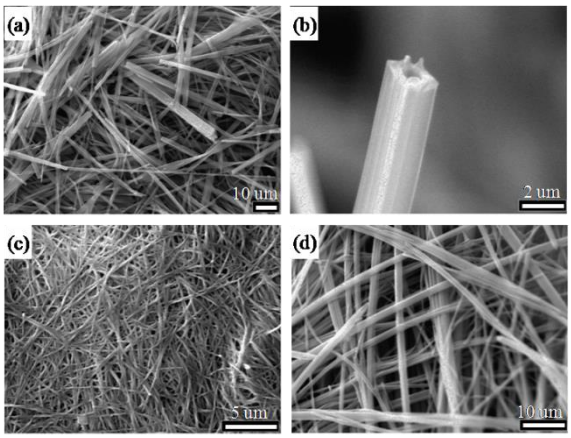

Figure 2. SEM images of (a) *rac*-$TBA_{1.0}DA_{1.5}$, (b) the hollow shape of the edge of *rac*-$TBA_{1.0}DA_{1.5}$, (c) *L*-$TBA_{1.0}DA_{1.0}$, and (d) *rac*-$TBA_{1.0}DA_{1.0}$.

As expected, self-assembled superstructures of TBA_xDA_y were

significantly changed by the addition of metal ions. As shown in **figure 3**, SEM and EF-TEM image of Cd(II) complexes of *L*-$TBA_{1.0}DA_{1.0}$ showed structural changes from fibrous to rod-like structures with diameters of about 100 nm. Surprisingly, tubule-shaped superstructures were obtained by adding Co(II) ion to *L*-$TBA_{1.0}DA_{1.0}$. The tubules had external and internal diameters of approximately 150 nm and 100 nm, respectively. However, the superstructure of *L*-$TBA_{1.0}DA_{1.0}$ did not show any significant change after adding Zn(II) ion (**Figure 10**).

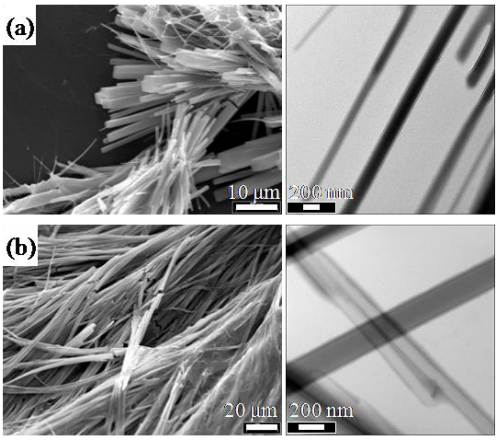

Figure 3. SEM (left) and EF-TEM (right) images of (a) *L*-$TBA_{1.0}DA_{1.0}$Cd(II) and (b) *L*-$TBA_{1.0}DA_{1.0}$Co(II).

Interestingly, while *L*-$TBA_{1.0}DA_{1.5}$ remained in a clear solution, metal complex with *L*-$TBA_{1.0}DA_{1.5}$ formed precipitates. According to SEM and EF-TEM images, the precipitates were a bundle of highly-ordered superstructures. As shown in **figure 4**, *L*-$TBA_{1.0}DA_{1.5}$Zn(II) and *L*-$TBA_{1.0}DA_{1.5}$Cd(II) self-assembled into nano-sized wire structures, with diameters of about 140 nm and 100 nm, respectively. However, Co(II) complex with *L*-$TBA_{1.0}DA_{1.5}$ self-assembled into tubule structure with external and internal diameters of about

160 nm and 50 nm, respectively.

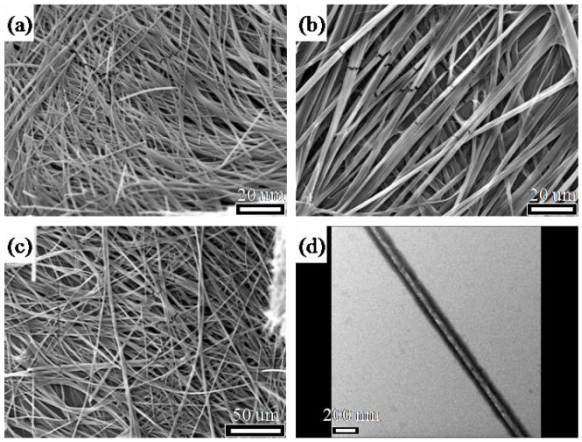

Figure 4. SEM images of (a) *L*-$TBA_{1.0}DA_{1.5}$Zn(II), (b) *L*-$TBA_{1.0}DA_{1.5}$Cd(II), and (c) *L*-$TBA_{1.0}DA_{1.5}$Co(II). (d) EF-TEM image of *L*-$TBA_{1.0}DA_{1.5}$Co(II) shows a hollow shape.

On the other hand, metal ion complex with *rac*-TBA_xDA_y exhibited different superstructures. SEM images revealed that the Cd(II) complexes with *rac*-$TBA_{1.0}DA_{1.0}$ and *rac*-$TBA_{1.0}DA_{1.5}$ had plate-like superstructure (**Figure 5**), while *rac*-$TBA_{1.0}DA_{1.0}$ and *rac*-$TBA_{1.0}DA_{1.5}$ showed wire and tubule structure, respectively (**Figure 2**). Zn(II) and Co(II) complexes with *rac*-$TBA_{1.0}DA_{1.0}$ and *rac*-$TBA_{1.0}DA_{1.5}$ did not form ordered superstructures.

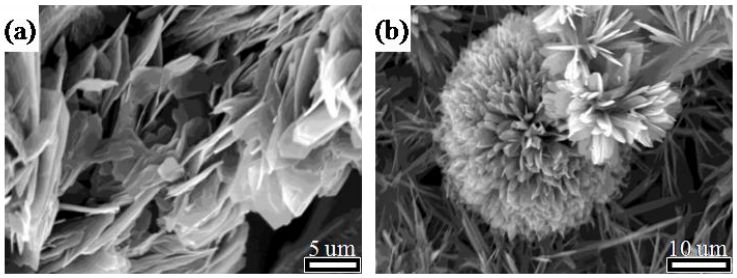

Figure 5. SEM images of Cd(II) complexes of (a) *rac*-$TBA_{1.0}DA_{1.0}$Cd(II) and (b) *rac*-$TBA_{1.0}DA_{1.5}$Cd(II).

Fourier transform infrared (FT-IR) spectroscopic analysis was employed to provide better insight into the self-assembled structures of the xerogels and the dried precipitates of the TBA_xDA_y aggregates. The FT-IR spectra of *L*- and *rac*-$TBA_{1.0}DA_{2.0}$ only showed two absorptions at 1611 and 1395 cm^{-1} corresponding to the typical asymmetrical and symmetrical stretching vibrations of the carboxylate, but didn`t show absorptions of the carboxylic acid (**Figure 6a**). These absorption spectra indicate that all carboxylic acids in *L*- and *rac*-$TBA_{1.0}DA_{2.0}$ are fully deprotonated during the self-assembling process. However, the absorption spectrum of *L*- and *rac*-$TBA_{1.0}DA_{1.0}$ showed three absorptions at 1743, 1603, and 1399 cm^{-1}. The absorption at 1743 cm^{-1} corresponds to the carboxylic acid stretching vibration and the absorption at 1603 and 1399 cm^{-1} correspond to the carboxylate stretching vibration. Therefore, the absorption spectra of *L*-$TBA_{1.0}DA_{1.0}$ indicate that both carboxylic acid and carboxylate ion moieties coexist in the complex during the self-assembling process. All complexes have absorptions corresponding to CH_2 asymmetrical and symmetrical stretching vibrations at 2918–2923 and 2850–2851 cm^{-1}, respectively. These CH_2 stretching absorptions signify that part of the hydrocarbon chains of DA have *gauche*-conformation in self-assembled structures, which indicates that the hydrocarbon chains are arrayed in a disordered state.[13]

There was no significant change in the carbonyl absorption bands of the carboxylic acids upon changing the chirality of H_2TBA. However, the absorption bands of the amide N-H stretching and amide I in *L*-TBA_xDA_y showed a slight shift to a lower wavenumber compared to *rac*-TBA_xDA_y, which means that *L*-TBA_xDA_y forms stronger intermolecular hydrogen-

bonding networks than *rac*-TBA_xDA_y (**Figure 6b**). The CH_2 asymmetrical and symmetrical stretching vibrations of *rac*-$TBA_{1.0}DA_{1.0}$ are almost the same as those of *L*-$TBA_{1.0}DA_{1.0}$. On the other hand, the CH_2 asymmetrical and symmetrical stretching vibrations of *rac*-$TBA_{1.0}DA_{2.0}$ shifted to lower wavenumbers, 2918 and 2850 cm^{-1}, than *L*-$TBA_{1.0}DA_{2.0}$. This indicates that the hydrocarbon chains in the self-assembled structure of *rac*-$TBA_{1.0}DA_{2.0}$ aggregates have more crystalline conformation when compared to the *L*-complex

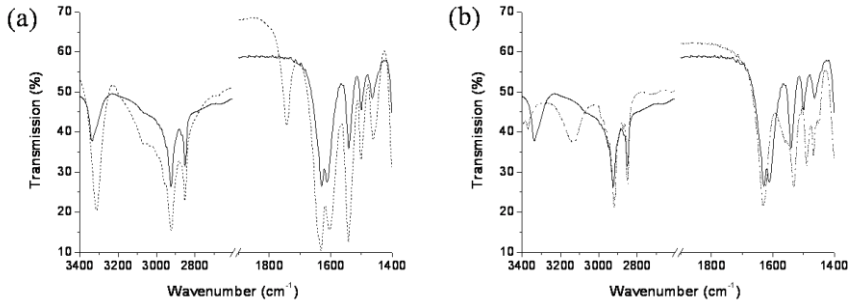

Figure 6. (a) FT-IR spectra of *L*-$TBA_{1.0}DA_{1.0}$ (dashed line) and *L*-$TBA_{1.0}DA_{2.0}$ (solid line). (b) FT-IR spectra of *L*-$TBA_{1.0}DA_{2.0}$ (solid line) and *rac*-$TBA_{1.0}DA_{2.0}$ (dashed dot line).

We performed powder X-ray diffraction (XRD) analysis on the dried samples of *L*-TBA_xDA_y, *rac*-TBA_xDA_y and *L*-$TBA_{1.0}DA_{1.0}$M(II) to obtain more information on the aggregation patterns in the two- and three-component systems. Diffraction pattern of $TBA_{1.0}DA_{1.0}$ showed three similar intense peaks in the small angle region, irrespective of the chirality (**Figure 13a, b**). These diffraction patterns indicate that both *L*- and *rac*-$TBA_{1.0}DA_{1.0}$ self-assembled into superstructures having monoclinic unit cell structures and that changing the chirality has little influence on the unit cell parameters (**Table 2**).

These results were also supported by the fact that *L*- and *rac*-$TBA_{1.0}DA_{1.0}$ have the same fibrous superstructure. However, $TBA_{1.0}DA_{2.0}$ showed distinct changes, not only in the diffraction pattern (**Figure 13c, d**), but also in EM images (**Figure 1**). Unlike $TBA_{1.0}DA_{1.0}$, ribbon-like superstructure of *L*- and *rac*-$TBA_{1.0}DA_{2.0}$ aggregate had different unit cell structure. When *rac*-H_2TBA was replaced by *L*-H_2TBA, the unit cell structure of $TBA_{1.0}DA_{2.0}$ aggregate changed from lamellar to columnar (**Table 2**). Close packing aggregation of *L*-$TBA_{1.0}DA_{2.0}$ due to stronger intermolecular hydrogen-bonding interactions promoted a one-directional self-assembling process. As a result, *L*-$TBA_{1.0}DA_{2.0}$ was able to self-assemble into a helical ribbon structure (**Figure 1a**). Interestingly, the diffraction pattern of *rac*-$TBA_{1.0}DA_{1.5}$ aggregates showed peaks from *rac*-$TBA_{1.0}DA_{1.0}$ and *rac*-$TBA_{1.0}DA_{2.0}$ (**Figure 7**). The mixed diffraction pattern revealed that both the monoclinic unit cell structure from *rac*-$TBA_{1.0}DA_{1.0}$ and the lamellar unit cell structure from *rac*-$TBA_{1.0}DA_{2.0}$ coexisted in one self-assembled structure. However, the two unit cell structures did not develop individually into original self-assembled structures, but participated in the self-assembly process to make one superstructure.

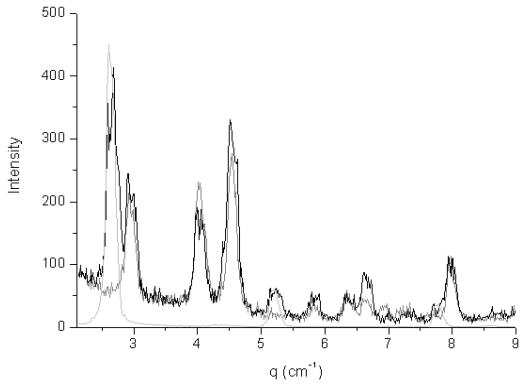

Figure 7. Overlapped X-ray diffraction patterns of *rac*-$TBA_{1.0}DA_{1.5}$ (black),

rac-$TBA_{1.0}DA_{1.0}$ (gray), and *rac*-$TBA_{1.0}DA_{2.0}$ (light grey).

To study the influence of metal ion on the self-assembled structures in the three-component system, X-ray diffraction patterns of Zn(II), Cd(II), and Co(II) complex with *L*-$TBA_{1.0}DA_{1.0}$ were compared to their non-metal complex. All the *L*-$TBA_{1.0}DA_{1.0}$M(II) aggregates had monoclinic unit cell structures like their non-metal complex. However, *L*-$TBA_{1.0}DA_{1.0}$M(II) aggregates had different unit cell parameters. The β value of the unit cell showed a gradual increase upon the respective addition of Zn(II), Cd(II), and Co(II) to *L*-$TBA_{1.0}DA_{1.0}$ (**Table 2**). Metal-TBA interaction did not influence the interaction between TBA and DA, which was reflected in the same unit cell structures of both $TBA_{1.0}DA_{1.0}$ and $TBA_{1.0}DA_{1.0}$M(II). However, different coordination geometry of metal ions should give rise to changes in unit cell parameters, which would cause different self-assembled superstructures.[14] Shimizu *et al.* also mentioned that the coordination geometry of metal ions induced morphological change in self-assembled structures.[10b]

Table 2. Unit cell structure and parameters of TBA_xDA_y and TBA_xDA_yM(II).

Composition	**a (Å)**	**b (Å)**	**c (Å)**	**α (°)**	**β (°)**	**γ (°)**	**unit cell structure**
L-$TBA_{1.0}DA_{1.0}$	16.21	14.11	24.86	90.00	60.50	90.00	Monoclinic
L-$TBA_{1.0}DA_{2.0}$	14.50	14.50				97.20	Columnar
rac-$TBA_{1.0}DA_{1.0}$	15.90	13.84	24.62	90.0	60.50	90.00	Monoclinic
rac-$TBA_{1.0}DA_{2.0}$	24.12						Lamellar
L-$TBA_{1.0}DA_{1.0}$Zn(II)	33.50	21.22	27.87	90.00	49.60	90.00	Monoclinic
L-$TBA_{1.0}DA_{1.0}$Cd(II)	32.91	25.96	26.39	90.00	52.10	90.00	Monoclinic
L-$TBA_{1.0}DA_{1.0}$Co(II)	30.12	26.59	28.40	90.00	62.00	90.00	Monoclinic

1.3. Conclusion

We have suggested a simple way to fabricate nano- or micro-sized superstructures using non-covalent interactions. Various superstructures were constructed by self-assembly of a simple amino acid derivative and aliphatic amine. The incorporation of metal ions into the mixtures of H_2TBA−DA resulted in a variety of new self-assembled superstructures, such as nano- and micro-structures. The diversity of superstructures resulting from the addition of metal ion might be due to different coordination numbers, geometry, and binding affinities of the metal ions. These differences can induce dramatic changes in the basic building blocks themselves and, eventually, in the aggregation mode. This method can be applied to the fabrication of various conducting nano-materials or to organic templates for inorganic nanostructures.

1.4. Experimental

1.4.1. Instrumentation

^{1}H and ^{13}C NMR spectra were measured on a Bruker Advance DPX-300 or a Bruker Advance 500 spectrometer. The XWINNMR program was used for the pulse program. Chemical shifts are reported as parts per million (δ) and referenced to residual solvent peak (δ 2.50 for DMSO and 7.27 for $CDCl_3$). ^{13}C NMR chemical shifts: δ = 39.51 ppm for DMSO. The GC-MS was obtained with a JEOL JMS-AX505WA and HP 5890 Series II, using the FAB method. Scanning electron microscope (SEM) images were obtained with a JEOL-JSM 5410LV. Energy-filtering electron microscope (EF-TEM)

images were obtained with a Carl Zeiss-LIBRA 120. FT-IR spectra was obtained with a JASCO FT/IR-660 plus. Powder X-ray diffraction analysis was performed with a Bruker D5005.

1.4.2. Materials

All reagents were purchased from either sigma-aldrich or TCI and used without any further purification. Deuterated solvents were acquired from cambridge isotopic laboratories. All anion salts were purchased from Aldrich or TCI.

1.4.3. Preparation of Self-assembled Samples

H_2TBA and DA were mixed in MeOH in various ratios. The suspensions were heated or sonicated until they turned into a clear solution. Then, the MeOH solution was evaporated in a vacuum until white solid was generated. Two-component amphiphilic complexes were prepared by suspending the resulting white solid (TBA_xDA_y) (10 mg) in deionized water (500 uL). The suspension was heated until clear, followed by cooling and incubating at room temperature until it turned into either a gel or insoluble solid. Three-component amphiphilic complexes were prepared by suspending TBA_xDA_y (10 mg) in deionized water (500 uL) containing 1 equiv. of $M(NO_3)_2 \cdot xH_2O$ (M = Zn, Cd, Co, Cu). The suspension was heated until clear, followed by cooling and incubating at room temperature until it turned into either a gel or insoluble solid.

1.4.4. Preparation of Electroscope Specimen and Their Images

For SEM imaging of the two- or three-component systems, the gels or

precipitates were diluted with deionized water (500 uL). The diluted suspensions were dropped onto slide glass, and then air-dried. The prepared specimens were coated with Au. For TEM imaging of the two- or three-component systems, gels or precipitates were diluted with deionized water (4.5 mL). The diluted suspensions were dropped onto a carbon grid, and then air-dried. TEM images were obtained without staining.

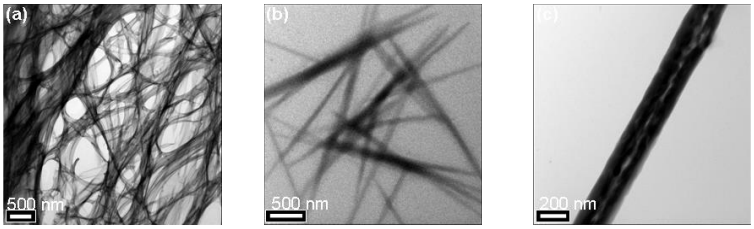

Figure 8. EF-TEM images of (a) a 1:1 mixture of *L*-H_2TBA−DA, (b) a 1:1 mixture of *rac*-H_2TBA−DA, and (c) a 1:1.5 mixture of *rac*-H_2TBA−DA.

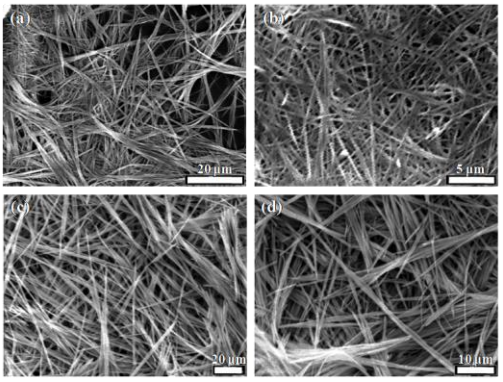

Figure 9. SEM images of H_2TBAenriched complex. (a) a *L*-$TBA_{1.5}DA_{1.0}$ and (b) *rac*-$TBA_{1.5}DA_{1.0}$. (c) a *L*-$TBA_{2.0}DA_{1.0}$ and (d) *rac*-$TBA_{2.0}DA_{1.0}$.

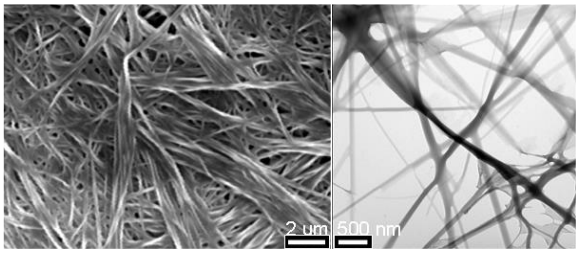

Figure 10. SEM (left) and EF-TEM (right) image of 1:1:1 mixtures of Zn(II)−*L*-H_2TBA−DA.

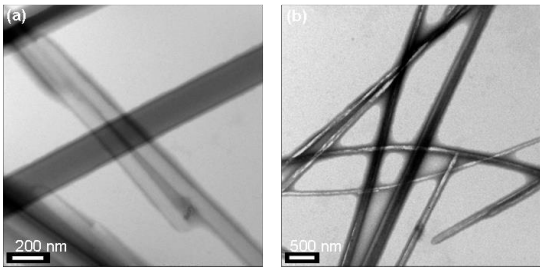

Figure 11. EF-TEM images of (a) 1:1:1 mixture of Co(II)−*L*-H_2TBA−DA and (b) 1:1:1.5 mixture of Co(II)−*L*-H_2TBA−DA.

1.4.5. Preparation of FT-IR Specimens and Their Spectrum

To obtain FT-IR spectra, the gels or precipitates were dried at room temperature. The dried samples and KBr were mixed and the mixtures ground to form a fine powder. Using the powder, a KBr and gel-containing pallet was prepared.

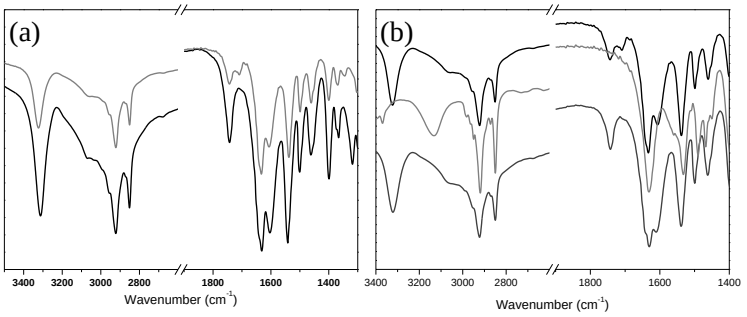

Figure 12. (a) Absorption spectra of a *L*-$TBA_{1.0}DA_{1.0}$ (red line) and *rac*-$TBA_{1.0}DA_{1.0}$ (black line). (b) Absorption spectra of *rac*-TBA_xDA_y. Black line is a *rac*-$TBA_{1.0}DA_{1.0}$, blue line is *rac*-$TBA_{1.0}DA_{1.5}$, and purple line is *rac*-$TBA_{1.0}DA_{2.0}$.

1.4.6. Preparation of X-ray Diffraction Specimens and Their Diffraction Patterns

To obtain X-ray diffraction patterns, the gels or precipitates were dried at room temperature. The dried samples were analyzed with a Bruker D5005. The diffraction radius was 2θ=3–13°, the step size was 0.02, and the scan speed was 1 deg/min. Wavelength of the X-ray was 1.5406 Å (the generator was 40 kV, and 40 mA).

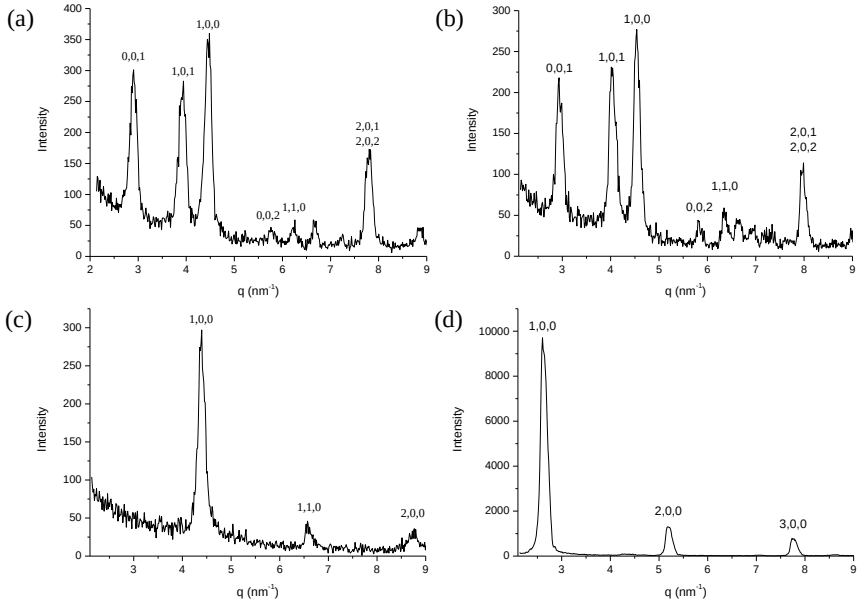

Figure 13. X-ray diffraction patterns at q=2.0~9.0 cm^{-1}. Diffraction pattern of a) *L*–$TBA_{1.0}DA_{1.0}$, b) *rac*–$TBA_{1.0}DA_{1.0}$, c) *L*–$TBA_{1.0}DA_{2.0}$, and d) *rac*–$TBA_{1.0}DA_{2.0}$.

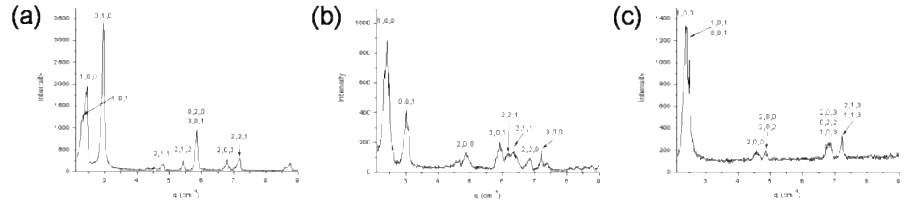

Figure 14. X-ray diffraction pattern of (a) a *L*-$TBA_{1.0}DA_{1.0}Zn(II)$, (b) *L*-$TBA_{1.0}DA_{1.0}Cd(II)$, and (c) *L*-$TBA_{1.0}DA_{1.0}Co(II)$ at q=2.0~9.0 cm^{-1}.

1.4.7. Synthesis of H_2TBA Component

Synthesis of H_2TBA

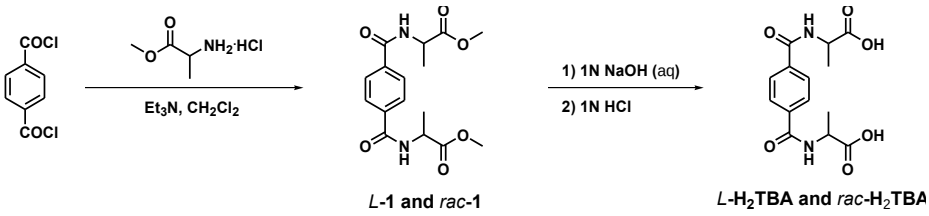

Terephthaloyl bisalanine methyl ester *L*(or *rac*)**-1** (*L*- and *rac*-Me_2TBA)**:** terephthaloyl chloride (2.37 g, 11.7 mmol) and *L(or rac)*-alanine methyl ester hydrochloride (3.06 g, 21.9 mmol) was suspended in 150 mL of CH_2Cl_2 under N_2 atmosphere at 0℃. To the mixture, triethylamine (6 mL, 43.0 mmol) was carefully added, and then stirred for 3 hrs at room temperature. The reaction mixture was washed 3 times with H_2O. The organic residues were dried over Na_2SO_4 and evaporated to give pale yellow solids. The crude *L*(or *rac*)-**1** was purified by recrystallization with CH_2Cl_2 and hexane to give rise to white solids (1.0774 g, 29.5 % yield).

^1H NMR (300 MHz, $CDCl_3$) *L*-**1**: 1.57 (6H, d, *J* = 7.14 Hz), 3.83 (6H, s), 4.83 (2H, m), 6.79 (2H, d, *J* = 6.64 Hz), 7.90 (4H, s).

^{1}H NMR (300 MHz, $CDCl_3$) *rac*-**1**: 1.57 (6H, d, *J* = 7.14 Hz), 3.83 (6H, s), 4.83 (2H, m), 6.79 (2H, d, *J* = 6.64 Hz), 7.90 (4H, s).

Terephthaloyl bisalanine *L*(or *rac*)-**H_2TBA:** To a solution of *L*(or *rac*)-**1** (1.0774 g, 3.20 mmol) in 10 mL EtOH, 30 mL 1 N aq. NaOH was added, and then stirred for 3 hr at room temperature. After EtOH was evaporated, the aqueous residue was acidified with 1 N HCl at pH 1. Crude **H_2TBA** was purified by recrystallization in acidic aqueous condition to give rise white solids.

^{1}H NMR (300 MHz, DMSO-d_6) *L*-**H_2TBA**: 1.41 (6H, d, *J* = 7.35 Hz), 4.44 (2H, m), 7.97 (4H, s), 8.80 (2H, d, *J* = 7.17 Hz), 12.72 (2H, bs).

^{1}H NMR (300 MHz, DMSO-d_6) *rac*-**H_2TBA**: 1.41 (6H, d, *J* = 7.35 Hz), 4.44 (2H, m), 7.97 (4H, s), 8.80 (2H, d, *J* = 7.17 Hz), 12.70 (2H, bs).

^{13}C NMR (75 MHz, DMSO-d_6) *L*-**H_2TBA**: 17.338, 48.697, 127.828, 136.723, 165.908, 174.541

^{13}C NMR (75 MHz, DMSO-d_6) *rac*-**H_2TBA**: 17.338, 48.697, 127.828, 136.723, 165.908, 174.541

HR-MS (FAB+) *L*-**H_2TBA**: calculated ($C_{14}H_{17}N_2O_6$) = 309.1087, found = 309.1086.

HR-MS (FAB+) *rac*-H_2**TBA**: calculated ($C_{14}H_{17}N_2O_6$) = 309.1087, found = 309.1086.

1.5. References and Notes

Donghak Jang, Ho Yong Lee, Miae Park, Seong Ryong Nam and Jong-In Hong, *Chem. Eur. J.* **2010**, *16*, 4836-4842.

1. Comprehensive reviews: (a) Rye, J.-H.; Hong, D.-J.; Lee, M. *Chem. Commun.* **2008**, 1043. (b) Shimizu, T.; Masuda, M.; Minamikawa, H. *Chem.*

Rev. **2005**, *105*, 1401. (c) Hoeben, F. J. M.; Jonkheijm, P.; Meijer, E. W.; Schening, A. P. H. J. *Chem. Rev.* **2005**, *105*, 1491. (d) Ulijn, R. V.; Smith, A. M. *Chem. Soc. Rev.* **2008**, *37*, 664. (e) Zhao, X.; Zhang, S. *Chem. Soc. Rev.* **2006**, *35*, 1105.

2. (a) Hartgerink, J. D.; Beniash, E.; Stupp, S. I. *Science*, **2001**, *294*, 1684. (b) Lim, Y. –B.; Lee, E.; Lee, M. *Angew. Chem. Int. Ed.* **2007**, *46*, 9011.
3. (a) Jung, J. H.; John, G.; Yoshida, K.; Shimizu, T. *J. Am. Chem. Soc.* **2002**, *124*, 10674. (b) Bhattacharya, S.; Acharya, S. N. G. *Chem. Mater.* **1999**, *11*, 3504.
4. (a) Zhang, J.; Song, Y.–F.; Cronin, L.; Liu, T. *J. Am. Chem. Soc.* **2008**, *130*, 14408. (b) Shirakawa, M.; Fujita, N.; Tani, T.; Kaneko, K.; Ojima, M.; Fujii, A.; Ozaki, M.; Shinkai, S. *Chem. Eur. J.* **2007**, *13*, 4155.
5. (a) Geiger, C.; Stanesau, M.; Chen, L.; Whitten, D. G. *Langmuir* **1999**, *15*, 2241. (b) Sangeetha, N. M.; Maitra, U. *Chem. Soc. Rev.* **2005**, *34*, 821. (c) Lin, Y. –C.; Kachar, B.; Weiss, R. G. *J. Am. Chem. Soc.* **1989**, *111*, 5542.
6. (a) Jang, W. D.; Jiang, D. L.; Aida, T. *J. Am. Chem. Soc.* **2000**, *122*, 3232. (b) Gröhn, F.; Klein, K.; Brand, S. *Chem. Eur. J.* **2008**, *14*, 6866.
7. (a) Kim, H.–J.; Lee, J.; Kim, T.–H.; Lee, T. S.; Kim, J. *Adv. Mater.* **2008**, *20*, 1117. (b) Kim, J.–K.; Lee, E.; Lim, Y.–B.; Lee, M. *Angew. Chem. Int. Ed.* **2008**, *47*, 4662. (c) Che, Y.; Datar, A.; Balakrishnan, K.; Zhang, L. *J. Am. Chem. Soc.* **2007**, *129*, 7234. (d) Hill, J. P.; Jin, W.; Kosaka, A.; Fukushima, T.; Ichihara, H.; Shimomura, T.; Ito, K.; Hashizume, T.; Ishii, N.; Aida, T. *Science*, **2004**, *304*, 1481. (e) Diegelmann, S. R.; Gorham, J. M.; Tovar, J. D. *J. Am. Chem. Soc.* **2008**, *130*, 13840.
8. (a) Hanabusa, K.; Miki, T.; Taguchi, Y.; Koyama, T.; Shirai, H. *J. Chem. Soc. Chem. Commun.* **1993**, 1382. (b) Fuhrhop, J. H.; Schneider, P.; Rosenberg, J.; Boekema, E. *J. Am. Chem. Soc.* **1987**, *109*, 3387. (c) Oda, R.; Huc, I.; Candau, S. J. *Angew. Chem. Int. Ed.* **1998**, *37*, 2689. (d) Lee, H. Y.; Nam, S. R.; Hong, J.-I. *J. Am. Chem. Soc.* **2007**, *129*, 1040. (e) Basit, H.; Pal, A.; Sen, S.; Bhattacharya, S. *Chem. Eur. J.* **2008**, *14*, 6534. (f) Zemb, T.; Dubois, M.; Deme, B.; Gulik-Krzywicki, T. *Science*, **1999**, *283*, 816.
9 (a) Oh, M.; Mirkin, C. A. *Nature*, **2005**, *438*, 651. (b) Maeda, H.; Hasegawa,

M.; Hashimoto, T.; Kakimoto, T.; Nishio, S.; Nakanishi, T. *J. Am. Chem. Soc.* **2006**, *128*, 10024. (c) Richard, A.; Marchi-Artzner, V.; Lalloz, M.-N.; Brienne, M.-J.; Artzner, F.; Gulik-Krzywicki, T.; Guedeau-Boudeville, M.-A.; Lehn, J.-M. *Proc. Natl. Acad. Sci. USA* **2004**, *101*, 15279. (d) Mart, R. J.; Liem, K. P.; Wang, X.; Webb, S. J. *J. Am. Chem. Soc.* **2006**, *128*, 14462.

10 (a) Shen, X.-F.; Yan, X.-P. *Angew. Chem. Int. Ed.* **2007**, *46*, 7659. (b) Kogiso, M.; Zhou, Y.; Shimizu, T. *Adv. Mater.* **2007**, *19*, 242. (c) Zhou, Y.; Kogiso, M.; He, C.; Shimizu, Y.; Koshizaki, N.; Shimizu, T. *Adv. Mater.* **2007**, *19*, 1055.

11 See the Experimental Section for the details of preparation and characterization.

12 (a) Gulik-Krzywicki, T.; Fouquey, C.; Lehn, J.-M. *Proc. Acad. Sci. U.S.A.* **1993**, *90*, 163. (b) Spector, M. S.; Selinger, J. V.; Singh, A.; Rodriguez, J. M.; Price, R. R.; Schnur, J. M. *Langmuir*, **1998**, *14*, 3493. (c) Thomas, B. N.; Lindemann, C. M.; Corcoran, R. C.; Cotant, C. L.; Kirsch, J. E.; Persichini, P. J. *J. Am. Chem. Soc.* **2002**, *124*, 1227. (d) Kim, H.-J.; Moon, D.; Lah, M. S.; Hong, J.-I. *Angew. Chem. Int. Ed.* **2002**, *41*, 3174.

13 Brizard, A.; Aimé, C.; Labrot, T.; Huc, I.; Berthier, D.; Artzner, F.; Debat, B.; Oda. R. *J. Am. Chem. Soc.* **2007**, *129*, 3754.

14 Lee, H. Y.; Park, J.; Lah, M. S.; Hong, J.-I. *Crystal Growth & Design*, **2008**, *8*, 587.

Section 2.
Effect of Solvent Polarity on Self-assembly of Hairpin Amphiphiles

2.1. Introduction

Ethylene glycol (=EG) subunit is widely used functional group for catalysts and chemical sensors. In particular, cyclic oligo (ethylene glycol), known as crown ether, is able to form complex with various metal cations.[1] Selectivity of binding ability in crown ether uses oxygen atoms such as nitrogen and sulphur.[2] The binding behavior with metal cation can induce conformation change of tethering groups in noncyclic crown ether.[3] The binding inherence of cyclic and non-cyclic EG subunit is cause for the popularity of ionophores and chemical sensors

Another characteristic feature of EG is hydrophilicity. Introducing the hydrophilic EG moiety is made hydrophilic dye or π-conjugated materials to soluble in polar solvent.[4] In particular, when EG oligomer is attached to hydrophobic segment, the compound can have amphiphilic features and self-assemble into various supramolecular architectures.[5] An occupied volume of EG oligomer on outside of assembly is able to change by

hydration/dehydration and the variation of ethylene glycol monomers.[6] Such occupied volume changes can be induced by the change in morphology of self-assembled architectures.

"Gemini amphiphiles (GP)" are made from two monomeric amphiphiles connected by a spacer between polar head groups.[7] Compared to conventional monomeric amphiphiles, the GP has characteristic features such as a low critical micelle concentration (CMC),[8] a tunable self-assembling process, and biocompatibility for gene delivery.[9] In particular, when the rigidity, length, and hydrophilic of the linker are changed, a GP is able to exhibit a different self-assembling behavior.[10] In this study, we introduced an oligo (ethylene glycol) moiety as a linker in GPs. We demonstrate the self-assemble of the GPs into various supramolecular architectures by changing several of oligo(ethylene glycol) linker and solvent polarity.

2.2. Results and Discussion

Oligo (ethylene oxide) bridged hairpin-amphiphiles (=EG_nA) were simply obtained from the reaction between (ethylene glycosyl) ditosylate, *N*-Boc-4-hydroxyaniline and dodecanoyl chloride (**Scheme 1**). From the hydrogen bonding interaction between amide moieties, the EG_nA pre-organize to a hairpin shape conformation in solution. The EG_nA may have specific self-assembling behavior like that of gemini amphiphile. Due to these characteristic features, the self-assembling process of the EG_nA influences external stimuli, such as solvent polarity and molecular volume of ethylene glycol moiety.

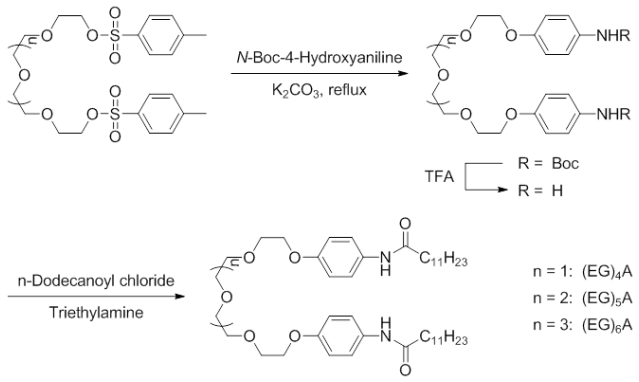

Scheme 1. Molecular structures and preparation of oligo(ethylene glycol) containing hairpin amphiphiles EG_nA.

To verify the influence of solvent polarity, self-assembling behavior of EG_nA was tested for both non-polar and polar solvent, such as *n*-hexane, toluene, CCl_4, *n*-propanol, THF and acetonitrile. An appropriate amount of EG_nA was suspended into the proper solvent, and then the suspended solution was heated to form a clear solution. These clear solutions were left at room temperature until a precipitate was formed, with the exception of the self-assembly of EG_4A and CCl_4 condition, where a gel was formed. Most of the EG_nA suspensions turned into an opaque gel or a precipitate within one day. The self-assembling behaviors of EG_nA at each solvent are listed in **table 1**.

Table 1. Self-assembling behavior of EG_nA in various organic solvent.[a)]

Solvent	**EG_4A**	**EG_5A**	**EG_6A**
n-Hexane	P[b)]	P	P
CCl_4	G[c)]	P	P
Toluene	P	P	P
n-Propanol	P	P	P

THF	P	P	S[d)]
Acetonitrile	P	P	P

a) All self-assembling behaviors of the EG_nA were tested at 1 wt% concentration in each solvent.

b) P=precipitate; c) G=gel; d) S=soluble.

To confirm the self-assembled structures of EG_nA, we applied scanning electron microscopy (SEM) analysis. According to SEM images, EG_4A•nHex and EG_6A•nHex self-assembled into precipitate with fibrous structures (**Figure 1**). However, for the case of EG_5A, the self-assembling process resulted in a precipitate with a flat-ribbon like structure. While EG_4A•CCl_4 was able to form a gel with a fibrous structure, the self-assembly of EG_5A and EG_6A result in the same morphology and structure as with other non-polar solvents, such as toluene and CCl_4.

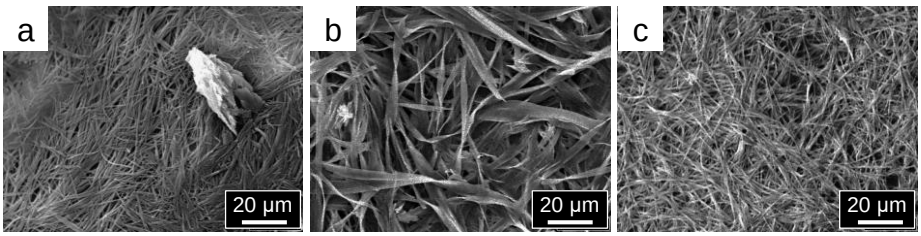

Figure 1. SEM images of (a) EG_4A•nHex, (b) EG_5A•nHex and (c) EG_6A•nHex self-assembly. EG_4A and EG_6A self-assembled into fibrous structure. However, EG_5A self-assembled into ribbon-like structure.

To study the influence of solvent polarity on self-assembling behaviors, we observed the self-assemblies of EG_nA in *n*-PrOH, THF and MeCN. According to the SEM analysis (**Figure 2**), the self-assemblies of EG_4A•nPrOH encompass only fibrous structures. On the other hand,

EG_5A•nPrOH and EG_6A•nPrOH could self-assemble into flat-sheet like structures. We also tested the self-assembling process of EG_nA with non-alcoholic polar solvents, such as THF and MeCN. While EG_6A is completely dissolved and does not show any self-assembled structure in THF, self-assembly in other solvent is able to self-assemble into precipitate with flat ribbon-like structure.

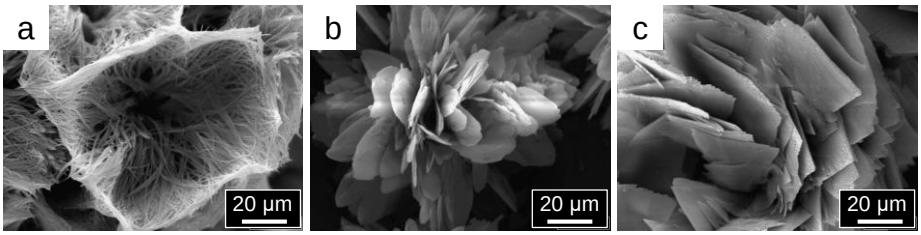

Figure 2. SEM images of (a) EG_4A•nPrOH, (b) EG_5A•nPrOH and (c) EG_6A•nPrOH self-assemblies. EG_4A self-assembled into fibrous structure. However, EG_5A and EG_5A self-assembled into flat-ribbon like structure.

We carried out X-ray diffraction (XRD) analysis for EG_nA•sol to obtain more information on aggregation. The diffraction spectrum of EG_nA•nHex showed two intense peaks at 2.32° and 3.97° (**Figure 3**). It is indicated that EG_nA•nHex self-assembled into fibrous and ribbon structure, with specific hexagonal unit cell structure. On the other hand, the diffraction spectrum of EG_nA•nHex showed diffraction patterns within wide angle regions with the length of ethylene glycol. While EG_4A•nHex and EG_6A•nHex could self-assemble into fibrous structure with typical hexagonal diffraction pattern, the self-assembly of EG_5A•nHex showed two intense peaks at 12-20°. This means that EG_4A•nHex self-assembled into ribbon-like structure with distorted hexagonal pattern. For the case of EG_nA•nPrOH, we also can obtain similar XRD pattern to that of EG_nA•nHex. Clearly, the XRD spectra of

EG_5A•nPrOH only exhibits two intense peaks at 12-20°, as with EG_5A•nHex. Self-assembly of EG_4A•nPrOH and EG_6A•nPrOH have hexagonal patterns that are more complicated than the self-assemblies in *n*-hexane. This shows that the self-assemblies in *n*-propanol contain hydrophobic chains that are more flexible, and aggregate with distorted hexagonal unit cells.

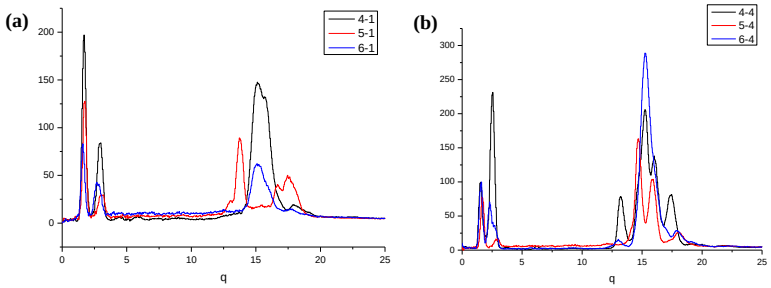

Figure 3. XRD spectra of EG_nA self-assembly in (a) *n*-hexane and (b) *n*-PrOH. EG_4A•sol (black line), EG_5A•sol (red line) and EG_6A•sol (blue line).

To gain insight into the different self-assembling behavior, we performed comparisons with the molecular structure of pre-organized EG_nA. As shown in **figure 4**, the hydrocarbon tails of EG_4A and EG_6A are stretched in parallel to each other. The small occupied volume of the hydrophobic section (rather than the hydrophilic section) can induce aggregation with the cylindrical micelle structure, resulting in fibrous self-assemblies. However, two hydrocarbon tails of EG_5A intersect each other, with a larger occupied volume. The large hydrophobic amphiphile self-assembles into bilayer structure, similar to ribbon structure.

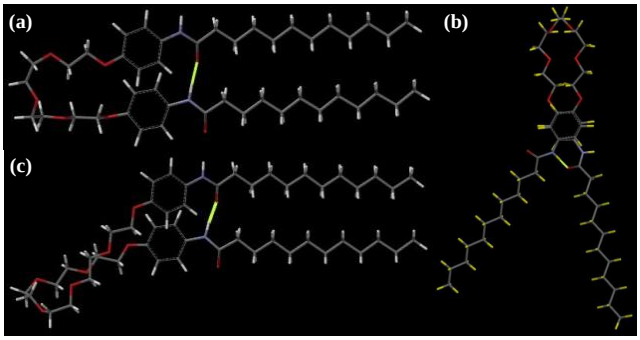

Figure 4. Molecular structures of pre-organized (a) EG_4A, (b) EG_5A and (c) EG_6A via hydrogen bonding interaction.

2.3. Conclusion

In conclusion, we prepared hairpin type EG_nA amphiphiles, which have an ethylene glycol linker between dodecanoyl benzene moieties. We observed their self-assembly into various structures. The self-assembled structure of EG_nA can be modulated by the length of the linker and solvent polarity. In non-polar systems, the self-assemblies could be controlled by the length of ethylene glycol linker. On the other hand, the self-assembling process of EG_nA in a polar solvent was determined by the spatial arrangement of hydrocarbon tails, decided by the hydrogen bonding interaction.

2.4. Experimental

2.4.1. Instrumentation

^{1}H and ^{13}C NMR spectra were measured on a Bruker Advance DPX-300 or a Bruker Advance 500 spectrometer. The XWINNMR program was used for the pulse program. Chemical shifts are reported as parts per million (δ) and referenced to residual solvent peak (δ 2.50 for DMSO and 7.27 for

$CDCl_3$). ^{13}C NMR chemical shifts: δ = 39.51 ppm for DMSO. The GC-MS was obtained with a JEOL JMS-AX505WA and HP 5890 Series II, using the FAB method. Scanning electron microscope (SEM) images were obtained with a JEOL-JSM 5410LV. FT-IR spectra were obtained with a JASCO FT/IR-660 plus. X-ray diffraction analysis was performed with a Bruker D5005.

2.4.2. Materials

All reagents were purchased from either sigma-aldrich or TCI and used without any further purification. Deuterated solvents were acquired from Cambridge Isotopic Laboratories. All anion salts were purchased from sigma-aldrich or TCI.

2.4.3. Preparation of Self-assembled Samples

The hairpin amphiphiles, EG_nA, samples were prepared by suspending the amphiphile (5 mg) in proper solvent (500 uL). The suspension was heated until clear, followed by cooling and incubating at room temperature until it turned into either a gel or insoluble solid.

2.4.4. Preparation of Electromicroscope Specimens and Their Images.

For SEM imaging of self-assemblies of EG_nA, the gels or precipitates were dropped onto slide glass, and then air-dried. The prepared specimen was coated with Au.

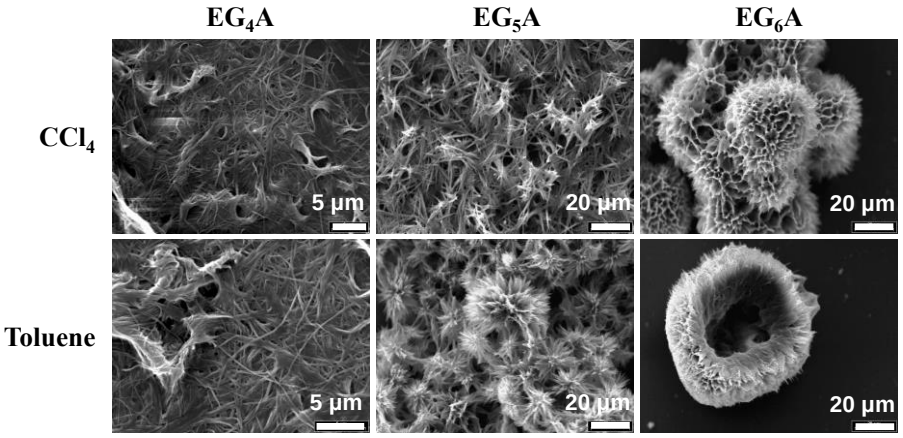

Figure 5. SEM images of EG_nA•CCl_4 and EG_nA•Tol self-assemblies.

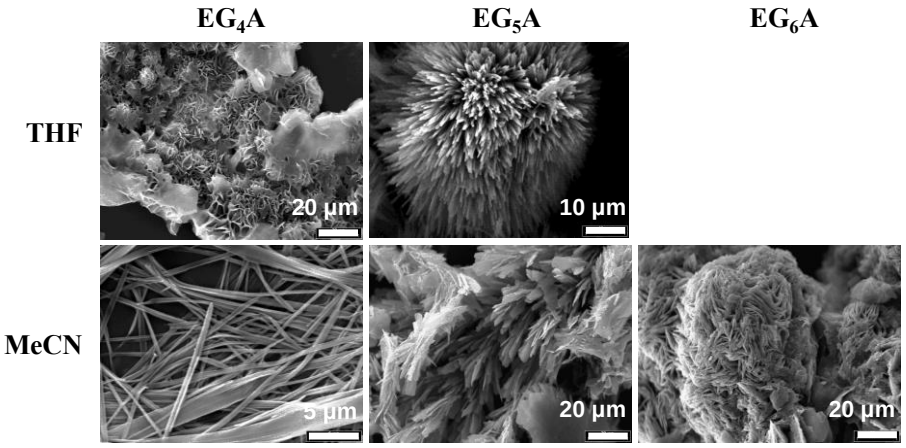

Figure 6. SEM images of EG_nA•THF and EG_nA•MeCN self-assemblies.

2.4.5. Synthesis of EG_nA

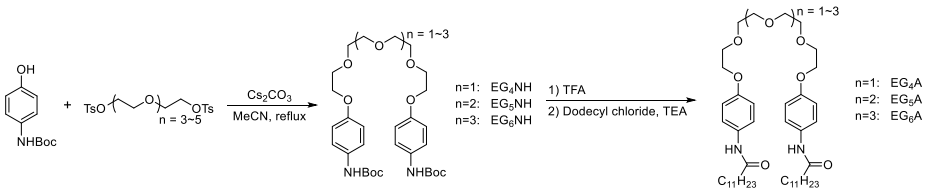

Figure 7. Preparation of hairpin amphiphile EG_nA.

Tetraethylene glycol di(*N*-Boc-4-aminophenolate) (EG_4NH): Tetraethylene glycol ditosylate (0.39 g, 0.80 mmol), *N*-Boc-4-aminophenol (0.37 g, 1.78 mmol) and Cs_2CO_3 (1.16 g, 3.50 mmol) was mixed in 100 mL MeCN. The mixture was heated to reflux and stirred for 18 hrs. After cooling to room temperature, all volatiles was removed by evaporating in vacuo. The residue was dissolved in CH_2Cl_2, and then washed with 1N HCl (×2) and brine (×1). The organic layer was dried over Na_2SO_4 and evaporated to give white solids. The crude product was purified by SiO_2 column chromatography with mixture of CH_2Cl_2 and MeOH (50/1, v/v) as a eluent. **EG_5NH** and **EG_6NH** was obtained with same manner, except use pentaethylene gylcol ditosylate for **EG_5NH** and hexaethylen glycol ditosylate for **EG_6NH**.

^{1}H NMR (300 MHz, $CDCl_3$) **EG_4NH:** 1.53 (18H, s), 3.69-3.74 (8H, m), 3.83-3.85 (4H, t, *J*=5.18Hz), 4.08-4.13 (4H, t, *J*=5.11Hz), 6.36 (2H, bs), 6.87-6.84 (4H, d, *J*=9.00Hz), 7.24-7.27 (4H, d, *J*=8.95Hz);

EG_5NH: 1.53 (18H, s), 3.67-3.74 (12H, m), 3.83-3.86 (4H, t, *J*=4.89Hz), 4.08-4.12 (4H, t, *J*=4.88Hz), 6.36 (2H, bs), 6.84-6.87 (4H, m), 7.24-7.27 (4H, d, *J*=8.91Hz);

EG_6NH: 1.52 (18H, s), 3.65-3.74 (16H, m), 3.82-3.85 (4H, t, *J*=4.87Hz), 4.08-4.11 (4H, t, *J*=4.87Hz), 6.44 (2H, bs), 6.82-6.88 (4H, m), 7.24-7.27 (4H, d, *J*=8.85Hz).

EG_4A: Tetraethylene glycol di(*N*-Boc-4-aminophenolate) (**EG_4NH**) (0.88 g, 1.52 mmol) was dissolved in 10 mL of CH_2Cl_2, and then 5 mL TFA was added. The mixture was stirred until disappearing **EG_4NH** which was confirmed by TLC analysis at room temperature. After completing the deprotection, all

volatiles were removed by evaporating. The resulting residue was re-dissolved in 30 mL anhydrous THF. To the solution TEA (1.50 mL, 10.6 mmol) and *n*-dodecanoyl chloride (0.87 mL, 3.65 mmol) was added droppwise under ice-bath. Resulting suspension was slowly warmed to room temperature, and stirred overnight. After removing solvent, the residue was re-dissolved in CH_2Cl_2. The organic layer was washed with H_2O (×2) and brine (×1). The organic layer was dried over Na_2SO_4 and evaporated to give white solids. The crude **EG_4A** was purified by SiO_2 column chromatography with mixture of CH_2Cl_2 and MeOH (10/1, v/v) as a eluent. Other amphiphile **EG_5A** and **EG_6A** was obtained with same manner, except use **EG_5NH** for **EG_5A** and **EG_6NH** for **EG_6A**. **EG_4A** as white solids (0.512 g, 65.7 % yield).

^{1}H NMR (300 MHz, $CDCl_3$) **EG_4A:** 0.88-0.92 (6H, t, *J*=6.68Hz), 1.28 (32H, bs), 1.71-1.76 (4H, t, *J*=6.96Hz) 2.33-2.38 (4H, t, *J*=7.56Hz), 3.69-3.76 (8H, m), 3.84-3.87 (4H, t, *J*=4.83Hz), 4.07-4.11 (4H, t, *J*=4.80Hz), 6.81-6.85 (4H, d, *J*=8.89Hz), 7.24 (2H, bs), 7.34-7.37 (4H, d, *J*=8.87Hz); **EG_5A:** 0.88-0.92 (6H, t, *J*=6.42Hz), 1.28 (32H, bs), 1.71-1.76 (4H, t, *J*=6.96Hz) 2.32-2.36 (4H, t, *J*=7.60Hz), 3.68-3.72 (12H, m), 3.84-3.87 (4H, t, *J*=4.56Hz), 4.08-4.12 (4H, t, *J*=4.57Hz), 6.83-6.86 (4H, d, *J*=8.66Hz), 7.20 (2H, bs), 7.37-7.39 (4H, d, *J*=8.56Hz); **EG_6A:** 0.87-0.92 (6H, t, *J*=6.68Hz), 1.27 (32H, bs), 1.71-1.76 (4H, t, *J*=6.96Hz) 2.30-2.36 (4H, t, *J*=7.56Hz), 3.65-3.72 (16H, m), 3.82-3.85 (4H, t, *J*=4.83Hz), 4.08-4.11 (4H, t, *J*=4.82Hz), 6.83-6.86 (4H, d, *J*=8.91Hz), 7.32 (2H, bs), 7.38-7.41 (4H, d, *J*=8.93Hz);

^{13}C NMR (75 MHz, $CDCl_3$) **EG_4A**: 14.33, 22.90, 25.96, 29.56, 29.64, 29.73, 29.84, 29.85, 32.13, 37.85, 67.99, 69.95, 70.94, 71.01, 115.11, 122.11, 131.42, 155.78, 171.61; **EG_5A:** 14.34, 22.91, 25.96, 29.56, 29.63, 29.73, 29.84, 32.13, 37.88, 67.99, 69.98, 70.89, 71.07, 115.15, 121.98, 131.46, 155.75, 171.53;

EG_6A: 14.33, 22.90, 25.94, 29.55, 29.62, 29.72, 29.83, 29.84, 32.13, 37.88, 67.98, 69.99, 70.83, 70.88, 71.07, 115.17, 121.87, 131.53, 155.71, 171.49

HR-MS (FAB+) **EG_4A**: calculated ($C_{44}H_{72}N_2O_7$)=740.5340, found=741.5418. **EG_5A**: calculated ($C_{46}H_{76}N_2O_7$)=784.5602, found=785.5680. **EG_6A**: calculated ($C_{48}H_{80}N_2O_7$)=828.5864, found=829.5942.

2.5. References and Notes

1 (a) Farago, M. E. *Inorg. Chim. Acta*. 1977, *25*, 71. (b) Lowe, N. D.; Garner, C. D. *J. Chem. Soc. Daltan Trans.* **1993**, 2197. (c) Buschmann, H.-J.; Mutihac, R.-C.; Schollmeyer, E. *J. Solution Chem.* **2009**, *38*, 209. (d) Wei, W.; Xu, C.; Ren, J.; Xu, B.; Qu, X. *Chem. Commun.* **2012**, *48*, 1284.

2 (a) Kang, S. O.; Llinares, J. M.; Day, V. W.; Bowman-James, K. *Chem. Soc. Rev.* **2010**, *39*, 3980. (b) Reuter, K.; Buchner, M. R.; Thiele, G.; von Hänisch, C. *Inorg. Chem.* **2016**, *55*, 4441.

3 (a) Jung, S. H.; Kim, E.; Lee, S. J.; Lee, C. G.; Lee, J.-K.; Lee, S. S.; Jung, J. H. *Bull. Korean Chem. Soc.* **2008**, *29*, 1630. (b) Gandolfi, C.; Moitzi, C.; Schurtenberger, P.; Morgan, G. G.; Albrecht, M. *J. Am. Chem. Soc.* **2008**, *130*, 14434. (c) Guan, B.; Jiang, M.; Yang, X.; Liang, Q.; Chen, Y. *Soft Matter*, **2008**, *4*, 1393.

4 (a) Seo, S. H.; Chang, J. Y.; Tew, G. N. *Angew. Chem. Int. Ed.* **2006**, *45*, 7526. (b) Che, Y.; Datar, A.; Balakrishnan, K.; Zang, L. *J. Am. Chem. Soc.* **2007**, *129*, 7234. (c) Hill, J. P.; Jin, W.; Kosaka, A.; Fukushima, T.; Ichihara, H.; Shimomura, T.; Ito, K.; Hashizume, T.; Ishii, N.; Aida, T. *Science*, **2004**, *304*, 1481.

5 (a) Ryu, J.-H.; Hong, D.-J.; Lee, M. *Chem. Commun.* **2008**, 1043. (b) Shim M. S.; Lee, H. T.; Shim, W. S.; Park, I.; Lee, H.; Chang, T.; Kim. S. W.; Lee, D. S. *J. Biomol. Mater. Res.* **2002**, *61*, 188. (c) Inoue, Y.; Kuad, P.; Okumura, Y.; Takashima, Y.; Yamaguchi, H.; Harada, A. *J. Am. Chem. Soc.* **2007**, *129*, 6396.

6 (a) de Greef, T. F. A.; Nieuwenhuizen, M. M. L.; Stals, P. J. M.; Fitié, C. F.

C.; Palmans, A. R. A.; Sijbesma, R. P.; Meijer, E. W. *Chem. Commun.* **2008**, 4306. (b) Kim, J.-K.; Lee, E.; Lim. Y.-B.; Lee, M. *Angew. Chem. Int. Ed.* **2008**, *47*, 4662.

7 Menger, F. M.; Keiper, J. S. *Angew. Chem. Int. Ed.* **2000**, *39*, 1906.

8 Sun, H.-S.; Lee, C.-H.; Lai, C.-S.; Chen, H.-L.; Tung, S.-H. *Soft Matter,* **2011**, *7*, 4198.

9 (a) Kumar, M.; Jinturkar, K.; Yadav, M. R.; Misra, A. *Crit. Rev. Ther. Drug Carrier Syst.* **2010**, *27*, 237. (b) Ding, A.-X.; Tan, Z.-L.; Shi, Y.-D.; Song, L.; Gong, B.; Lu, Z.-L. *ACS Appl. Mater. Interfaces*, **2017**, *9*, 11546. (c) Ivanova, E. A.; Filatov, A. V.; Morozova, N. G.; Zenkova, M. A.; Maslov, M. A. *RSC Adv.* **2015**, *5*, 93262.

10 (a) Ghauhan, V.; Singh, S.; Kaur, T.; Kaur, G. *Langmuir*, **2015**, *31*, 2956. (b) Aggarwal, R.; Singh, S. *Ind. Eng. Chem. Res.* **2014**, *53*, 2549. (c) Sharma, V. D.; Ilies, M. A. *Med. Res. Rev.* **2014**, *34*, 1. (d) Shimizu, T.; Masuda, M.; Minamikawa, H. *Chem. Rev.* **2005**, *105*, 1401. (e) Vemula, P. K.; John, G. *Acc. Chem. Res.* **2008**, *41*, 769.

Section 3.
Control of Self-assembled Structures through Co-assembly of NDI Based Amphiphiles.

3.1. Introduction

Amphiphilic molecules, which have both of hydrophobic and hydrophilic moiety, self-assemble into highly organized aggregates with various morphologies such as spherical micelles, wormlike micelles, spherical and hollow vesicles, planar bilayers and nano-tubes.[1] The formation of these morphologies depends on solvent environment, molecular structures and shapes as well as the relative fraction of hydrophilic and hydrophobic part.[2]

Aromatic diimide derivatives serve as electron acceptors for solar energy conversion,[3] molecular electronics[4] and *n*-type organic semiconductors.[5] Among the aromatic diimide derivatives, 1,4,5,8-naphthalenediimides (NDIs) have attracted much attention due to tendency to form *n*-type over *p*-type semiconductor materials.[6] The naphthalenediimide are a compact, electron deficient class of aromatic compound capable of self-organization[6] and being incorporated into larger multi-component assemblies through intercalation.[7] Functionalization through diimide nitrogen produces analogues whose

absorption and emission properties are variable. Here we reported a surface modified tubular materials by controlled self-assembly of NDI and PDI (1,4,9,10-perylenediimide) derivatives which both have an electron acceptor and donor moiety in one molecule.

3.2. Results and Discussion

In this work, we prepared NDI•R derivatives, which bear an acetyl, carbazole, and pyrene moiety at terminus of TEG (tetraethylene glycol) chain *via* click chemistry (**Figure 1**). Particulary, NDI•Car amphiphile containing carbazole donor and naphthalenediimide (NDI) acceptor can self-assemble and elaborate nano-object which is expected to serve as a nanoscopic energy converter. The terminal functionalized amphiphilic naphthalenediimide (NDI·Car) and perylenediimdie (PDI·Car) were obtained by asymmetric condensation, and then attaching proper functional moiety with “click” chemistry.

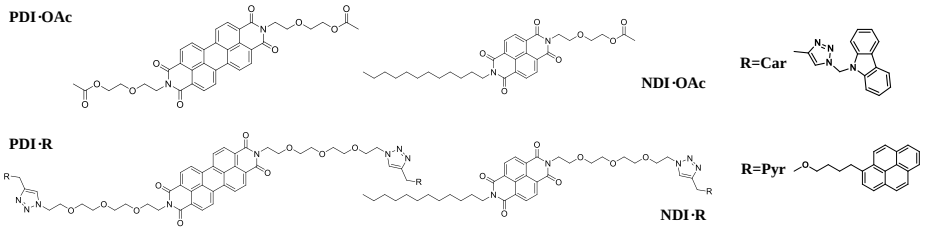

Figure 1. Molecular structures of amphiphilic NDI and PDI derivatives.

While the fluorescence spectrum of molecularly dissolved NDI•Pyr display no relationship between NDI and pyrene moiety, fluorescence spectrum of NDI•Car shows an energy transfer property from NDI to the carbazole moiety (**Figure 2**). This means that the structure creates an extremely wide interface for the spatially segregated redox couple. Hence, the

heterojunction amphiphile can attain electrical conductivity upon photo-irradiation.

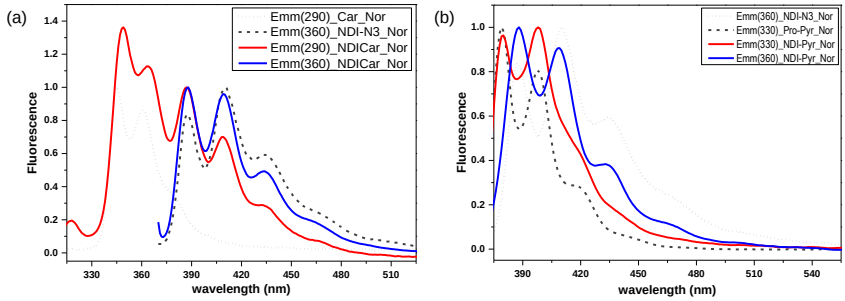

Figure 2. Emission spectra of (a) NDI•Car and (b) NDI•Pyr in $CHCl_3$ at 25 ℃. (λ_{car} = 290 nm, λ_{NDI} = 360 nm, λ_{pyr} = 330 nm)

Firstly, we tested the self-assemble behavior of NDI•OAc and NDI•Car using diffusion solvent system with $CHCl_3$ and EtOH. A yellow precipitate was formed when 10 times of the volume of EtOH was added to the NDI solution in $CHCl_3$ with 60 μM. For the NDI•Car, Israelachvili's critical packing parameter (P_c)[8] was calculated to be approximately 1.0, implying that spherical vesicle should be favorably formed in self-assembling condition. On the other hand, NDI•OAc has $P_c \geq 1$ value, which should be favorably self-assembled into bilayer structure. According to SEM studies (**Figure 3**), the self-assemblies of NDI•Car consisted of ten micro-sized spherical structure with small rolling sheet on the surface. In contrast, NDI•OAc, which occupied a small volume, self-assembled into fibril structure through one-dimension (1D) π-π stacking process. However, the self-assembling behavior of PDI•R is different to the case of NDI•R due to its strong π-π stacking ability. Despite the difference in hydrophilic moiety volume, PDI•OAc and PDI•Car self-assembled into ribbon- and rod-like structure, respectively with 1D aggregating process.

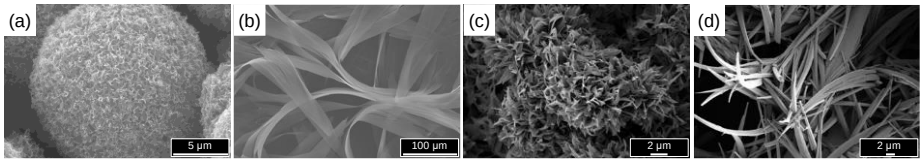

Figure 3. SEM images for self-assemblies of (a) NDI•Car, (b) NDI•OAc, (c) PDI•Car and (d) PDI•OAc in mixture of $CHCl_3$ and EtOH.

More interestingly, nano-tubules were observed for the co-assembly system of NDI•Car and NDI•OAc in mixture of $CHCH_3$ and EtOH (1:10 v/v) as shown in **figure 4**. The nano-tubules can be observed at the molar ratio of NDI•Car and NDI•OAc, from 9:1 to 5:5 mixture. The nano-tubules were formed with the average outer-diameter of 500 nm. For the co-assembly system with higher NDI•OAc contents (>50%), coiled nano-fibril structure were observed. Finally, the coiled nano-fibrils were transformed into flat-nano-ribbon at pure NDI•OAc contents (**Figure 3b**).

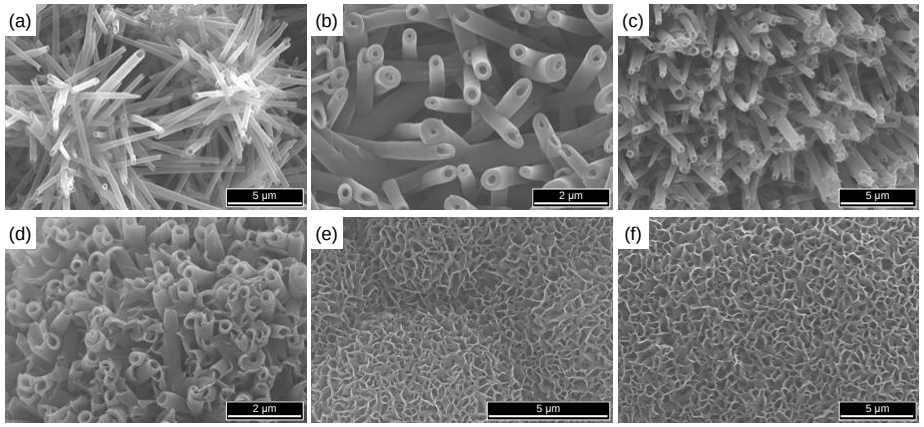

Figure 4. SEM images of co-assembly of NDI•OAc and NDI•Car in $CHCl_3$ and EtOH mixture (1/10, v/v): A ratio of NDI•OAc and NDI•Car is (a) 1:9, (b) 2:8, (c) 3:7, (d) 5:5, (e) 6:4, and (f) 8:2.

The observed transformation of the self-assembled structures for the co-

assembly of NDI•OAc and NDI•Car can be rationalized by considering spontaneous curvature. When bulky-hydrophilic NDI•Car is co-assembled with a flat shaped NDI•OAc, the average hydrophobic part decreases, and the interface between the hydrophilic and hydrophobic part changes from a flat interface to a more of a curved one. The resulting increase in spontaneous curvature get the strain to the formed nano-ribbon, leading to twist and a transition to nano-tubes[9] as illustrated in **figure 5**. It is interesting to note that such mechanism for control of self-assembly by spontaneous curvature is present in biology. A typical example is the deformation of flat lipid membranes by protein coating into transport spherical vesicles.[10]

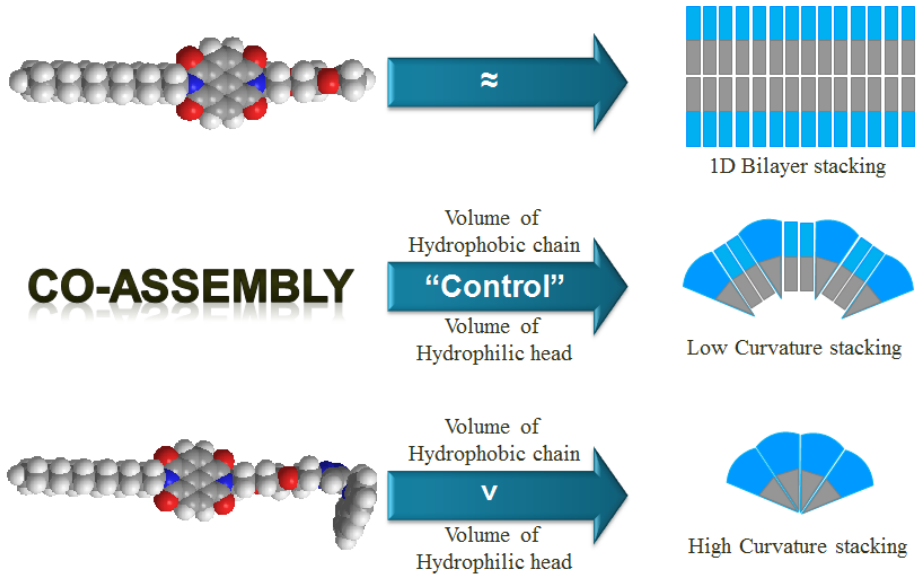

Figure 5. Schematic representation of control of self-assembled structure through co-assembly between NDI•OAc and NDI•Car.

3.3. Conclusion

In conclusion, the heterojunction amphiphile, NDI•Car, attached between

an electron donating and accepting moiety by “click” reaction, successfully shows electron transfer ability from NDI to carbazole moiety. Interestingly, the aggregate morphologies of amphiphilic NDI are dependent on their shapes. The co-assembly of NDI•OAc and NDI•Car generated nano-tubes owing to the changes in spontaneous curvature. The morphology changes from the co-assembly of different amphiphiles provide a guideline for the rational design of particular morphologies such as nano-tubes.

3.4. Experimental

3.4.1. Instrumentation

^{1}H and ^{13}C NMR spectra were measured on a Bruker Advance DPX-300 or a Bruker Advance 500 spectrometer. The XWINNMR program was used for the pulse program. Chemical shifts are reported as parts per million (δ) and referenced to residual solvent peak (δ 2.50 for DMSO and 7.27 for $CDCl_3$). ^{13}C NMR chemical shifts: δ = 39.51 ppm for DMSO. The GC-MS was obtained with a JEOL JMS-AX505WA and HP 5890 Series II, using the FAB method. Scanning electron microscope (SEM) images were obtained with a JEOL-JSM 5410LV. Phosphorescence spectra were recorded on a Jasco FP-6500 spectrophotometer. UV/vis spectra were collected on a Beckman DU-800.

3.4.2. Materials

All reagents were purchased from either sigma-aldrich or TCI and used without any further purification. Deuterated solvents were acquired from cambridge isotopic laboratories

3.4.3. Preparation of Naphthalenediimide and Perylenediimide Derivatives

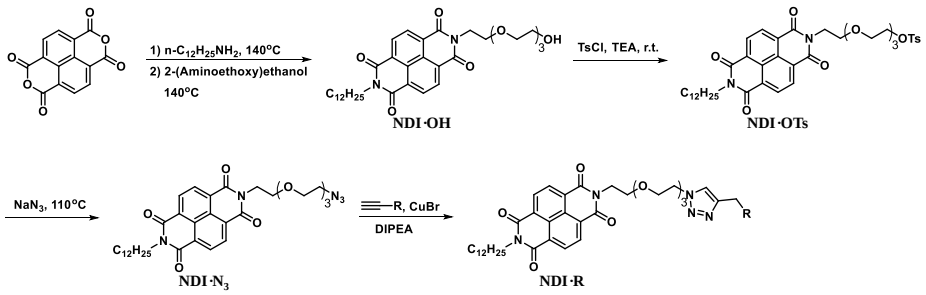

Figure 6. Schematic representation of preparation of **NDI•R**.

NDI•OH: 1,4,5,8-Naphthalenetetracarboxylic dianhydride (2.68 g, 10.0 mmol) was dissolved in 30 ml DMF. The suspension was heated to 140 ℃, and then added for 10 mins a dodecylamine (1.85 g, 10.0 mmol) at that temperature. The mixture was stirred for 16 hrs at 140 ℃. To the reaction mixture was added a solution of 2-(2-(2-(2-aminoethoxy)ethoxy)ethoxy)ethanol (1.93 g, 10.0 mmol) in 6 ml DMF. The reaction was more stirred for 16 hrs at 140℃. After cooling to room temperature, the solvent was removed by evaporating, and then the residue was diluted with CH_2Cl_2. The organic layer was washed with H_2O (×2) and brine (×1). The organic layer was dried with Na_2SO_4, filter, and concentrated in vacuo. The crude product was purified with SiO_2 column chromatography with mixture of CH_2Cl_2 and MeOH (40:1, v/v) as a eluent.

^{1}H NMR (300 MHz, $CDCl_3$): 0.85-0.89 (3H, t, *J*=6.48Hz), 1.25-1.38 (18H, m), 1.72-1.74 (2H, m), 3.51-3.54 (2H, t, *J*=4.27Hz), 3.59-3.63 (8H, m), 3.70-3.71 (2H, t, *J*=2.46Hz), 3.84-3.88 (2H, t, *J*=5.68Hz), 4.16-4.18 (2H, m), 4.44-4.48 (2H, t, *J*=5.74Hz), 8.74 (4H, s).

NDI•OTs: NDI•OH (1.92 g. 3.10 mmol) and TsCl (1.20 g, 6.30 mmol) was dissolved in 30 ml distilled CH_2Cl_2. To the mixture was added TEA (2.20 ml,

15.70 mmol) at 0 ℃. Reaction was stirred for 2 hrs at 0 ℃, and then warmed to room temperature with 16 hrs stirring. The solution was washed with 1N HCl (*aq*) (×1) and brine (×2), dried with Na_2SO_4, and filtered. The filtrate was concentrated in vacuo. The crude product was purified with re-crystallization in mixture of CH_2Cl_2 (10 ml) and MeOH (70 ml).

^{1}H NMR (300 MHz, $CDCl_3$): 0.87-0.92 (3H, t, *J*=6.47Hz), 1.27-1.40 (18H, m), 1.74-1.76 (2H, m), 2.46 (3H, s), 3.59-3.71 (8H, m), 3.84-3.88 (2H, t, *J*=5.93Hz), 4.13-4.21 (4H, m), 4.45-4.47 (2H, m), 7.33-7.36 (2H, d, *J*=8.01Hz), 7.78-7.80 (2H, d, *J*=8.26), 8.77 (4H, s).

NDI•N_3: NDI•OTs (1.01 g, 1.30 mmol) and NaN_3 (0.86 g, 13.20 mmol) was suspended in 30 ml DMF. The mixture was heated to 110 ℃ and stirred for 16 hrs. After cooling to room temperature, solvent was removed by evaporating. The residue was diluted in CH_2Cl_2, washed with H_2O (×2) and brine (×1). The organic layer was dried with Na_2SO_4, filtered, and concentrated in vacuo. A crude product was purified by SiO_2 chromatography with mixture of CH_2Cl_2 and EA (10/1, v/v) as a eluent.

^{1}H NMR (300 MHz, $CDCl_3$): 0.85-0.89 (3H, t, *J*=6.48Hz), 1.25-1.38 (18H, m), 1.72-1.74 (2H, m), 3.36 (2H, m), 3.63 (8H, m), 3.70-3.71 (2H, t, *J*=2.46Hz), 3.75 (2H, m), 3.89 (2H, m), 4.47-4.49 (2H, m), 8.74 (4H, s).

NDI•R: NDI•N_3 (0.10 g, 0.16 mmol) was dissolved in THF. To the solution was added a CuBr (0.24 g, 0.16 mmol), "R-≡" (0.16 mmol) and DIPEA (0.10 ml, 0.53 mmol). The mixture was stirred for 2 days at room temperature. The solvent was evaporated in vacuo. The crude product was purified with SiO_2 chromatography with mixture of CH_2Cl_2 and MeOH (50/1, v/v) as a eluent.

^{1}H NMR (400 MHz, $CDCl_3$) **NDI•Car**: 0.84-0.88 (3H, t, *J*=6.80Hz), 1.24-1.43 (22H, m), 1.72-1.75 (2H, t, J=7.20Hz), 3.35-3.46 (8H, m), 3.82-3.85 (2H,

t, *J*=5.60Hz), 4.11-4.15 (2H, t, *J*=7.60Hz), 4.34-4.37 (4H, m), 5.35 (2H, s), 7.06-7.09 (2H, t, *J*=7.20Hz), 7.29-7.37 (4H, m), 7.53 (1H, s), 7.76-7.78 (2H, d, J=7.60Hz), 8.44-8.48 (4H, m). **NDI•Pyr**: 0.84-0.88 (3H, t, *J*=6.40Hz), 1.25 (16H, m), 1.39-1.44 (6H, m), 1.70-1.89 (6H, m), 3.18-3.22 (2H, t, *J*=7.80Hz), 3.52-3.53 (4H, m), 3.61-3.63 (4H, m), 3.71 (2H, m), 3.77-3.79 (2H, t, *J*=4.40Hz), 3.84-3.87 (2H, t, *J*=5.60Hz), 4.06-4.10 (2H, t, *J*=7.40Hz), 4.33-4.36 (2H, t, *J*=5.80Hz), 4.56-4.48 (2H, t, *J*=4.40Hz), 4.64 (2H, s), 7.70-7.71 (2H, d, *J*=7.60Hz), 7.52 (2H, s), 7.82-7.98 (6H, m), 8.22 (4H, s).

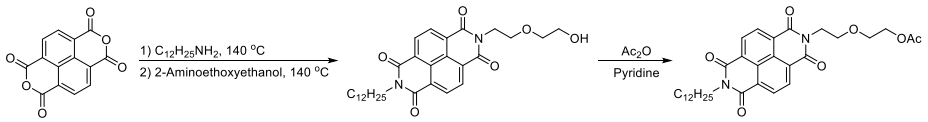

Figure 7. Schematic representation of preparation of **NDI•OAc**.

NDI•OEtOH: 1,4,5,8-Naphthalenetetracarboxylic dianhydride (2.00 g, 7.50 mmol) was dissolved in 30 ml DMF. The suspension was heated to 140 ℃, and then added for 10 mins a dodecylamine (1.38 g, 7.50 mmol) at that temperature. The mixture was stirred for 16 hrs at 140 ℃. To the reaction mixture was added a solution of (2-aminoethoxy)ethanol (1.44 g, 7.50 mmol) in 6 ml DMF. The reaction was more stirred for 16 hrs at 140 ℃. After cooling to room temperature, the solvent was removed by evaporating, and then the residue was diluted with CH_2Cl_2. The organic layer was washed with H_2O (×2) and brine (×1). The organic layer was dried with Na_2SO_4, filter, and concentrated in vacuo. The crude product was purified with SiO_2 column chromatography with mixture of CH_2Cl_2 and MeOH (80:1, v/v) as a eluent.

^{1}H NMR (300 MHz, $CDCl_3$): 0.87-0.92 (3H, t, *J*=6.67Hz), 1.27-1.40 (18H, m), 1.74-1.79 (2H, t, *J*=7.42Hz), 3.66-3.69 (4H, m), 3.88-3.92 (2H, t, *J*=5.54Hz),

4.19-4.24 (2H, t, *J*=7.61Hz), 4.48-4.52 (2H, t, *J*=5.57Hz), 8.79 (4H, s).

NDI•OAc: **NDI•OEtOH** (0.18 g, 0.40 mmol) and acetic anhydride (0.10 ml, 1.10 mmol) was mixed in 5 ml pyridine. The mixture was stirred for 24 hrs at room temperature. All volatiles were removed by evaporating. The crude product was purified with SiO_2 column chromatography with mixture of CH_2Cl_2 and MeOH (80:1, v/v) as a eluent.

^{1}H NMR (300 MHz, $CDCl_3$): 0.87-0.91 (3H, t, *J*=6.58Hz), 1.27-1.40 (18H, m), 1.74-1.78 (2H, t, *J*=6.12Hz), 2.00 (3H, s), 3.75-3.78 (2H, t, *J*=4.71Hz), 3.86-3.90 (2H, t, *J*=5.77Hz), 4.18-4.21 (2H, t, *J*=4.58Hz), 4.47-4.51 (2H, t, *J*=5.76Hz), 8.78 (4H, s).

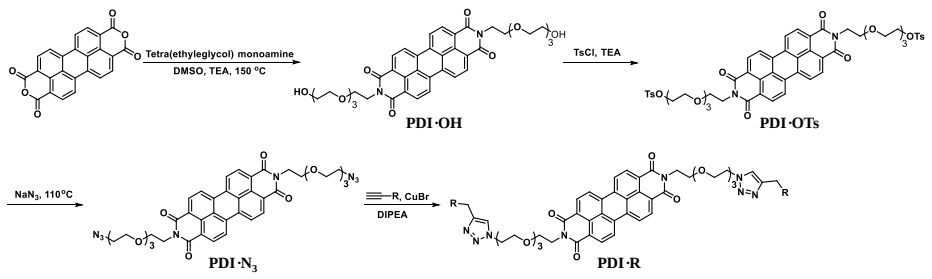

Figure 8. Schematic representation of preparation of **PDI•R**.

PDI•OH: 3,4,9,10-Perylenetetracarboxylic dianhydride (0.42 g, 1.10 mmol), 2-(2-(2-(2-aminoethoxy)ethoxy)ethoxy)ethanol (0.49 g, 2.60 mmol) and TEA (5.00 ml) was mixed in 10 ml DMSO. The suspension was heated to 150 ℃ and stirred for 4 hrs. After cooling to 70 ℃, 60 ml MeOH was added one portion. The solution was poured into 120 ml 10% HCl(*aq*), and stirred for 2 hrs at 60 ℃. The suspension was filtered and the filter-cake was purified by SiO_2 chromatography with CH_2Cl_2 and MeOH (5/1, v/v) as eluent.

^{1}H NMR (300 MHz, $CDCl_3$): 3.56-3.78 (24H, m), 3.88-3.92 (4H, t, *J*=5.91Hz),

4.48-4.52 (4H, t, *J*=5.89Hz), 8.55-8.58 (4H, d, *J*=8.00Hz), 8.65-8.67 (4H, t, *J*=7.98Hz).

PDI•OTs: **PDI•OH** (1.08 g. 1.40 mmol) and TsCl (1.50 g, 8.00 mmol) was dissolved in 100 ml distilled CH_2Cl_2. To the mixture was added TEA (10.00 ml, 72.00 mmol) at 0 ℃. Reaction was stirred for 2 hrs at 0 ℃, and then warmed to room temperature with 16 hrs stirring. All volatiles were removed in vacuo, and the residue was diluted with $CHCl_3$. The organic layer was washed with 1N HCl(*aq*) (×1) and brine (×2), dried with Na_2SO_4, and filtered. The filtrate was concentrated in vacuo. The crude product was purified with SiO_2 chromatography with mixture of CH_2Cl_2 and MeOH (40/1, v/v).

^{1}H NMR (300 MHz, $CDCl_3$): 2.44 (6H, s), 3.55-3.73 (20H, m), 3.86-3.90 (4H, t, *J*=5.15Hz), 4.13-4.16 (4H, t, *J*=3.86Hz), 4.45-4.47 (4H, m), 7.33-7.35 (4H, d, *J*=7.92Hz), 7.78-7.80 (4H, d, *J*=7.91Hz), 8.40-8.43 (4H, d, *J*=7.92Hz), 8.53-8.56 (4H, d, *J*=7.87Hz).

PDI•N_3: PDI•OTs (0.49 g, 0.50 mmol) and NaN_3 (0.56 g, 8.40 mmol) was suspended in 15 ml DMF. The mixture was heated to 110 ℃ and stirred for 16 hrs. After cooling to room temperature, solvent was removed by evaporating. The residue was diluted in CH_2Cl_2, washed with H_2O (×2) and brine (×1). The organic layer was dried with Na_2SO_4, filtered, and concentrated in vacuo. A crude product was purified by SiO_2 chromatography with mixture of CH_2Cl_2 and MeOH (40/1, v/v) as a eluent.

^{1}H NMR (300 MHz, $CDCl_3$): 3.36 (4H, m), 3.63 (16H, m), 3.75 (4H, m), 3.89 (4H, m), 4.47-4.49 (4H, m), 8.53-8.56 (4H, d, *J*=7.94Hz), 8.63-8.66 (4H, d, *J*=7.83Hz).

PDI•R: PDI•N_3 (0.10 g, 0.16 mmol) was dissolved in THF. To the solution was added a CuBr (0.24 g, 0.16 mmol), "R-≡" (0.16 mmol) and DIPEA (0.10

ml, 0.53 mmol). The mixture was stirred for 2 days at room temperature. The solvent was evaporated in vacuo. The crude product was purified with SiO_2 chromatography with mixture of CH_2Cl_2 and MeOH (50/1, v/v) as a eluent.

^{1}H NMR (400 MHz, $CDCl_3$) **PDI•Car**: 3.10-3.13 (4H, m), 3.35-3.36 (10H, m), 3.43-3.45 (4H, m), 3.61-3.72 (14H, m), 3.81-3.84 (8H, m), 4.31-4.33 (4H, t, *J*=4.60Hz), 4.38-4.41 (4H, t, *J*=5.60Hz), 5.39 (4H, s), 6.97-7.00 (4H, t, *J*=7.40Hz), 7.27-7.29 (4H, m), 7.34-7.36 (4H, m), 7.41 (2H, s), 7.71-7.73 (4H, d, *J*=7.60Hz), 8.07-8.09 (4H, d, *J*=8.00Hz), 8.31-8.33 (4H, d, *J*=7.60Hz). **PDI•Pyr**: 1.68-1.71 (16H, m), 2.97-2.99 (4H, m), 3.51-3.56 (20H, m), 3.62-3.64 (4H, m), 3.74-3.79 (4H, m), 3.89-3.92 (4H, m), 4.43-4.48 (8H, m), 4.60 (4H, s), 7.51-7.53 (2H, d, *J*=7.60Hz), 7.68 (4H, s), 7.70-7.74 (8H, m), 7.81-7.86 (8H, m), 8.21-8.23 (4H, d, *J*=8.00Hz).

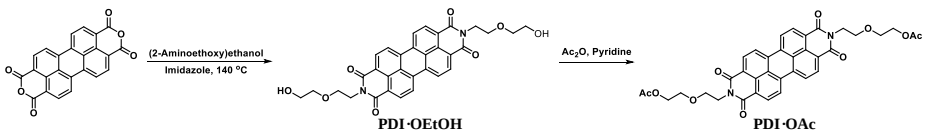

Figure 9. Schematic representation of preparation of **PDI•OAc**.

PDI•OEtOH: 3,4,9,10-Perylenetetracarboxylic dianhydride (1.10 g, 2.80 mmol), TEA (12.50 ml, 87.00 mmol) and 2-(2-aminoethoxy)ethanol (0.70 ml, 6.70 mmol) was mixed in 25 ml DMSO. The suspension was heated to 140 ℃ and stirred for 4 hrs. After cooling to 70 ℃, 60 ml MeOH was added one portion. The solution was poured into 120 ml 10% HCl(*aq*), and stirred for 2 hrs at 60 ℃. The suspension was filtered and the filter-cake was purified by SiO_2 chromatography with CH_2Cl_2 and MeOH (5/1, v/v) as eluent.

^{1}H NMR (300 MHz, $CDCl_3$): 3.69-3.72 (4H, m), 3.82-3.83 (4H, m), 4.22-4.26

(4H, m), 4.48-4.52 (4H, m), 8.57-8.59 (4H, d, *J*=8.00Hz), 8.65-8.67 (4H, d, *J*=8.00Hz).

PDI•OAc: **PDI•OEtOH** (0.20 g, 0.30 mmol) and acetic anhydride (0.20 ml, 2.10 mmol) was mixed in 6 ml pyridine. The mixture was stirred for 36 hrs at room temperature. All volatiles were removed by evaporating. The crude product was purified with SiO_2 column chromatography with mixture of CH_2Cl_2 and MeOH (99/1, v/v) as a eluent.

^{1}H NMR (300 MHz, $CDCl_3$): 3.75-3.77 (4H, m), 3.86-3.89 (4H, t, *J*=6.00Hz), 4.18-4.19 (4H, m), 4.46-4.48 (4H, t, *J*=5.80Hz), 8.59-8.61 (4H, d, *J*=8.00Hz), 8.66-8.68 (4H, d, *J*=8.00Hz).

3.4.4. Co-assembling Process between NDI•R (or PDI•R) and NDI•OAc (or PDI•OAc)

Both of solution of NDI•OAc (or PDI•OAc) and NDI•R (or PDI•R) in $CHCl_3$ (0.60 mM) was mixed in given weight ratio. To the solution was added carefully 10 times volume of EtOH. Resulting separated mixture was kept still on table, and diffused into each other layers. After 2 days, the mixture of NDI (or PDI) derivative was formed precipitate.

3.4.5. SEM Analysis

For SEM imaging of the NDI (or PDI) co-assemblies, the precipitates in suspension were dropped onto slide glass, and then air-dried. The prepared specimens were coated with Au.

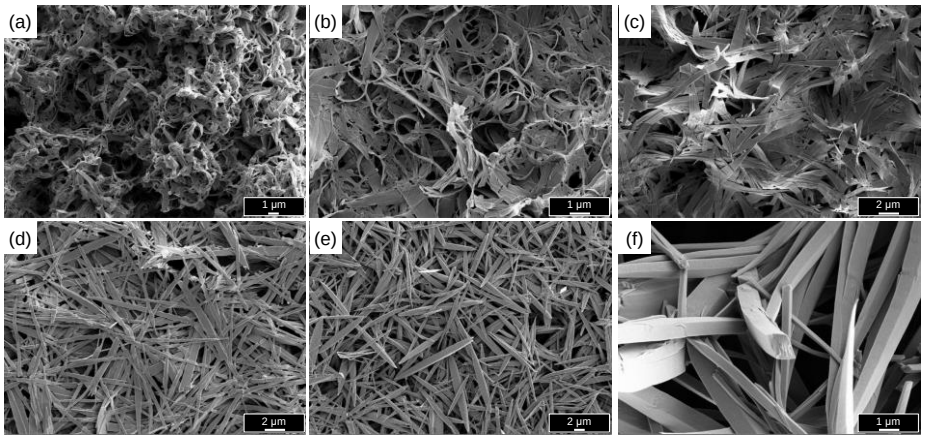

Figure 10. SEM images of co-assembly of PDI•OAc and PDI•Car in $CHCl_3$ and EtOH mixture (1/10, v/v): A ratio of PDI•OAc and PDI•Car is (a) 1:9, (b) 2:8, (c) 3:7, (d) 5:5, (e) 8:2, and (f) 9:1.

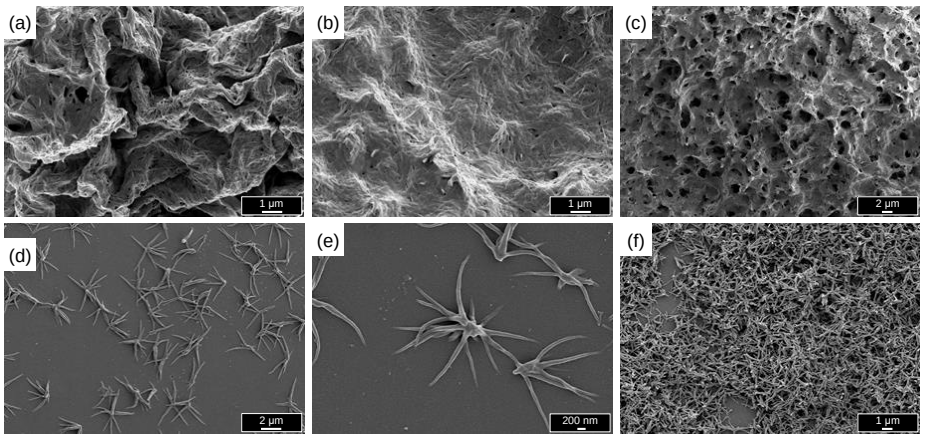

Figure 11. SEM images of co-assembly of NDI•OAc and NDI•Pyr in $CHCl_3$ and EtOH mixture (1/10, v/v): ratio of NDI•OAc and NDI•Pyr is (a) 7:3, (b) 6:4, (c) 5:5, (d) 4:6, (e) 3:7, and (f) 2:8.

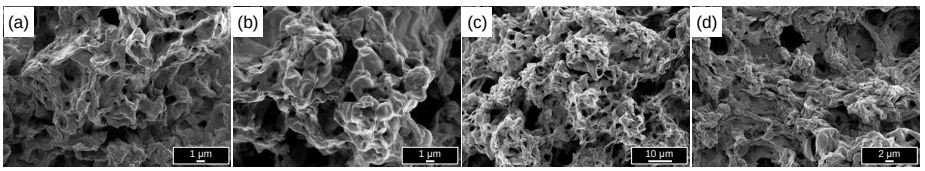

Figure 12. SEM images of co-assembly of PDI•OAc and PDI•Pyr in $CHCl_3$

and EtOH mixture (1/10, v/v): ratio of PDI•OAc and PDI•Pyr is (a) 7:3, (b) 6:4, (c) 4:6, (d) 3:7.

3.4.6. UV/vis Absorption and Fluorescence Spectrum

NDI (or PDI) derivatives were dissolved in $CHCl_3$ to afford a concentration of 10 mM stock solution, which was diluted with $CHCl_3$ up to 10 μM. The diluted solution was used for the UV-vis and fluorescence absorption and emission analysis.

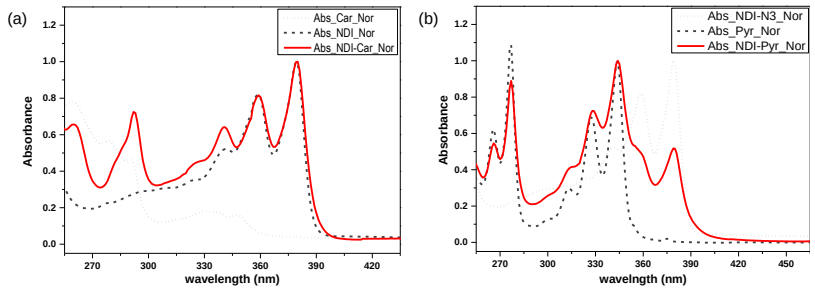

Figure 13. UV-vis absorption spectra of (a) NDI•Car and (b) NDI•Pyr in $CHCl_3$ at 25 ℃.

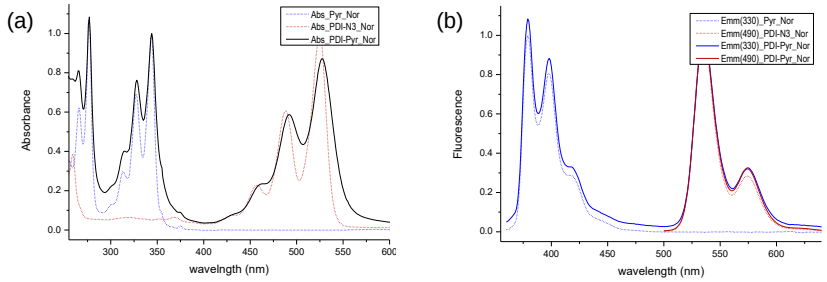

Figure 14. (a) UV-vis and (b) fluorescence spectra of the solution of PDI•Pyr in $CHCl_3$ at 25 ℃.

3.5. References and Notes

1 (a) Percec, V.; Dulcey, A. E.; Balagurusamy, V. S. K.; Maiura, Y.; Smidrkal, J.; Peterca, M.; Nummelin, S.; Edlund, U.; Hudson, S. D.; Heiney, P. A.; Hu, D. A.; Magonov, S. N.; Vinogradov, S. A. *Nature*, **2004**, *430*, 764. (b) Antonietti, M.; Förster, S. *Adv. Mater.* **2003**, *15*, 1323. (c) Hill, J. P.; Jin, W. S.; Kosaka, A.; Fukushima, T.; Ichihara, H.; Shimomur, T.; Ito, K.; Hashizume, T.; Ishii, N.; Aida, T. *Science*, **2004**, *304*, 1481. (d) Hartgerink, J. D.; Beniash, E.; Stupp, S. I. *Science*, **2001**, *294*, 1684.

2 (a) Uzun, O.; Sanyal, A.; Nakade, H.; Thibault, R. J.; Rotello, V. M. *J. Am. Chem. Soc.* **2004**, *126*, 14773. (b) Arnt, L.; Tew, G. N. *J. Am. Chem. Soc.* **2002**, *124*, 7664. (c) percec, V.; Ahn, C. H.; Ungar, G.; Yeardley, D. J. P.; Möller, M.; Sheiko, S. S. *Nature*, **1998**, *391*, 161.

3 Bhosale, S.; Sisson, A. L.; Talukdar, P.; Fürstenberg, A.; Banerji, N.; Vauthey, E.; Bollot, G.; Mareda, J.; Röger, C.; Würthner, F.; Sakai, N.; Matile, S. *Science*, **2006**, *313*, 84.

4 Wen, Y.; Liu, Y.; Di, C. A.; Wang, Y.; Sun, X.; Guo, Y.; Zheng, J.; Wu, W.; Ye, S.; Yu, G. *Adv. Mater.* **2009**, *21*, 1631.

5 Katz, H. E.; Lovinger, A. J.; Johnson, J.; Kloc, C.; Slegrist, T.; Li, W.; Lin, Y. Y.; Dodabalapur, A. *Nature*, **2000**, *404*, 478.

6 Mukhopadhyay, P.; Iwashita, Y.; Shirakawa, M.; Kawano, S.; Fujita, N.; Shinkai, S. *Angew. Chem. Int. Ed.* **2006**, *45*, 1592.

7 Stewart, W. W. *Nature*, **1981**, *292*, 17.

8 (a) Israelachvili, J. *Intermolecular and Surface Foreces, 2nd Ed.*; Academic Press, San Diego, CA, **1991**. (b) $Pc= v/a\times l$, where v is the effective molecular volume, a is the occupied area by hydrophilic chains, and l is optimal molecular length.

9 (a) John, G.; Vemula, P. K. *Soft Matter*, **2006**, *2*, 909. (b) Sorrenti, A.; Illa, O.; Ortuño, R. M. *Chem. Soc. Rev.* **2013**, *42*, 8200. (c) Zhang, X.; Chen, Z.; Würthner, F. *J. Am. Chem. Soc.* **2007**, *129*, 4886.

10 (a) Bigay, J.; Gounon, P.; Robineau, S.; Antonny, B. *Nature*, **2003**, *426*, 563. (b) Lippincott-Schwartz, J.; Liu, W. *Nature*, **2003**, *426*, 507.

Part II

Development of Functional Material through Surface Modification on Self-assembled Structure

Background

1. Introduction to Self-assembly of Functional Materials

The biological membrane provides many functions necessary for biological activities, including acquisition of nutrients, energy sources, reproduction, and cellular recognition. Most of these functions are provided by membrane proteins and carbohydrates on the lipid bilayer surfaces. Recently, functionalization of vesicles via modification with various functional ligands, including biological molecules, has attracted significant interest.[1] These studies require an efficient and convenient method for the introduction of functional ligands onto the surfaces of vesicles.[2] For example, covalent anchorage of poly-peptides onto phospholipid bilayers has been accomplished by functionalizing the peptide part with a lipoidic moiety.[3]

Very recently, the physical and chemical properties of nano-materials have inspired scientists to create new devices that are able to interact with biological systems at the nano-scale. While still in its early stages of development, the field of nano-technology has already made a tremendous impact in medicine and biology in general.[4] In particular, the field of nano-bio-technology – which refers to the use of biological system and molecules to build nano-scale materials – is currently leading to promising applications in diagnostics and therapeutics. It is clear that recent progress in nano-technology has deeply impacted the field of drug delviery.[5] In particularly, self-assembled nano-structures are highly valuable for therapeutic and delivery applications. Their size, high loading capacity and reversible character are major assets for the controlled release of therapeutics.

Liposomes are closed spherical lipid bilayers obtained by the aqueous

self-assembly of lipids. Due to their ease of preparation, their fine tunable properties, and their functionalization through co-assembly of different lipids, liposomes are among the most common self-assembled nano-scale vectors for a wide range of therapeutic agents such as drug or nucleic acid (**Figure 1**). The principle behind the design of these vectors is simple as it aims to take advantage of electrostatic interactions between charged lipids and charged therapeutic agents.[6] The most advanced supramolecular system for drug delivery was developed with cyclodextrin-containing polymer. Polymersomes, which are vesicles formed by the self-assembly of amphiphilic block copolymers, can be also loaded with hydrophilic or hydrophobic drug, functionalized with PEG segments for prolonged circulation times, and decorated with targeting moieties on their surface.[7] Inorganic nano-particles, such as gold nano-particles and silica nano-particles, can serve as versatile scaffolds for delivering drugs and nucleic acids as they can bind molecular cargos *via* a wide range of non-covalent interactions.[8] This system enables the targeted release of drugs in response to heat or chemical additives.

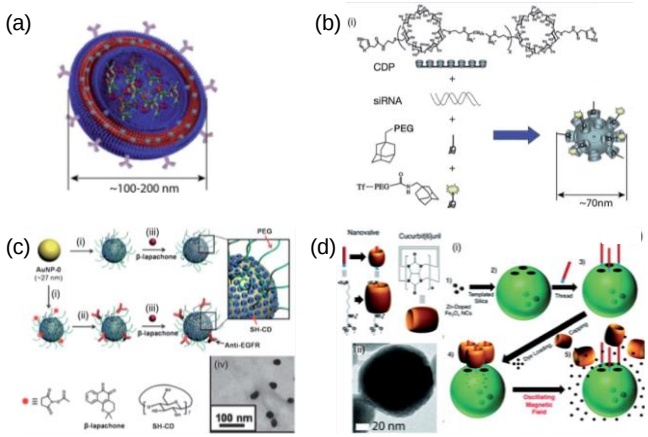

Figure 1. Self-assembled nano-materials for gene and drug delivery. (a) Polymersome decorated with antibodies for targeted delivery. (b) The siRNA and a cationic cyclodextrin containing polymer and their inclusion complex.

(c) Functionalization of the surface on gold nano-particle with a cyclodextrin and PEG thiol derivatives. (d) Silica nano-particles loaded with a dye and zinc-doped iron nano-crystals.

2. Current Developments of Self-assembled Functional Materials

The construction of functional nano-scopic materials and components through molecular self-assembly has the potential to deliver totally new concept in fields as widespread as electronic and tissue engineering.[9] The route of self-assembled functional materials may eventually allow cheap mass production of complex three-dimensional electronic nano-materials and nano-devices. Such bottom-up construction approaches depend on molecular materials with the desired functionality and also on molecular template materials with inherent molecular recognition properties for self-assembly from liquid.

2.1. Introducing Functionality to Self-assembly through Covalent Bond

Aida group have shown photoconductive coaxial nano-materials formed by controlled self-assembly (**Figure 2**).[10] A building block of the self-assemblies has trinitrofluorenone (TNF) moiety as electron acceptors which attach to hexabenzocoronene (HBC) amphiphiles via covalent bond. A gemini-shaped amphiphilic HBCs can self-assemble into well-defined nano-tubular objects, whose walls consist of a graphitic layer of π-stacked HBC and whose inner and outer surface are covered by hydrophilic triethylene glycol

(TEG) chains.[11] In this work, they prepared HBC-TNF derivatives, which bear an electron accepting 4,5,7-trinitro-9-fluorenone functionality with carboxylate linker at each terminus of the TEG chains. A self-assembly of HBC-TNF is achieved by diffusing MeOH vapor into THF solution. Depending on the initial concentration of HBC-TNF, either nano-tubules or nano-fibers with different photochemical property are selectively formed. When vapor-diffused suspension of either nano-tubules or nano-fibers was cast on the electrodes, the nano-tubules only exhibited a photo-current upon irradiation. The nano-tubule is characterized by a coaxial configuration, where a molecular layer of electron-accepting TNF laminates an electron donating π-stacked HBC. Such a spatial separation of the components would prevent charge recombination. The coaxial donor-acceptor configuration with covalent bond provides an ultimate molecular design strategy to achieve a wide interface for spatially segregated redox couples.

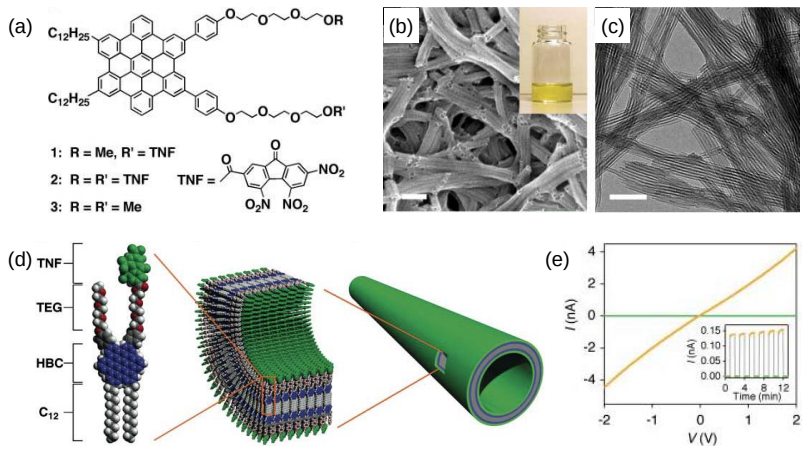

Figure 2. (a) Molecular structure of HBC derivatives. (b) SEM (optical) and (c) TEM image of self-assembled nano-tubules formed from HBC-TNF. (d) Schematic representation of HBC building block and nano-tubule. (e) I-V profiles at 25 °C of nano-tubules of with (yellow) and without (green) photo-

irradiation.

2.2. Introducing Post-functionalization of Self-assembly with Chemical Reaction.

The server condition and unpredictable deformation of the self-assemblies by incorporation of the functional group proved difficult for introducing various functional groups. One of the most promising approaches for functionalization of self-assemblies is post-modification by chemical reactions such as carbonyl-hydrazine (or hydroxylamine),[12] and azide-acetylene cycloaddition ("click chemistry") (**Figure 3**).[13]

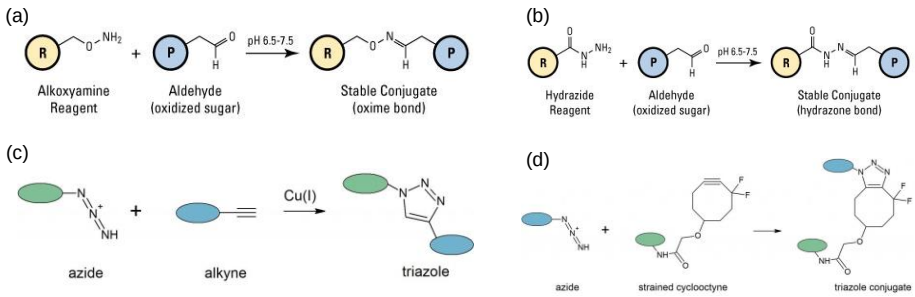

Figure 3. Schematic representation of chemical reaction with nucleophilic addition of (a) ketone and hydroxylamine, (b) ketone and hydrazine, click chemistry of (c) Cu(I) catalyst, and (d) ring strain.

Wagner group reported lipid micelles containing an in-chain diacetylene and a terminal alkyne moiety that can be polymerized by UV-irradiation and further functionalized, *via* "click" chemistry of fluorescent dye (**Figure 4**).[14] Synthetic lipids used in this study bearing a malonic acid polar head group, a diacetylene moiety in the middle of the carbon chain, and core functionalization alkyne in the terminal of the carbon chain. Lipid micelles

were obtained by solubilizing lipid at a concentration of 5 mg/mL in Tris solution upon sonication with a narrow distribution of size between 5~7 nm, and polymerization with UV irradiation not inducing any change in size. To functionalize the micelle with fluorophore, they reacted with different amounts of dansyl azide. The micelles did not significantly change in size after the reaction with dansyl. In contrast, the control lipid-dansyl conjugates form aggregates of approximately 200 nm in aqueous solution. These results demonstrate the stability of micelles, even after the labeling reaction. To further characterize the structure of micelle conjugates, they used the fluorescence properties of the nano-constructs. Non-polymerized micelles of lipid grafted with dansyl had a blue-shift in the fluorescence emission compared to the free label in Tris solution. It means that dansyl probe is located within the polymerized micelles of lipid **1**.

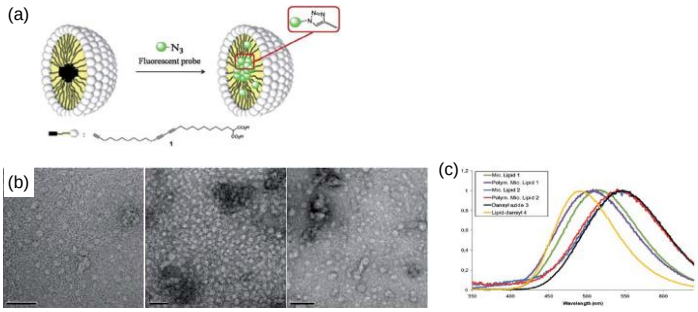

Figure 4. (a) Proposed strategy for core functionalization in micelles. (b) TEM images of micelles from lipid **1** (left) after polymerization, (middle) before reaction, and (right) after reaction with dansyl derivative **3**. (c) Normalized fluorescence spectra of the different compounds in aqueous solution.

2.3. Introducing Post-functionalization of Self-assemblies through Non-covalent Interaction.

Self-assembled π-electronic nano-objects[15] with post-functionalization into surface group *via* non-covalent interactions are expected to serve as potential scaffold for the ultimate molecular design of finely integrated electronic and optoelectronic materials.[16] To achieve this goal, the nano-objects must be sufficiently robust to allow the accommodation of a guest without structural disruption. Furthermore, proper choice of surface groups that enable selective non-covalent interactions is essential.

Zang group demonstrated that highly photo-conductive organic nano-fibril heterojunctions have been fabricated through simple interfacial engineering of the hydrophobic interaction between alkyl side-chain (**Figure 5)**.[17] The strong π-π stacking interaction between the acceptor amphiphile results in effective π-electron delocalization, that is, enhanced electron migration along the long axis of nano-fiber.[18] The nano-fibril heterojunctions were fabricated simply by drop-casting an ethanol solution of the donor compound onto the nano-fibers deposited on silica substrate. The spontaneous adsorption of compound onto the nano-fibers is likely driven by the hydrophobic interaction between the alkyl side-chains. High photo-conductivity was observed for the nano-fibril heterojunctions, whereas negligible photo-current was measured for the pristine the nano-fibers or pure the donor compound film. These approaches represent a simple, adaptable method allowing for the development and optimization of photoconductive supramolecular organic materials.

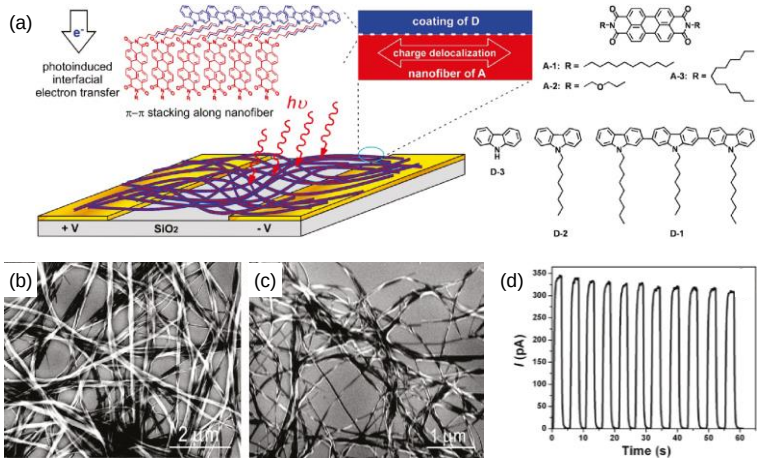

Figure 5. (a) Schematic illustration of nano-fibril heterojunctions composed of perylene and carbazole derivative. SEM images of (b) pristine nano-fibers and (c) nano-fibers after being coated with the donor. (d) Photocurrent measured at 10 V of bias in response to turning on and off the white irradiation.

2.4. Introducing Post-functionalization of Self-assembly through Host-guest Interaction.

The intra-cellular signaling is initiated by molecular recognition events on bio-membranes, where receptor proteins and lipids are dynamically and successively self-assembled into specific supramolecular complex to the binding of receptor ligands. They activate signaling pathway, leading to the amplification into cellular response.[19] The sophisticated interfacial functions of bio-membranes manifest the importance of pre-organized supramolecular systems which dynamically convert and amplify molecular information into the other physiochemical signals.

Kimizuka group have developed a novel amphiphilic receptor TbL^{+}

complex which spontaneously self-assembles in water and form stable vesicles (**Figure 6**).[20] The aqueous vesicles of TbL^+ complex shows luminescence in water as a consequence of energy transfer from the coordinating bis(pyridine) unit to Tb^{3+} ion. Upon addition of varied nucleotides, sigmoidal increase in luminescence intensity was observed for ATP, followed by ADP, whereas almost no enhancement was observed for AMP. The enhanced luminescence intensity is ascribed to the displacement of coordinating water molecules by the phosphate groups. They demonstrate synergistic interactions between highly organized receptors at the membrane surface. Self-assembly of receptor molecules to form nano-interfaces thus open a new strategy to the recognition, conversion and amplification of molecular information. Together with adaptive self-assemblies formed in water from nucleotides and lanthanide ions,[21] it allows for a wide range of applications for these coordination nano-interfaces, including sensing and diagnostics.

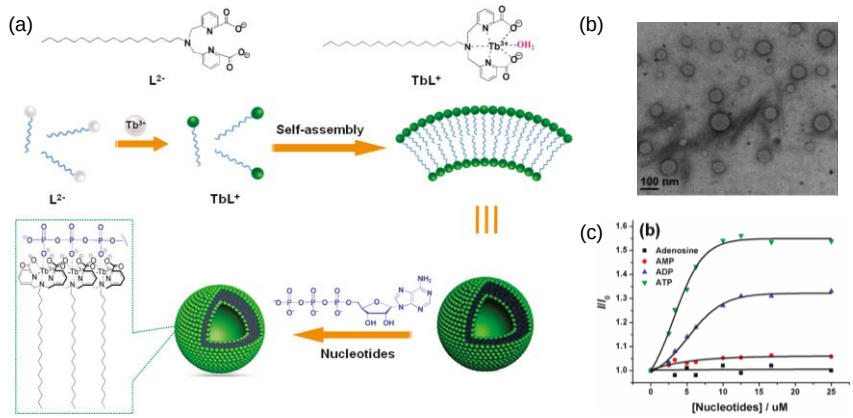

Figure 6. (a) Schematic representation for self-assembly of amphiphilic TbL^+ complex and binding of ATP molecule. (b) TEM image of [TbL]Cl in 10 mM HEPES buffer. (c) I/I_0 evolution as a function of the concentration of nucleotides.

3. References and Notes

1 (a) D'Souza G. G.; Wang, T.; Rockwell, K.; Torchilin, V. P. *Pharm Res.* **2008**, *25*, 2567. (b) Li, B.; Martin, A. L.; Gillies, E. R. *Chem. Commun.* **2007**, 5217. (c) Cavalli, S.; Tipton A. R.; Overhand, M.; Kros, A. *Chem. Commun.* **2006**, 3193.

2 (a) Ringsdorf, H.; Schlarb, B.; Venzmer, J. *Angew. Chem. Int. Ed. Engl.* **1988**, *27*, 113. (b) Best, M. D.; Rowland, M. M.; Bostic, H. E. *Acc. Chem. Res.* **2011**, *44*, 686.

3 (a) Schelre, P.; Boeckler, C.; Frischand, B.; Schuber, F. *Bioconjugate Chem.* **2000**, *11*, 118. (b) Lowik, D. W. P. M.; Linhardt, J. G.; Adams, P. J. H. M.; van Hest, J. C. M. *Org. Biomol. Chem.* **2003**, *1*, 1827. (c) Epand, R. M. *Biopolymers*, **1997**, *43*, 15. (d) Shahinian, S.; Sivius, J. R. *Biochemistry*, **1995**, *34*, 3813.

4 (a) Fuchs, H.; Grätzel, M.; Krug, H.; Schmid, G.; Vogel, V.; Waser, R. *Nanomedicine, in Nanotechnology*, WILEY-VCH Verlag GmbH, Weinheim, **2010**. (b) Aguilar, Z. P. *Nanomaterials for Medical Applications*, Elsevier, Amsterdam, **2013**.

5 Farokhzad, O. C.; Langer, R. *ACS Nano*, **2009**, *3*, 16.

6 (a) Caracciolo, G.; Amenitsch, H. *Eur. Biophys. J.* **2012**, *41*, 815. (b) Bilalov, A.; Olsson, U.; Lindman, B. *Soft Matter*, **2012**, *8*, 11022.

7 Lee, J. S.; Feijen, J. *J. Controlled Release*, **2012**, *161*, 473.

8 (a) Rana, S.; Bajaj, A.; Mout, R.; Rotello, V. M. *Adv. Drug Delivery Rev.* **2012**, *64*, 200. (b) Dreaden, E. C.; Mackey, M. A.; Huang, X.; Kang, B.; El-Sayed, M. A. *Chem. Soc. Rev.* **2011**, *40*, 3391. (c) Kim, C. K.; Ghosh, P.; Pagliuca, C.; Zhu, Z.-J.; Menichetti, S.; Rotello, V. M. *J. Am. Chem. Soc.* **2009**, *131*, 1360. (d) Ambrogio, M. W.; Thomas, C. R.; Zhao, Y.; Zink, J. I.; Stoddart, J. F. *Acc. Chem. Res.* **2012**, *44*, 903.

9 (a) Whitesides, G. M.; Grzybowski, B. *Science*, **2002**, *295*, 2418. (b) Zhang, S. *Nat. Biotechnol.* **2003**, *21*, 1171.

10 (a) Yamamoto, Y.; Fukushima, T.; Suna, Y.; Ishii, N.; Saeki, A.; Seki, S.; Tagawa, S.; Taniguchi, M.; Kawai, T.; Aida, T. *Science*, **2006**, *314*, 1761. (b) Yamamoto, Y.; Fukushima, T.; Saeki, A.; Seki, S.; Tagawa, S.; Ishii, N.; Aida, T. *J. Am. Chem. Soc.* **2007**, *129*, 9276.

11 (a) Hill, J. P.; Jin, W.; Kosaka, A.; Fukushima, T.; Ichihara, H.; Shimomura, T.; Ito, K.; Hashizume, T.; Ishii, N.; Aida, T. *Science*, **2004**, *304*, 1481. (b) Jin, W.; Fukushima, T.; Niki, M.; Kosaka, A.; Ishii, N.; Aida, T. *Proc. Natl. Acad. Sci. U.S.A.* **2005**, *102*, 10801.

12 (a) Carrico, I. S.; Carlson, B. L.; Bertozzi, C. R. *Nat. Chem. Biol.* **2007**, *3*, 321. (b) Mahal, L. K.; Yarema, K. J.; Bertozzi, C. R. *Science*, **1997**, *276*, 1125. (c) Zhang, Z.; Smith, B. A. C.; Wang, L.; Brock, A.; Cho, C.; Schultz, P. G. *Biochemistry*, **2003**, *42*, 6735. (d) Chen, I.; Howarth, M.; Lin, W.; Ting, A. Y. *Nat. Methods*, **2005**, *2*, 99.

13 (a) Deiters, A.; Cropp, T. A.; Mukherji, M.; Chin, J. W.; Anderson, J. C.; Schultz, P. G. *J. Am. Chem. Soc.* **2003**, *125*, 11782. (b) Rostovtsev, V. V.; Green, L. G.; Fokin, V. V.; Sharpless, K. B. *Angew. Chem. Int. Ed.* **2002**, *41*, 2596. (c) Agard, N. J.; Prescher, J. A.; Bertozzi, C. R. *J. Am. Chem. Soc.* **2004**, *126*, 15046. (d) Baskin, J. M.; Prescher, J. A.; Laughlin, S. T.; Agard, N. J.; Chang, P. V.; Miller, I. A.; Lo, A.; Codelli, J. A.; Bertozzi, C. R. *Proc. Natl. Acad. Sci. U.S.A.* **2007**, *104*, 16793.

14 Contal, E.; Klymchenko, A. S.; Mély, Y.; Meunier, S.; Wagner, A. *Soft Matter*, **2011**, *7*, 1648.

15 (a) Simpson, C. D.; Wu, J.; Watson, M. D.; Müllen, K. *J. Mater. Chem.* **2004**, *14*, 494. (b) Würthner, F. *Chem. Commun.* **2004**, 1564. (c) Hoeben, F. J. M.; Jonkheijm, P.; Meijer, E. W.; Schenning, A. P. H. J. *Chem. Rev.* **2005**, *105*, 1491. (d) Elemans, J. A. A. W.; van Hameren, R.; Nolte, R. J. M.; Rowan, A. E. *Adv. Mater.* **2006**, *18*, 1251.

16 (a) Carroll, R. L.; Gorman, C. B. *Angew. Chem. Int. Ed.* **2002**, *41*, 4378. (b) Schenning, A. P. H. J.; Meijer, E. W. *Chem. Commun.* **2005**, 3245.

17 Che, Y.; Xu, H. M.; Zhang, C.; Bunes, B. R.; Yang, X.; Zang, L. *J. Am. Chem. Soc.* **2011**, *133*, 1087.

18 (a) Che, Y.; Yang, X.; Liu, G.; Yu, C.; Ji, H.; Zuo, J.; Zhao, J.; Zang, L. *J.*

Am. Chem. Soc. **2010**, *132*, 5743. (b) Neuteboom, E. E.; Meskers, S. C. J.; van Hal, P. A.; van Duren, J. K. J.; Meijer, E. W.; Janssen, R. A. J.; Dupin, H.; Pourtois, G.; Cornil, J.; Lazzaroni, R.; Bredas, J.-L.; Beljonne, D. *J. Am. Chem. Soc*. **2003**, *125*, 8625. (c) Coropceanu, V.; Cornil, J.; Da Silva Filho, D. A.; Olivier, Y.; Silbey, R.; Bredas, J.-L. *Chem. Rev.* **2007**, *107*, 926. (d) Che, Y.; Datar, A.; Yang, X.; Naddo, T.; Zhao, J.; Zang, L. *J. Am. Chem. Soc*. **2007**, *129*, 6354.

19 (a) Stern, C. M.; Mermelstein, P. G. *cell. Mol. Life Sci.* **2010**, *67*, 3785. (b) Fröjdö, S.; Vidal, H.; Pirola, L. *Biochim, Biophys. Acta*, **2009**, *1792*, 83.

20 Liu, J.; Morikawa, M.-a.; Kimizuka, N. *J. Am. Chem. Soc.* **2011**, *133*, 17370.

21 (a) Aimé, C.; Nishiyabu, R.; Gondo, R.; Kimizuka, N. *Chem. Eur. J.* **2010**, *16*, 3604. (b) Nishiyabu, R.; Aimé, C.; Gondo, R.; Kaneko, K.; Kimizuka, N. *Chem. Commun.* **2010**, *46*, 4333.

Section 1.
Surface Functionalization of Liposomes through Host-guest Interactions

1.1. Introduction

Studies on liposome have received much attention in recent years due to their potential applications in various area such as the biomimetic system,[1] drug/gene delivery system[2] and smart material.[3] In all such applications, the incorporation of functional moieties on the surface of liposome has been extremely important. However, the functionalization of liposome surfaces is mostly achieved by attaching target moiety to compound in the liposome *via* covalent bonds. A non-covalent interaction, which would provide a more versatile method for fabricating liposomes with desired property and function, has recently received increasing attention.[4]

Recent reports reveal that transition metal complexes with vacant coordination site are well suited to serve as phosphate ion binding sites.[5] Macrocyclic 1,4,7,10-tetraazacyclododecane (cyclen) transition metal complexes were reported as phosphate binding receptors by König,[6] Kikuchi[7] and Kimura.[8] A widely used binding unit in phosphate chemosensor is the

Zn(II)-dipicolylamine (= dpa) receptors as demonstrated by Hamachi[9] and Smith.[10] We recently reported the use of Zn(II)-dpa complex to detect phosphorylated biomolecule.[11] Taking advantage of the complementary host-guest interaction, we describe here the preparation and morphological change of amphiphilic dpa-**1** by metal cation and anion (**Figure 1**). We also demonstrate that functionalization of liposome surface can be achieved by complementary host-guest interaction.

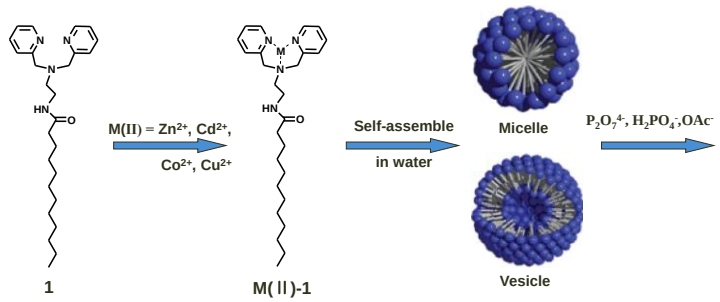

Figure 1. Molecular structure of amphiphilic dpa-**1** and schematic representation of M(II)-**1** self-assembling process.

1.2. Results and Discussion

The amphiphilic 2-(dipicolylamino)ethyldodecanoyl amide, lipid-1, was simply prepared by coupling 2-(dipicolylamino)ethylamine with dodecanoyl chloride. Self-assembling characteristic of M(II)-**1** was investigated by diffusion method. Clearly, solution of M(II)-**1** in MeOH is carefully dropped into Tris buffer at pH 7.4, which formed two separated layer. The separated mixture diffused into each other and finally self-assembled into micellar structure. According to TEM analysis (**Figure 2**), morphology of self-assemblies was changed by species of metal cation. While self-assembling process of Zn(II) and Cd(II) complex exhibited the formation of vesicular

structure, other metal-dpa complexes self-assembled into micellar structure. Light scattering studies also revealed that different metal cation have induced different self-assembled morphologies at solution state. The hydrodynamic radius of the Zn(II) and Cd(II) complex is ~200 nm, larger than that of Co(II) and Cu(II) complex.

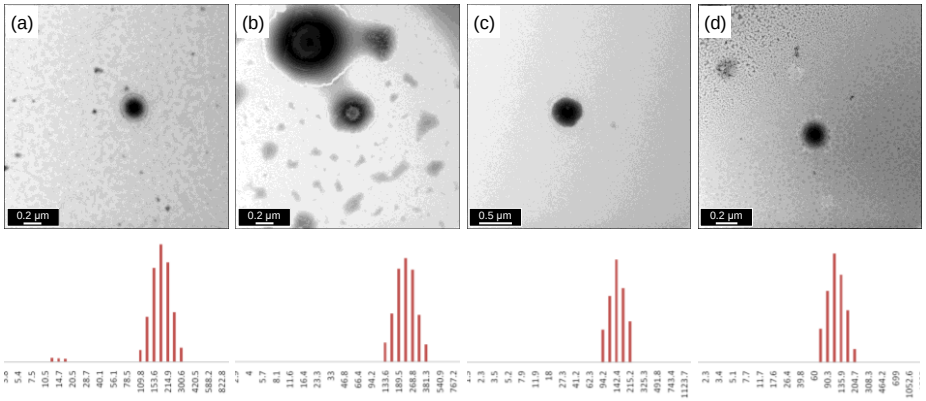

Figure 2. TEM images (top) and particle size distribution (bottom) of (a) Zn(II)-**1**, (b) Cd(II)-**1**, (c) Cu(II)-**1**, and (d) Co(II)-**1**.

To confirm the influence of anion (**A**) binding event, we choose three anions, such as pyrophosphate ($P_2O_7^{4+}$), dihydrogen phosphate ($H_2PO_4^+$) and acetic acetate (AcO^-), which have different binding affinity to dpa-M(II) receptor. TEM analysis (**Figure 3**) of M(II)-**1**-A^- self-assemblies indicated that addition of pyrophosphate, with a higher binding affinity to dpa-M(II) complex, is significantly influence morphology. For the case of Cu(II)-**1**, the self-assembly is changed from micellar structure to vesicular structure upon adding pyrophosphate. Interestingly, Cd(II)-**1** self-assembly underwent liposome fusion upon adding pyrophosphate. The two neighboring vesicles are closed and fuzzed by interaction between pyrophosphate and Cd(II)-dpa moiety, which are placed on surface of the vesicles.

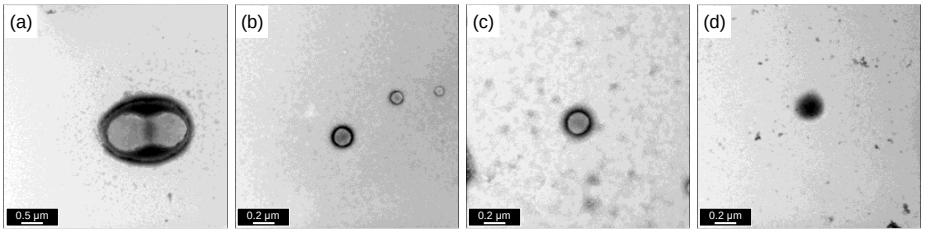

Figure 3. TEM images of self-assemblies of (a) Cd(II)-**1** + $P_2O_7^{4-}$, (b) Cd(II)-**1** + AcO^-, (c) Cu(II)-**1** + $P_2O_7^{4-}$ and (d) Cu(II)-**1** + AcO^-.

Since dpa-Zn(II) compound is known to form stable host-guest complex with phosphate group[12], we anticipated that the surface of the vesicle can be easily modified using host-guest interaction., that is, non-covalent interaction between the accessible dpa-Zn(II) receptors in the vesicle membrane and phosphate derivatives. Treatment FMN fluorophore to self-assembly of Zn(II)-**1**, followed by purification using dialysis for 1 days. Green fluorescent spheres were observed under a confocal microscope, which confirmed the accessibility of the receptor molecule in the vesicle membrane towards phosphorylate ligand, which resulted in a facile non-covalent modification of the vesicle surface with the fluorescent tag (**Figure 4**).

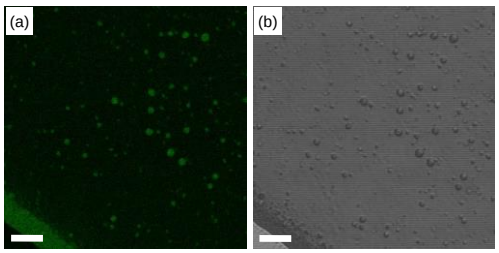

Figure 4. Surface modification with FMN. (a) Fluorescence (confocal) and (b) optical image of Zn(II)-**1**+FMN complex. (scale bar = 10 μm)

1.3. Conclusion

In conclusion, we have demonstrated the formation of various spherical materials from M(II)-**1**, which possesses several remarkable features. Most notable is its ability for easy modification on its surface by receptor-ligand binding pathway. Particularly, self-assembled micelle of Zn(II)-**1** is easily modified their surface by FMN through complementary receptor-guest interaction. The ability for facile surface modification suggests the potential for many applications, including its use in targeted drug delivery and immunization.

1.4. Experimental

1.4.1. Instrumentation

^{1}H and ^{13}C NMR spectra were measured on a Bruker Advance DPX-300 or a Bruker Advance 500 spectrometer. The XWINNMR program was used for the pulse program. Chemical shifts are reported as parts per million (δ) and referenced to residual solvent peak (δ 2.50 for DMSO and 7.27 for $CDCl_3$). ^{13}C NMR chemical shifts: δ = 39.51 ppm for DMSO. The GC-MS was obtained with a JEOL JMS-AX505WA and HP 5890 Series II, using the FAB method. Energy-filtering transmission electron microscope (EF-TEM) images were obtained with a Carl Zeiss-LIBRA 120. Analytical thin-layer chromatography was performed using Kieselgel 60_F-254 plate from Merck. Column chromatography was carried out on Merck silica gel 60 (70 - 230 mesh). Size-distrubution of particles was recorded on a Photal ELS-8000.

1.4.2. Materials

All reagents were purchased from either sigma-aldrich or TCI and used without any further purification. Deuterated solvents were acquired from cambridge isotopic laboratories

1.4.3. Synthesis of Lipid 1

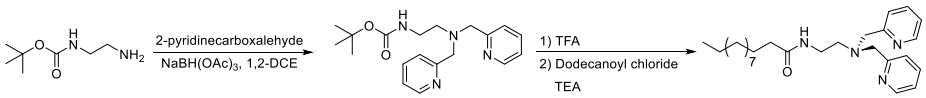

Figure 5. Preparation of lipid 1.

***N-Boc*-2-(di-2-picolylamino)ethylamine:** *N*-Boc-ethylene-1,2-diamine (0.46 g, 2.87 mmol) was dissolved in 1,2-dichloroethane. 2-Pyridinecarboxaldehyde (0.57 ml, 5.99 mmol) and $NaBH(OAc)_3$ (1.73 g, 8.16 mmol) was added to the solution, and the mixture stirred for 16 hrs at room temperature. Resulting solution was washed with brine (×3) and dried with Na_2SO_4. After removing Na_2SO_4 by filtration, the organic layer was concentrated by evaporating. The crude product was purified with SiO_2 column chromatography with mixture of CH_2Cl_2 and MeOH (20/1) as eluent. Yield: 0.83g, 84.3%.

^{1}H NMR (300 MHz, Acetone-d_6): 1.42 (9H, s), 2.67-2.71 (2H, t, *J*=6.13Hz), 3.22-3.28 (2H, m), 3.86(4H, s), 6.28(1H, bs), 7.20-7.24 (2H, t, *J*=6.58) 7.57-7.60 (2H, d, *J*=7.80Hz), 7.70-7.75 (2H, t, *J*=7.68Hz), 8.50-8.52 (2H, d, *J*=4.57Hz).

***N*-(2-(bis(pyridin-2-ylmethyl)amino)ethyl)dodecanamide (**Lipid-**1):** To a solution of *N*-Boc-2-(di-2-picolylamino)ethylamine (0.34 g, 1.00 mmol) in 10 ml CH_2Cl_2 was added 2 ml TFA dropwisely at 0 ℃. The mixture was stirred for 2 hrs at room temperature. All volatiles were removed by evaporating, and

the residue was re-dissolved in 15 ml 2N NaOH (*aq*). The aqueous layer was extracted with CH_2Cl_2 (×3). The combined organic layer was washed with brine (×1), dried with Na_2SO_4, and filtered. The filtrate was concentrated by evaporating and re-dissolved in 10 ml distilled CH_2Cl_2. TEA (0.13 ml, 0.96 mmol) and dodecanoyl chloride (0.37 ml, 1.60 mmol) was added to the solution at 0 ℃. The reaction was stirred for 16 hrs upon slowly warming to room temperature. The organic layer was washed with H_2O (×2) and brine (×1), dried with Na_2SO_4, and filtered to remove Na_2SO_4. The organic layer was concentrated in vacuo. The crude product was purified with SiO_2 column chromatography with mixture of CH_2Cl_2, MeOH and TEA (50/1/0.1). Yield 0.30g, 88.7%.

^{1}H NMR (300 MHz, Acetone-d_6): 0.86-0.91 (3H, t, *J*=6.71Hz), 1.29 (16H, m), 1.57-1.62 (2H, t, *J*=7.01Hz), 2.05-2.08 (2H, m), 2.68-2.72 (2H, t, *J*=6.16Hz), 3.24-3.38 (2H, q, *J*=5.67Hz), 3.86 (4H, s) 7.21-7.25 (2H, m), 7.55-7.58 (2H, d, *J*=7.81Hz), 7.70-7.73 (2H, m), 8.50-8.53 (2H, m).

1.4.4. Preparation of Artificial Liposomes with Lipid-**1**

Appreciate metal(II) nitrate (0.093 mmol) was dissolved in 100 μl MeOH. To the metal solution was added lipid-**1** (39.4 mg, 0.093 mmol). The metal-complex solution was carefully added to the 3.90 ml Tris buffer at pH 7.40. The separated mixture was kept still on table for 7 days at room temperature which can diffuse into each other layers. The homogenous suspension was measured electrophoretic light scattering spectrophotometer (ELS) for confirming particle size.

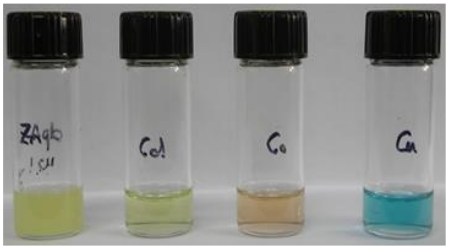

Figure 6. Optical image of M(II)-**1** suspensions.

Appreciate $Na^{+}A^{-}$ (0.024 mmol) was dissolved in 100 ul tris-buffer at pH 7.4. The M(II)-**1** suspension was taken to another vials with 1.0 ml volume, and then mixed with prepared anion solution. The mixture was gently shook for 1 day at 400 rpm.

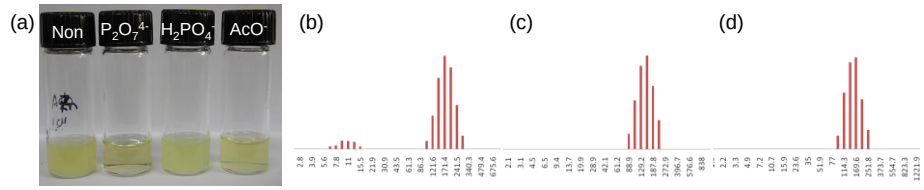

Figure 7. (a) Optical image and size-distribution spectrum of (b) Zn(II)-**1**-$P_2O_7^{4-}$, (c) Zn(II)-**1**-$H_2PO_4^-$ and (d) Zn(II)-**1**-AcO^-.

Figure 8. (a) Optical image and size-distribution spectrum of (b) Cd(II)-**1**-$H_2PO_4^-$ and (d) Cd(II)-**1**-AcO^-. The suspension of Cd(II)-**1**-$P_2O_7^{4-}$ finally formed a precipitate.

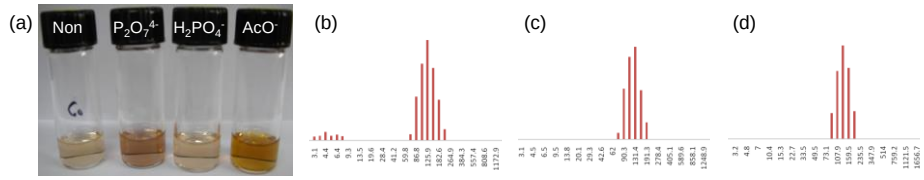

Figure 9. (a) Optical image and size-distribution spectrum of (b) Co(II)-**1**-$P_2O_7^{4-}$, (c) Co(II)-**1**-$H_2PO_4^-$ and (d) Co(II)-**1**-AcO^-.

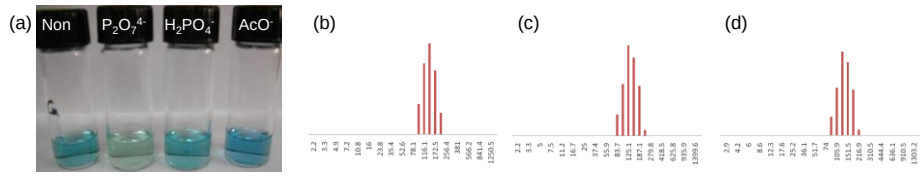

Figure 10. (a) Optical image and size-distribution spectrum of (b) Cu(II)-**1**-$P_2O_7^{4-}$, (c) Cu(II)-**1**-$H_2PO_4^-$ and (d) Cu(II)-**1**-AcO^-.

1.4.5. Self-assembled Behaviors of M(II)-1-A^{n-}

For TEM analysis of the liposome, the suspension of M(II)-**1**-A^{n-} were dropped onto a carbon grid, and then air-dried. TEM images of the self-assembly of M(II)-**1** and M(II)-**1**-A^{n-} were obtained with post-staining method by phosphotungstate and uranylacetate, respectively.

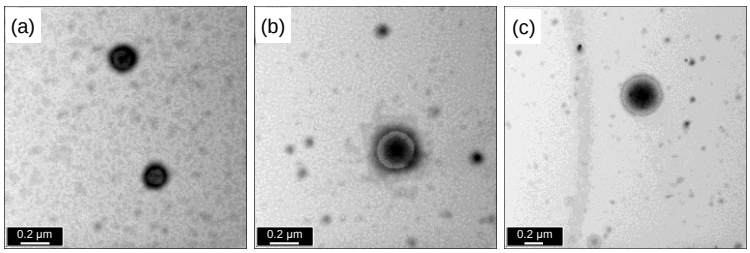

Figure 11. TEM images of self-assembly of (a) Zn(II)-**1**-$P_2O_7^{4-}$, (b) Zn(II)-**1**-$H_2PO_4^-$ and (c) Zn(II)-**1**-AcO^-.

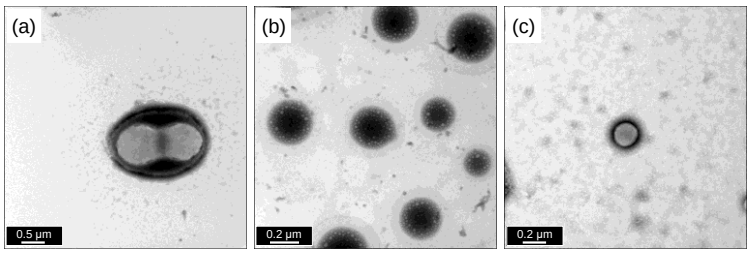

Figure 12. TEM images of self-assembly of (a) Cd(II)-**1**-$P_2O_7^{4-}$, (b) Cd(II)-**1**-$H_2PO_4^-$ and (c) Cd(II)-**1**-AcO^-.

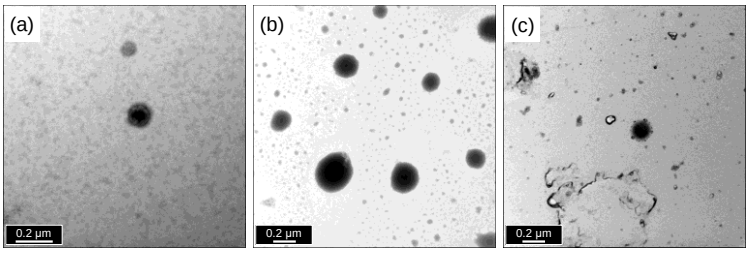

Figure 13. TEM images of self-assembly of (a) Co(II)-**1**-$P_2O_7^{4-}$, (b) Co(II)-**1**-$H_2PO_4^-$ and (c) Co(II)-**1**-AcO^-.

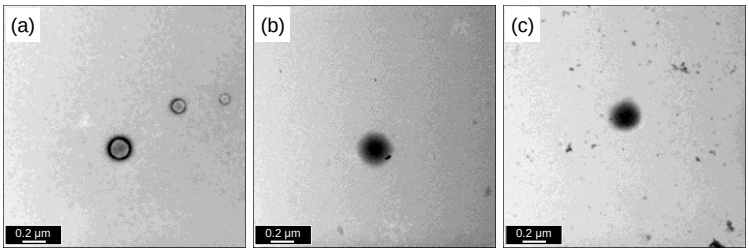

Figure 14. TEM images of self-assembly of (a) Cu(II)-**1**-$P_2O_7^{4-}$, (b) Cu(II)-**1**-$H_2PO_4^-$ and (c) Cu(II)-**1**-AcO^-.

1.5. References and Notes

1 Blumenthal, R.; Clague, M. J.; Durell, S. R.; Epand, R. M. *Chem. Rev.* **2003**, *103*, 53.

2 Allen, T. M.; Cullis, P. R. *Science*, **2004**, *303*, 1818.

3 (a) Mueller, A.; O'Brien, D. F. *Chem. Rev.* **2002**, *102*, 727. (b) Hentze, H.-P.; Co, C. C.; McKelvey, C. A.; Kaler, E. W. *Top. Curr. Chem.* **2003**, *226*, 197. (c) Discher, D. E.; Eisenberg, A. *Science*, **2002**, *297*, 967.

4 (a) Marchi-Artzner, V.; Jullien, L.; Gulik-Krzywicki, T.; Lehn, J.-M. *Chem. Commun.* **1997**, 117. (b) Jeon, Y. J.; Bharadwaj, P. K.; Choi, S. W.; Lee, J.

W.; Kim, K. *Angew. Chem. Int. Ed.* **2002**, *41*, 4474. (c) Kawasaki, T.; Tokuhiro, M.; Kimizuka, N.; Kunitake, T. *J. Am. Chem. Soc.* **2001**, *123*, 6792. (d) Liu, Y.; Xu, J.; Craig, S. L. *Chem. Commun.* **2004**, 1864. (e) Zhou, M.; Haldar, S.; Franses, J.; Kim, J.-M.; Thompson, D. H. *Supramol. Chem.* **2005**, *17*, 101.

5 (a) Tamaru, S.; Hamahci, H. *Recent progress of phosphate derivaties recognition utilizing artificial small molecular receptors in aqueous media. Structure and Bonding (Recognition of Anions)*, Springer, Berlin, Germany, **2008**, *129*, 95-125. (b) Kruppa, M.; König, B. *Chem. Rev.* **2006**, *106*, 3520.

6 (a) Amilan Jose, D.; Stadlbauer, S.; König, B. *Chem. Eur. J.* **2009**, *15*, 7404. (b) Grauer, A.; Riechers, A.; Ritter, S.; König, B. *Chem. Eur. J.* **2008**, *14*, 8922. (c) Riechers, A.; Schmidt, F.; Stadlbauer, S.; König, B. *Bioconjugate Chem.* **2009**, *20*, 804. (d) Turygin, D. S.; Subat, M.; Raitman, O. A.; Selector, S. L.; Arslanov, V. V.; König, B.; Kalinina, M. A. *Langmuir*, **2007**, *23*, 2517.

7 Mizukami, S.; Nagano, T.; Urano, Y.; Odani, A.; Kikuchi, K. *J. Am. Chem. Soc.* **2002**, *124*, 3920.

8 (a) Aoki, S.; Zulkefeli, M.; Shiro, M.; Kohsako, M.; Takeda, K.; Kimura, E. *J. Am. Chem. Soc.* **2005**, *127*, 9129. (b) Kimura, E.; Shiota, T.; Koike, T.; Shiro, M. *J. Am. Chem. Soc.* **1990**, *112*, 5805. (c) Koike, T.; Kajitani, S.; Nakamura, I.; Kimura, E.; Shiro, M. *J. Am. Chem. Soc.* **1997**, *119*, 3068.

9 (a) Sakamoto, T.; Ojida, A.; Hamachi, I. *Chem. Commun.* **2009**, 141. (b) Ojida, A.; Mito-oka, Y.; Inoue, M.; Mamachi, I. *J. Am. Chem. Soc.* **2002**, *124*, 6256. (c) Ojida, A.; Takashima, I.; Kohir, T.; Nonaka, H.; Hamachi, I. *J. Am. Chem. Soc.* **2008**, *130*, 12095. (d) Wongkongkatep, J.; Miyara, Y.; Ojida, A.; Hamachi, I. *Angew. Chem. Int. Ed.* **2006**, *45*, 5518. (e) Anai, T.; Nakata, E.; Koshi, Y.; Ojida, A.; Hamachi, I. *J. Am.Chem. Soc.* **2007**, *129*, 6232.

10 (a) Lakshmi, C.; Hanshaw, R. G.; Smith, B. D. *Tetrahedron*, **2004**, *60*, 11307. (b) Leevy, W. M.; Johnson, J. R.; Maxwell, D. J.; Jackson, E. N.; Marquez, M.; Piwnica-Worms, D.; Smith, B. D. *Chem. Commun.* **2006**, 1595. (c) Leevy, W. M.; Gammon, S. T.; Jiang, H.; Johnson, J. R.; Maxwell,

D. J.; Jackson, E. N.; Marquez, M.; Piwnica-Worms, D.; Smith B. D. *J. Am. Chem. Soc.* **2006**, *128*, 16476.

11 (a) Lee, D. H.; Im, J. H.; Son, S. U.; Chung, Y. K.; Hong, J.-I. *J. Am. Chem. Soc*. **2003**, *125*, 7752. (b) Lee, D. H.; Kim, S. Y. *Angew. Chem. Int. Ed.* **2004**, *43*, 4777. (c) Cho, H. K.; Lee, D. H.; Hong, J.-I. *Chem. Commun*, **2005**, 1690.

12 Ngo, H. T.; Liu, X.; Jolliffe, K. A. *Chem. Soc. Rev.* **2012**, *41*, 4928.

Part III

Selective Detection of Small Molecules through Reaction-triggered Gelation by Self-assembly of Coumarin Based Amphiphiles

Background

1. Introduction to Low Molecular Weight Gelators

By definition, gels are solid, jelly-like materials formed from colloidal mixture. They are colloidal in nature because of the dispersion of the gelators within a solvent. What makes gels so interesting is that by weight and volume they are mostly liquid, yet they behave like a solid. Many applications of gels have been designed due to the ability to trap and immobilize large volume of liquid and sometimes active guest molecules using relatively low masses of gelators. Gels have been applied in the photographic, food, cosmetic and petroleum industries, and have additional potential uses in drug delivery, lithography, catalysis and scaffold as separation material, to name but a few.[1]

Gels can be divided in two separate classes, chemical and physical gels. Chemical gels are classified as gels in which the aggregation is driven by the formation of covalent cross-link between the compounds. This aggregation leads to the formation of a thermally irreversible network.[2,3] On the other hand, physical gels system are formed by non-covalent interaction and, hence, the gel formation is thermally reversible, which makes this type of gelators an excellent subject for studies into supramolecular chemistry.

The set of compounds that act as gelators is surprisingly diverse, and virtually all liquids can be immobilized within a physical gel. Gelators such as polymers, proteins, inorganic substances – like clay and silica – and certain small organic compounds have been studied extensively. Compounds of this latter group are called low molecular weight gelators (LMWGs) (**Figure 1**). Although LMWGs were identified a long time ago, it is only recently that they have become a focused area of supramolecular chemistry and materials

science. This increased interest has occurred because of the high versatility of such compounds towards synthetic modification. In practice, this 'molecular tunability' allow for greater control of the property of the gel phase assemblies

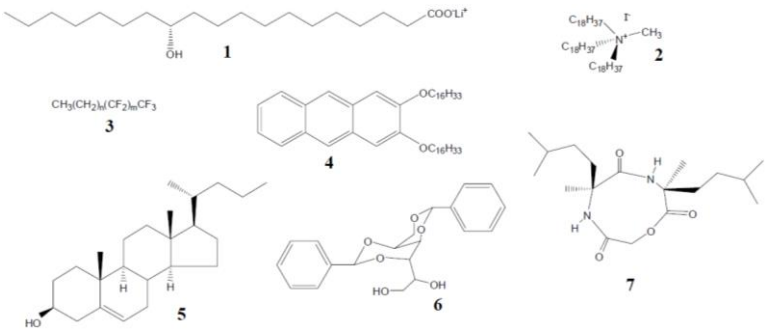

Figure 1. Structure of various low molecular weight gelators.

The formation of a gel occurs, in general, *via* the following steps (**Figure 2**). At elevated temperature the gelator molecules are completely dissolved. The temperature is required to overcome the driving force for aggregation by strong inter-molecular interactions. Upon cooling of the solution, these inter-molecular interactions provide the driving force for the molecules to self-assemble. Due to anisotropy in these interactions self-assembly is favored in one dimension and leads to the formation of thin fibers. Along these fibers, new fibers can grow or assemble, thereby creating bundles consisting of several thin fibers which minimize the large surface free energy of the single fibers. Over time these bundles grow and can occasionally split, leading ultimately to the formation of a 3D network

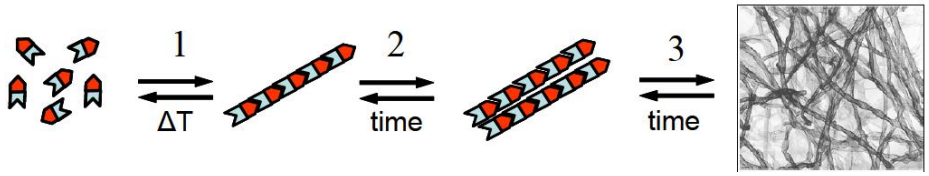

Figure 2. Schematic representation of the formation of a 3D network starting

from dissolved gelator molecules.

The reversibility of non-covalent intermolecular interactions, including hydrogen bonding, π-π stacking, hydrophobic effects, metal coordination and van der Waals interaction, means that LMWGs are easily manipulated by external stimuli, allowing for the tuning of the physical properties of the gel. This has been accomplished using mechanical stimuli,[4] as well as thermal,[5] electrochemical, electromagnetic[6] and chemical stimuli. Chemical stimuli, as additives, have also been reported to change the characteristics of the gel, for example, variations of pH[7], addition of biologically relevant compounds such as vancomycin and insulin[8], incorporation of metal (metallogel)[9] and the subject of this perspective - the addition and incorporation of anions.[10]

2. Current Developments of Stimuli Responsive Low Molecular Weight Gelators

Recent studies have demonstrated that physical gels may have a potential application in a number of area including nano-material and delivery/ modification agent for paints, ink, cleaning agent, drug, etc.[11] As a result, they have received increasing attention in recent years, apart from studies on gel formation and structure, extensive efforts have been made to investigate functional and stimuli responsive gels. Several critical reviews have been published highlighting the advances of gel chemistry from different aspects.[12]

Stimuli responsive physical gels offer us promising opportunities for designing and constructing new functional materials, such as sensors and actuators. Apart from thermal response, various physical gels also respond to other stimuli including light irradiation and redox. The molecular design

rationales for these stimuli responsive gelation is incorporation of photoresponsive-, electroactive- and chemoreactive-segments into the respective LMWGs. For instance, organogels which respond to light irradiation have been attained by incorporating photo-responsive moiety (e.g. azobenzene and stillbene)[12b] into a corresponding LMWG. By designing LMWGs with electro-active moiety, organogels showing response to redox reaction have been described.[12c] In the following, we will introduce the representative examples of stimuli responsive gels based on LMWGs, demonstrate the molecular design principle and perspectives for these fascinating physical gels.

2.1. Redox Responsive Low Molecular Weight Gelators

A redox-sensitive system is expected to respond to a redox process which is in most cases is either an oxidant or a reductant and in a few cases, a species capable of catalyzing a redox process.[13] The key in developing a redox sensitive gel is to functionalize the LMWG with a moiety that is capable of undergoing a redox transition and as a result, the system should exhibit detectable changes in its physico- or chemical-property. One of the most widely used functional motifs in this category is tetrathiafulvalene (TTF) redox active group that can be reversibly transformed into radical cation and dication (**Figure 3a**). The organometallic compound ferrocene (Fc) is capable of undergoing a redox transformation to ferrocenium cation (Fc^+). This redox switching property of Fc/Fc^+ and the self-assembly and gelating property of LMWG have been coupled to develop redox responsive ferrocene-LMWG conjugate (**Figure 3b**). Copper chelate complex feature a structural inter-conversion between tetrahedral and planar geometry by redox treatments.[14]

The difference in their π-π stacking ability was further applied to a redox-controlled gel formation (**Figure 3c).**

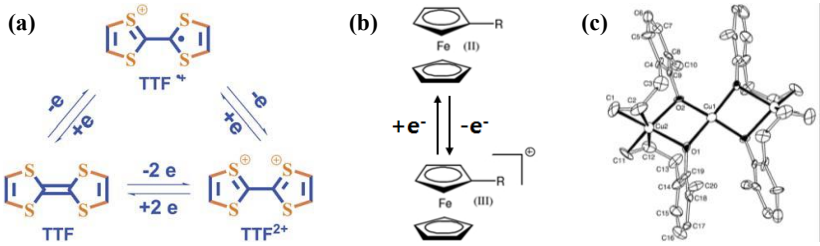

Figure 3. Redox responsive property of (a) TTF and (b) ferrocene. (c) The structure of tetrakis(2-allyl-6methylphenoxo)tricopper(I, II), showing distorted square-planar copper(II) and tetrahedral coordinated copper(I) contres.

2.1.1. Tetrathiafulvalene Based LMWGs

It is known that tetrathiafulvalene (TTF) and its derivatives can be reversibly transformed into the respective radical cation (TTF^{+}) and dication (TTF^{2+}) by either chemical or electrochemical redox reaction.[15] By taking advantage of this unique feature, Zhu group reported TTF based gelators and the resulting gels that show response to redox reaction.[16] Apart from the electroactive TTF segment, a urea group is also present, forming intermolecular extended hydrogen bonding and is widely employed as a gelating group. The gelator can gel several solvent such as cyclohexane and 1,2-dichloroethane (DCE). Either addition of Fe^{3+} or applying of an oxidation potential to the gel can lead to gel to sol transition (**Figure 4**). Interestingly, the gel state can be restored by electro-chemical reduction, followed by heating and cooling. Therefore, the gel to sol transition can be tuned as a function of the redox state of the TTF moiety in gelator. Alternatively, the gel phase can also be modulated by reaction with tetracyanoquinodimethane

(TCNQ) which is a strong electron acceptor. Addition of TCNQ to the gel of **1** from DCE results in the destruction of the gel state.

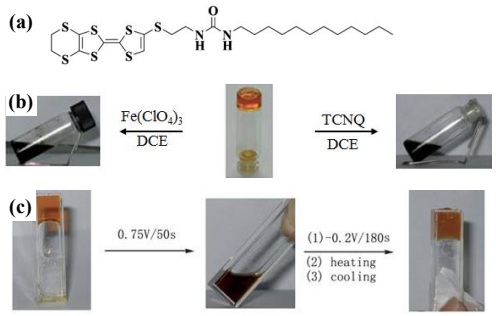

Figure 4. (a) Chemical structure of LMWG. Tuning the gel formation by (b) oxidation and (c) electrochemical oxidation/reduction.

2.1.2. Ferrocene Based LMWGs

As a remarkable organometallic compound, ferrocene (Fc) contains an oxidizable metal ion, Fe(II), is a nonpolar compound in the neutral state, and thereby it dissolves readily in hydrocarbon system. This property, however, can be easily reversed by simple oxidation of the central ion. A neutral-cation redox transition of Fc moiety may be employed on redox-responsive gel system by tune the hydrophilicity of gelator. Actually, the idea has been adopted by a number of groups for study of switchable complexation and molecular aggregation in micelles and vesicles.[17]

Fang group reports four novel cholesterol-appended ferrocene derivatives.[18] These gelators contain a redox-active ferrocenyl moiety and one cholesteryl residue linked by different diamino units. Gelation behavior studies demonstrated that compound **1** is more efficient than its analogues with longer spacers (**Figure 5**). Increasing the length of the spacer as compound **3** and **4** results in complete loss of the gelating ability. To confirm redox responsive gelating ability, an equal amount of $(NH_4)_2Ce(NO_3)_6$, as

oxidant, was carefully placed above the gel of **1**/cyclohexane. It was found that the gel gradually turned into a dark green suspension. Afterwards, an equivalent amount of hydrazine, as reductant, was added, and the mixture was stirred or shaken at room temperature for a few seconds, producing an organogel.

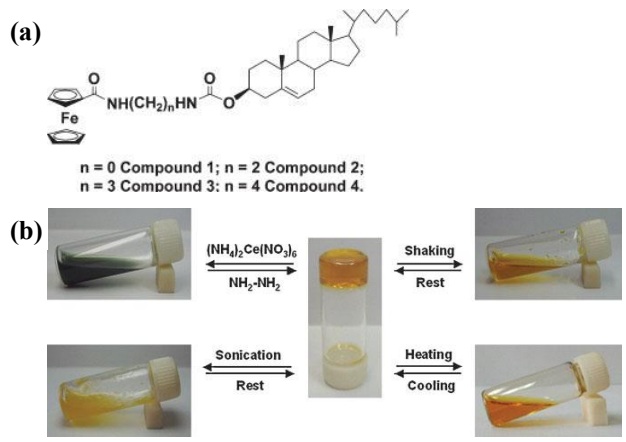

Figure 5. (a) Chemical structure of cholesterol-appended ferrocene derivatives gelators. (b) Reversible sol-gel phase transition of the gel **1**/cyclohexane triggered by chemical redox reaction, shear stress, sonication, and temperature.

2.1.3. Transition Metal Cation Based LMWGs

Various transition metal ions including iron,[19] cobalt,[20] copper,[21] ruthenium,[22] osmium[23] etc., are useful inparting redox properties to gels. Hydrogels cross-linked with metal cation centers that undergo redox reactions were found to undergo a change in geometry. The presence of transition metal ions in gels provides a simple and efficient way for producing electoactive materials.

Shinkai group reported a class of coordination gelators that exhibit reversible sol-gel phase-transition phenomena controlled by redox state of the

Cu(I)/Cu(II) metal-ligand complex.[21b] This system features a Cu(I) complex in which the ligand is a 2,2'-bipyridine derivative bearing two cholesteryl moieties (**Figure 6**). They found that the color of the gel including the Cu(I)•$\mathbf{1}_2$ complex in 1-PrCN gradually changed from reddish brown to greenish blue. The chromatic change in the Cu(I)•$\mathbf{1}_2$ complex is induced by the gel to sol phase transition, which is associated with the distortion of the coordination complex and air oxidation of Cu(I) to Cu(II) in the specific cholesteric gel fibril. When ascorbic acid was added to the Cu(I)•$\mathbf{1}_2$ complex and the mixture was heated until the solid dissolved completely, a greenish blue gel was formed after cooling to room temperature. On the other hand, when the oxidant $NOBF_4$ was added to the Cu(I) complex and the mixture was heated, the deep-green gel turned into a sol with a small amount of pale-blue precipitate.

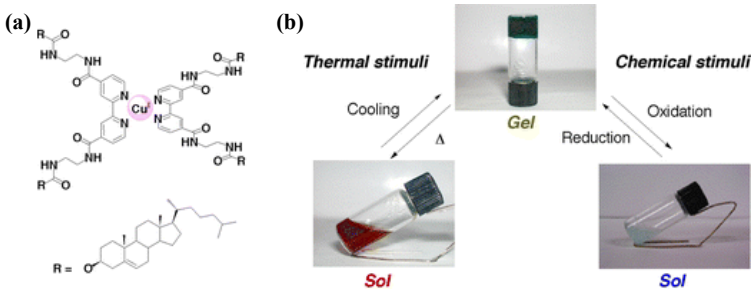

Figure 6. (a) Chemical structure of Cu(I)•$\mathbf{1}_2$. (b) Phase transition and thermochromic behavior of Cu(I)•$\mathbf{1}_2$ at thermal- and redox-stimuli

2.2. Photo-responsive Low Molecular Weight Gelators

The use of light as an external stimulus to modify gels is of particular interest due to the ability to create patterned gel surfaces[24]. This is useful for applications such as microfluidic, cell culture and differentiation and

electronic materials. Light is also often a non-invasive trigger, so the addition of another reagent is not needed.

Gelators that are inherently photo-responsive will contain a chromophore, belonging to the photo-responsive group, attached to other functional groups that drive or aid with gelation. For instance, organogel that respond to light irradiation to effect the gel-sol transition have been achieved by incorporating photo-responsive moiety (e.g., azobenzene [25] and stilbene [26]) into the corresponding LMWGs. The chromophores collect light of a specific wavelength and convert it, leading to photo-reactions that include isomerization, dimerization, bond formation, bond cleavage and exciton formation depending on the chromophore present.

2.2.1 Azobenzene Based LMWGs

The most common photo-responsive LMWGs are based on an azobenzene core. *trans*-Azobenzene is isomerized to the *cis*-form when it is irradiated with UV light. The *trans*-isomer is more stable than the *cis*-isomer, meaning that the *cis*-to-*trans* isomierzation can also be achieved using heat.

Kitamura group reported that photo-responsive rosette composed of azobenzene-appended melamine (**1**) and barbiturate (**3**), is capable of being hierarchically organizing into higher order fibrous aggregates.[26b] As a consequence of the formation of higher-order columnar aggregates, a freshly prepared concentrated cyclohexane solution of rosette $\mathbf{1_3 \bullet 3_3}$ gradually became viscous at room temperature, and eventually a transparent organogel was obtained over 24 hrs (**Figure 7**). When cyclohexane gel of rosette $\mathbf{1_3 \bullet 3_3}$ in glass vial was irradiated at around 350 nm for 1 hr at 20 ℃, the gel turned into a complete fluid with the increase of *cis* contents to ca. 34%. When the gel was irradiated at the wavelength regions not overlapping the absorption

band of the *trans*-azobenzene moiety, no transition to sol was observed. The photo-generated sol phase recovered the original gel state when it was kept in the dark at r.t. for 48 hrs.

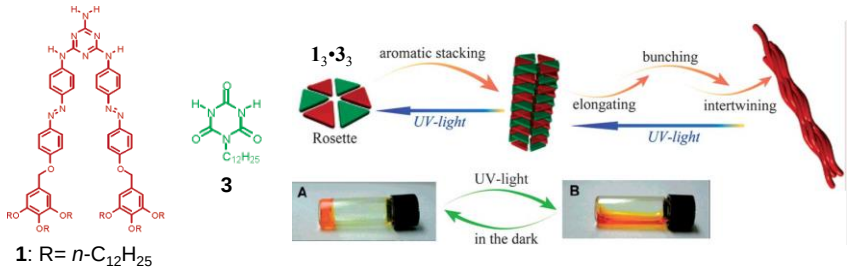

Figure 7. Schematic representation of aggregation of melamine-azobenzene conjugate **1** with barbit. Photograph of a cyclohexane gel (10 mM) of $\mathbf{1_3 \bullet 3_3}$ (A) before and (B) after UV-irradiation for 1 hr.

2.2.2 Stilbene Based LMWGs

Stilbenes act similarly to the azobenzene, with the *trans* to *cis* isomerisation occurring upon irradiation with UV light. The *cis*-stilbene is less thermally stable than the *trans*-stilbene and so in the dark the *cis*-isomer can re-convert to the *trans*-isomer. However, the wavelength needed for the *trans* to *cis* isomerization is shorten than that needed for azobenzene, and the *cis*-stilbene is more stable than *cis*-azobenzene.[27]

Heenan group reported photo-responsive organogel based on stilbene-containing gemini compound, which display a UV-induced gel to sol transition.[26d] The organogel of *E*-SGP was prepared by refluxing a sample containing 8% *E*-SGP and 0.4% *N,N'*-dimethyldodecylamine in toluene for several hours, then cooling slowly it to room temperature (**Figure 8**). Upon irradiation for 1 hour with a mercury lamp, the gels changed to a clear solution. ^{1}H NMR spectroscopy showed that complete conversion to the non-

gelling *cis*-isomer occurred. For the initial *E*-SGP π-π stacking interactions may promote aggregation, with the organophilic pendant chains protecting central polar moieties, in a similar fashion to classic organogelators.[28] On the other hand, the UV-produced photodimers are sterically hindered resulting in much weaker intermolecular association and reduced aggregation. A mask was then used and selectively de-gelled parts of gel. This selective removal could be used to create patterned surfaces.

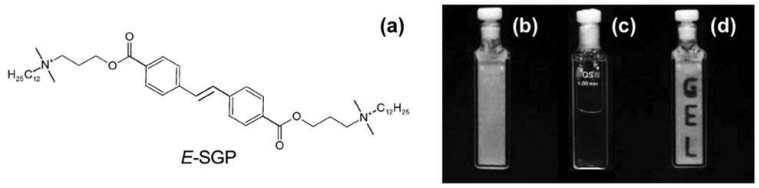

Figure 8. Molecular structure of stilbene gemini surfactant gelator, *E*-SGP. Photographs of (b) the organogel, (b) after irradiation and (c) selective removal of part of the gel.

2.2.3 Ring Opening and Closing Based LMWGs

Another useful photoreaction is where bonds are made or broken. For photo-responsive gelators, this is most likely a ring opening or ring closing reaction.[29] This ring opening or ring closing (**Figure 9**) can have several result; these include a change in color,[30] a change in electronic properties,[31] and or gel to sol transition.[32]

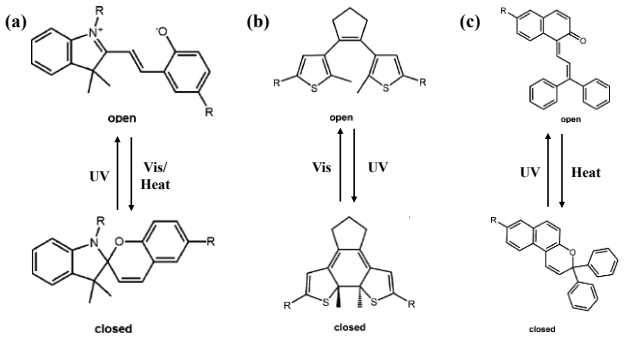

Figure 9. Molecular structures and photo-isomerization of (a) spiropyran, (b) dithienylethene and (c) *2H*-chromene.

Zhang group reported photo-responsive gelator encompassing a spiropyran and dipeptide containing to alanine amino acid.[34] The open form of the gelator (**1**-MC) was dissolved at neutral pH and formed dark red gel when the pH was lowered to 3 using HCl at concentration of around 11 mM. Upon irradiation of the gel with wavelengths of light >400 nm, the red hydrogel rapidly turned into a yellow slurry and the hydrogel disassembled thoroughly within 5 min (**Figure 10**). On the other hand, the yellow slurry, upon irradiation with UV light, turned into red slurry instead of the original red hydrogel. The intrinsic driving force for the sensitive photo-response hydrogel formed by **1**-MC should be photo-induced isomerization from planar MC form to the non-planar SP (closed) form. The π-π stacking between the merocyanine moieties in the self-assembled hydrogel was destroyed when the **1**-MC converted to **1**-SP. The delicate balance between π-π stacking and hydrogen bonding was then disturbed, which resulted in the disassembly of the hydrogel.

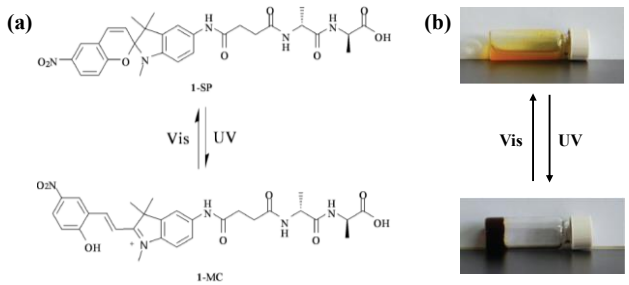

Figure 10. (a) Chemical structure of the spiropyran-linked dipeptide in SP form (**1**-SP) and MC form (**1**-MC). (b) Optical image of the hydrogel formed by **1**-MC and its response to photo-irradiation.

2.3. Chemo-responsive Low Molecular Weight Gelators

In the past decade, several LMWGs gel system have been reported that respond to chemical triggers, either *via* specific non-covalent intermolecular interactions or a reversible chemical reaction between the additive and the gelators. Most interestingly, the interaction between the trigger molecules and the gel can take place at different hierarchical level, leading to different responses.

Although the structural characteristics of the LMWGs involved are very different, the responsive gel systems known so far can be conveniently divided into four distinct groups according to the nature of the chemical trigger (i.e., anions, cations, neutral chemical species, and biomaterials). We will discuss each of these groups and will address the major factors that characterize the responsiveness of the gel system. (i.e., the trigger and its interaction with the gel, as well as the nature, kinetics, and reversibility of the response)

2.3.1 Anion Responsive LMWGs

Among the parameters that determine gel formation, the use of anion has been reported in recent decade, possibly as a result of the smaller number of candidate anion receptors that can act as gelators. Most of the anion responsive gels reported thus far comprise of anion receptors bearing amide or urea unit, which also act as hydrogen bonding sites that support molecular assembly. If the hydrogen bonding donor NH sites interact with anions, the gelators may not form stable assemblies, resulting in the transformation of the gel into a solution.

Amide NH unit is well known anion binding sites, owing to the polarization by π-conjugation with the neighboring carbonyl moiety.[33] For example, Thordarson group reported an alkyl-substituted pyromellite tetraamide derivative (**Figure 11**) that gels in cyclohexane, *n*-hexane, diethyl ether and toluene because of the hydrogen bonding interaction between gelators. The tetraamide binds to anion by adding tetrabutylammonium (TBA) salts through conformation changes of its amide units in dilute solutions. Therefore, the cyclohexane gel of **1** is transformed into a solution by addition of 0.25 equiv. of TBA salts (Cl^-, Br^-, I^-, AcO^-, and NO_3^-) owing to the weaker association between the gelators caused by the interaction of anions at the hydrogen bonding NH sites. The transformation from gel to sol upon the addition of TBA salts as a solid on the gel surface takes times (several seconds to minutes), depending on the affinity of **1** to the anions (Cl^->AcO^->Br^->NO_3^- >I_3^-). In contrast to organic salts, NaI does not induce such a transition to sol state.[34]

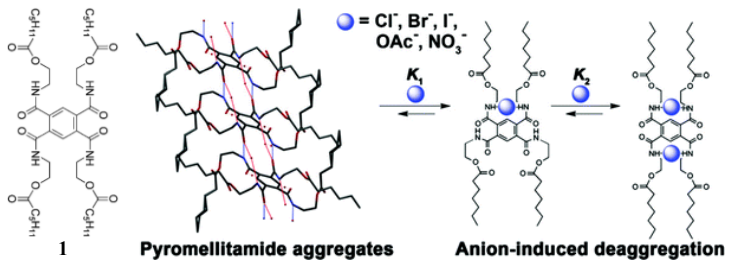

Figure 11. Molecular structure of **1** and schematic representation of anion responsive gel to sol transition.

2.3.2 Cation Responsive LMWGs

Smith group reported metal cation responsive gelator, G1-ene, which is a bolaform gelator with *L*-lysine head group and peripheral alkenes.[35] This

compound formed opaque gels in ethyl acetate containing 0.18 wt% gelator. These gels were tested for their response to a number of salts; A solution of $AgSbF_6$, $LiPF_6$, $NaPF_6$, and $KSbF_6$, in ethyl acetate was gently pipetted onto the pre-formed gel (**Figure 12**). The gels showed a response to Ag^+ and Li^+ by undergoing a gel to sol transition, with the gel breaking down from top to bottom as the salt diffuses through the gel. However, the gels were completely unresponsive to Na^+ or K^+. The addition of Li^+ perturbed intermolecular hydrogen bond interactions, and led to gel breakdown. However, the response to Ag^+ in gels of G1-ene is caused by repulsive electrostatic repulsions between alkene-bound Ag^+ ions.

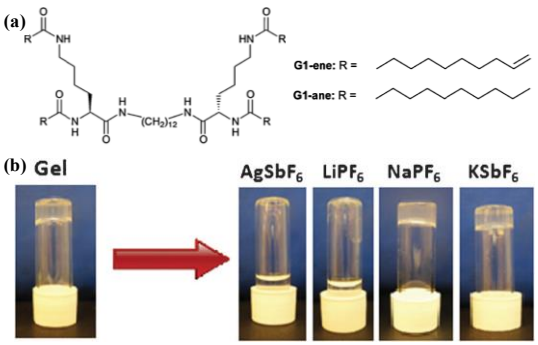

Figure 12. (a) Chemical structure of G1-ene and G1-ane. (b) Response of gels of **G1-ene** in ethyl acetate to solutions of metal salts. All gels are 3 mM, salt solutions are 90 mM, except for $AgSbF_6$ which is 30 mM.

2.3.3 Neutral Compound Responsive LMWGs

Escuder group reported a hydrogelator bearing a nucleophilic reactive site that reacts with aldehydes.[36] A *L*-proline attached hydrogelator (Pro-G1) formed hydrogels above a concentration of 2 mM after dissolution in hot water and suddenly cooling at 25 ℃ accompanied by 1 min of sonication. When a small amount of phenol-red was added together with Pro-G1,

hydrogelation was accompanied by a color change from yellow solution to pink gels (**Figure 13**). A 20 mM solution of the aldehyde in water was added on top of the gel and changes in both macroscopic aspect and color of the gel followed. Acetaldehyde turns initial pink color into yellow after 1hr whereas phenylacetaldehyde and 3-phenylpropanal react immediately after addition. This fact points to the relevance of the hydrophobic interactions that will locate the more hydrophobic compounds within aggregates hidden from water and in close proximity to the reaction centre of Pro-G1.

Figure 13. (a) Chemical structure of hydrogelator Pro-G1 and schematic representation of the hydrogel disassembly mechanism after reaction with aldehydes. (b) Pro-G1/phenol-red mixture at 25℃ in water before (up) and after (down) self-assembly. (c) Gel Pro-G1/phenol-red system at 25 ℃ (1) after addition 20 mM solution of propanol; (2) after 72 hrs; (3) after 96 hrs.

2.3.4 Bio-material Responsive LMWGs

Yang group have developed hydrogelator, which is phosphorylate Fmoc-*L*-tyrosine, as a substrate of phosphatase.[37] Treating a clear solution of the gelator in PBS buffer with high concentrations of phosphatase (>16 units/mL) resulted in the formation of suspensions within 1 min. Interestingly, opaque hydrogels were formed when lower concentrations of enzyme were used

(**Figure 14**). Final concentration of 16 and 4 units/mL gave gel **I** and gel **II** formed within 10 min, and HPLC results indicated that 64.3 and 62.8% of the gelator had been converted at the gelling points of gel **I** and gel **II**, respectively. According to fluorescence spectroscopy of the gel, the fluorenyl groups in gelator favor the anitiparallel overlap. Most of the fluorenyl groups are stacked in antiparallel mode, providing one of the major driving forces for nano-fiber formation. They assume that the nano-fibers were mainly formed by **2** and doped with hydrophilic **1**, making the nano-fibers stable in aqueous solutions.

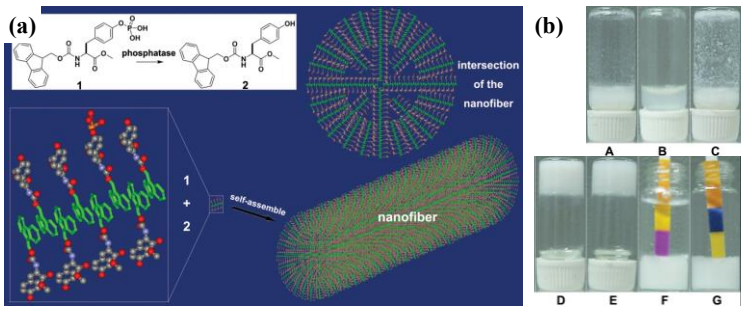

Figure 14. (a) Schematic illustration of enzymatic conversion and proposed molecular arrangements of **1** and **2** in nano-fibers. (b) A: Optical images of 0.5 mL of 1.0 wt% **2** in PBS buffer after sonication; B: 1.0 wt% **1** in PBS buffer; C: suspension formed by solution in (B) with enzyme (20 units/mL); D: gel **I** formed by the solution in (B) with enzyme (16 units/mL); E: gel **II** formed by the solution in (B) with enzyme (4 untis/mL); F: pH 0.0 and G: 9.0.

3. References and Notes

1 (a) Hirst, A. R.; Escuder, B; Miravet, J. F.; Smith, D. K. *Angew. Chem. Int. Ed.* **2008**, *47*, 8002. (b) van Esch, J. H.; Feringa, B. L. *Angew. Chem. Int. Ed.* **2000**, *39*, 2263. (c) Fages, F. *Top. Curr. Chem.* **2005**, *256*, 1. (d)

Sangeetha, N. M.; Maitra, U. *Chem. Soc. Rev.* **2005**, *34*, 821. (e) Estroff, L. A.; Hamilton, A. D. *Chem. Rev.* **2004**, *104*, 1201.

2 Gesser, H. D.; Goswami, P. C. *Chem. Rev.* **1989**, *89*, 765.

3 (a) Daganli, R. *Chem & Eng. News*, **1997**, *23*, 26. (b) Dorski, C. M.; Doyle, F. J.; Peppas, N. A. *Polym. Mater. Sci. Eng. Proc.* **1997**, *76*, 281. (c) Boury, B.; Corriu, R. J. P.; Le Strat, V.; Delord, P.; Nobili, M. *Angew. Chem. Int. Ed.* **1999**, *38*, 3172.

4 (a) Naota, T.; Koori, H. *J. Am. Chem. Soc.* **2005**, *127*, 9324. (b) Anderson, K. M.; Day, G. M.; Paterson, M. J.; Byrne, P.; Clarke, N.; Steed, J. W. *Angew. Chem. Int. Ed.* **2008**, *47*, 1058.

5 Chung, J. W.; An, B.-K.; Park, S. Y. *Chem. Mater.* **2008**, *20*, 6750.

6 (a) Sugiyasu, K.; Fujita, N.; Takeuchi, M.; Yamada, S.; Shinkai, S. *Org. Biomol. Chem.* **2003**, *1*, 895. (b) Sako, Y.; Takaguchi, Y. *Org. Biomol. Chem.* **2008**, *6*, 3843.

7 Ghoussoub, A.; Lehn, J.-M. *Chem. Commun.* **2005**, 5763.

8 (a) Zhang, Y.; Gu, H.; Yang, Z.; Xu, B. *J. Am. Chem. Soc.* **2003**, *125*, 13680. (b) Bhuniya, S.; Kim, B. H. *Chem. Commun.* **2006**, 1842.

9 (a) Sreenivasachary, N.; Lehn, J.-M. *Proc. Natl. Acad. Sci. U.S.A.* **2005**, *102*, 5938. (b) Fages, F. *Angew. Chem. Int. Ed.* **2006**, *45*, 1680.

10 Maeda, H. *Chem. Eur. J.* **2008**, *14*, 11274.

11 (a) Piepenbrock, M. O. M.; Lloyd, G. O.; Clarke, N.; Steed, J. W. *Chem. Rev.* **2010**, *110*, 1960. (b) Steed, J. W. *Chem. Soc. Rev.* **2010**, *39*, 3686. (c) Suzuki, M.; Hanabusa, K. *Chem. Soc. Rev.* **2010**, *39*, 455. (d) Suzuki, M.; Hanabusa, K. *Chem. Soc. Rev.* **2010**, *39*, 5067.

12 (a) Adams, D. J. *Macromol. Biosci.* **2011**, *11*, 160. (b) Dawn, A.; Shiraki, T.; Haraguchi, S.; Tamaru, S.; Shinkai, S. *Chem. Asian. J.* **2011**, *6*, 266. (c) Diaz, D. D.; Kuhbeck, D.; Koopmans, R. J. *Chem. Soc. Rev.* **2011**, *40*, 427.

13 (a) Kawano, S.-I.; Fujita, N.; Shinkai, S. *Chem. Eur. J.* **2005**, *11*, 4735. (b) Kitahara, T.; Shirakawa, M.; kawano, S.-I.; Beginn, U.; Fujita, N.; Shinkai, S. *J. Am. Chem. Soc.* **2005**, *127*, 14980. (c) Liu, J.; He, P.; Yan, J.; Fang, X.; Peng, J.; Liu, K.; Fang, Y. *Adv. Mater.* **2008**, **20**, 2508.

14 Gustafsson, B.; Håkansson, M.; Jagner, S. *New J. Chem.* **2003**, *27*, 459.

15 (a) Pease, A. R.; Jeppesen, J. O.; Stoddart, J. F.; Luo, Y.; Collier, C. P.; Heath, J. R. *Acc. Chem. Res*. **2001**, *34*, 433. (b) Jeppesen, J.; Nielsen, M.; Becher, J. *Chem. Rev.* **2004**, *104*, 5115. (c) Martín, N.; Sánchez, L.; Herranz, M. A.; Illescas, B.; Guldi, D. *Acc. Chem. Res.* **2007**, *40*, 1015. (d) Dichtel, W.; Mijanić, O.; Zhang, W.; Spruell, J.; Patel, K.; Aprahamian, I.; Health, J.; Stoddart, J. *Acc. Chem. Res.* **2008**, *41*, 1750.

16 Wang, C.; Zhang, D.; Zhu, D. *J. Am. Chem. Soc.* **2005**, *127*, 16372.

17 (a) Fery-Forgues, S.; Delavaux-Nicot, B. *J. Photochem. Photobiol. A*, **2000**, *132*, 137. (b) Medina, J. C.; Gay, I.; Chen, Z. H.; Echegoyen, L.; Gokel, G. W. *J. Am. Chem. Soc.* **1991**, *113*, 365. (c) Wang, K.; Muñoz, S.; Zhang, L. T.; Castro, R.; Kaifer, A. E.; Gokel, G. W. *J. Am. Chem. Soc.* **1996**, *118*, 6707.

18 Liu, J.; He, P.; Yan, J.; Fang, X.; Peng, J.; Liu, K.; Fang, Y. *Adv. Mater.* **2008**, *20*, 2508.

19 Peng, F.; Li, G. Z.; Liu, X. X.; Wu, S. Z.; Tong, Z. *J. Am. Chem. Soc*. 2008, 130, 16166.

20 Chujo, Y.; Sada, K.; Saegusa, T. *Macromolecules*, **1993**, *26*, 6320.

21 (a) Fei, S. T.; Phelps, M. V. B.; Wang, Y.; Barrett, E.; Gandhi, F.; Allcock, H. R. *Soft Matter*, **2006**, *2*, 397. (b) Kawano, S.; Fujita, N.; Shinkai, S. *J. Am. Chem. Soc.* **2004**, *126*, 8592.

22 (a) Yoshida, R.; Takahashi, T.; Yamaguchi, T.; Ichijo, H. *J. Am. Chem. Soc.* **1996**, *118*, 5134. (b) Maeda, S.; Hara, T.; Sakai, R.; Yoshida, R.; Hashimoto, S. *Adv. Mater.* **2007**, *19*, 3480.

23 Mao, F.; Mano, N.; Heller, A. *J. Am. Chem. Soc.* **2003**, *125*, 4951.

24 (a) Yagai, Y.; Kitamura, A. *Chem. Soc. Rev.* **2008**, *37*, 1520. (b) Yagai, Y.; Karatsu, T.; Kitamura, A. *Chem. Eur. J.* **2005**, *11*, 4054. (c) Khetan, S.; Burdick, J. A. *Soft Matter*, **2011**, *7*, 830.

25 (a) Murata, K.; Aoki, M.; Suzuki, T.; Harada, T.; Kawabata, H.; Komori, T.; Ohseto, F.; Ueda, K.; Shinkai, S. *J. Am. Chem. Soc*. **1994**, *116*, 6664. (b) Yagai, S.; Nakajima, T.; Kishikawa, K.; Kohmoto, S.; Karatsu, T.; Kitamura, A. *J. Am. Chem. Soc.* **2005**, *127*, 11134. (c) Suzuki, T.; Shinkai, S.; Sada, K. *Adv. Mater.* **2006**, *18*, 1043. (d) Eastoe, J.; Sànchez-Dominguez, M.; Wyatt,

P.; Heenan, R. K. *Chem. Commun.* **2004**, 2608. (e) Ji, Y.; Kuang, G. C.; Jia, X. R.; Chen, E. Q.; Wang, B. B.; Li, W. S.; Wei, Y.; Lei, J. *Chem. Commun.* **2007**, 4233. (f) Kim, J. H.; Seo, M.; Kim, Y. J.; Kim, S. Y. *Langmuir*, **2009**, *25*, 1761.

26 (a) Geiger, C.; Stanescu, M.; Chen, L. H.; Whitten, D. G. *Langmuir*, **1999**, *15*, 2241. (b) Wang, R.; Geiger, C.; Chen, L. H.; Swanson, B.; Whitten, D. G. *J. Am. Chem. Soc.* **2000**, *122*, 2399.

27 Dugave, C.; Demange, L. *Chem. Rev.* **2003**, *103*, 2475.

28 (a) Terech, P.; Ostuni, E.; Weiss, R. G. *J. Phys. Chem.* **1996**, *100*, 3759. (b) Terech, P.; Furman, I.; Weiss, R. G. *J. Phys. Chem.* **1995**, *99*, 9558.

29 (a) Ahmed, S. A.; Sallenave, X.; Fages, F.; Mieden-Gundert, G.; Müller, W. M.; Müller, U.; Vögtle, F.; Pozzo, J.-L. *Langmuir*, **2002**, *18*, 7096. (b) Li, Y.; Wong, K. M.-C.; Tam, A. Y.-Y.; Wu, L.; Yam, V. W.-W. *Chem. Eur. J.* **2010**, *16*, 8690.

30 Katritzky, A. R.; Sakhuja, R.; Khelashvili, L.; Shanab, K. *J. Org. Chem.* **2009**, *74*, 3062.

31 Xiao, S.; Yi, T.; Li, F.; Huang, C. *Tetrahedron Lett.* **2005**, *46*, 9009.

32 Qiu, Z.; Yu, H.; Li, J.; Wang, Y.; Zhang, Y. *Chem. Commun.* **2009**, 3342.

33 Stibor, I. *Topics in Current Chemistry*, Springer-Verlag, Berlin, **2005**, *225*, pp. 238.

34 Webb, J. E. A.; Crossley, M. J.; Turner, P.; Thordarson, P. *J. Am. Chem. Soc.* **2007**, *129*, 7155.

35 Edwards, W.; Smith D. K. *Chem. Commun.* **2012**, *48*, 2767.

36 (a) Rodríguez-Llansola, F.; Miravet, J. F.; Escude, B. *Chem. Commun.* **2011**, *47*, 4706. (b) Rodríguez-Llansola, F.; Miravet, J. F.; Escude, B. *Chem. Commun.* **2009**, 7303.

37 Gao, J.; Wang, H.; Wang, L.; Wang, J.; Kong, D.; Yang, Z. *J. Am. Chem. Soc.* **2009**, *131*, 11286.

Section 1.
Reaction Based Gelation System Showing Fluorescence and Sol to Gel Transition for Fluoride Anion in Aqueous Media

1.1. Introduction

Self-assembled supramolecular gels consist of low molecular weight gelators (LMWGs) and solvent molecules, in which non-covalent interactions, such as hydrogen bonding, van der Waals interaction, π–π stacking, electrostatic force, and metal coordination, are crucial to forming three-dimensional networks.[1] Compared to gels derived from polymers or inorganic materials, self-assembled supramolecular gels made from LMWGs are relatively easy to modify to control their physical or optoelectronic properties.[2] Furthermore, the properties of gels derived from LMWGs can be tuned using the external stimuli that arise from reversible non-covalent interactions.[3]

In recent years, many researchers have shown an interest in the construction of anion-responsive supramolecular gels.[4] Among these, fluoride-responsive gels have received a great deal of attention because fluoride is involved in preventing dental caries and in medical treatment for

osteoporosis.[5] Fluoride and proton was reported to trigger gel-to-sol transition and fluorescence emission after interacting with bisurea-functionalized naphthalene organogelators.[6] In addition, organogelators made with urea,[7] oxalamide,[8] or hydrazide[9] was also reported to induce gel-to-sol transition and optical change after the addition of fluoride anion, because the amidic NHs of these organogelators could interact with the fluoride anions thus disrupting the effective hydrogen-bonding interactions between the gelators. However, because the amidic NHs in the organogelators could also interact with other anions, the initiation of their gel-to-sol transitions and optical changes would not necessarily be selective to fluoride.

Taking advantage of the selective cleavage of a Si–O bond by fluoride,[10] we developed "reaction-based gelators" **1** and **2** (**Scheme 1**) having a silyl ether protecting group and a fluorescent-signaling backbone[11,12] that can selectively detect fluoride anion by a formation of fluorescent gels in aqueous media.

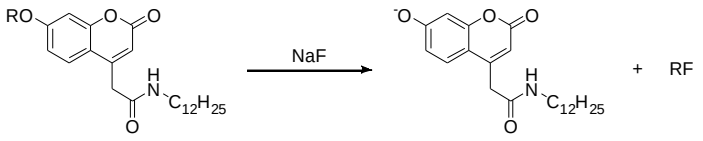

1: R = TBDMS (*tert*-Butyldimethylsilane)
2: R = TBDPS (*tert*-Butyldiphenylsilane)
3: R = H

Scheme 1. Molecular structures of silyl ether-based gelators **1**, **2** and **3**, and S–O bond cleavage by fluoride.

A simple silyl ether protection of a 7-hydroxycoumarin gelator (**3**) not only quenches its fluorescence emission but also prevents gelation. However, when the silyl ether protecting group is selectively cleaved by fluoride anion, the reaction triggers gelation and fluorescence emission. The effective

aggregation between gelators (**1** or **2**) is suppressed because the *tert*-butyldimethylsilane (TBDMS) and *tert*-butyldiphenylsilane (TBDPS) groups are relatively bulky. Therefore, removal of a bulky silyl ether protecting group by fluoride could induce gelation. At the same time, fluorescence emission increases as a result of a recovering intramolecular charge transfer (ICT) upon release of phenolate in coumarin.

1.2. Results and Discussion

Reaction-based gelator **1** was prepared by coupling 7-hydroxycoumarin-4-acetic acid with dodecylamine, after which a silyl ether moiety was attached by the reaction with *tert*-butyldimethylsilyl chloride.[13] We also prepared a control gelator, **3**, without a silyl ether moiety to examine whether or not 3 would form a gel. First, we tested the gelation behavior of **3** using varying solvent conditions. A white opaque gel was formed, but with little fluorescence emission, in a 1:1 methanol/water cosolvent[14] after cooling a hot solution of **3**. The critical gelation concentration for **3** was 0.25 wt%, and was determined using the upside-down method. We then tested the gelation ability of **1** at 0.6 wt%. **1** was fully dissolved in methanol, but when an equal amount of water was added to the methanol solution, a turbid solution formed. Although this turbid solution turned to a clear solution when heated, the clear solution turned turbid again after cooling to room temperature. As expected, the bulky TBDMS prevented gelator **1** from aggregating in an orderly way and forming gels. In the presence of 1.0 equivalent of F^-, however, an opaque gel was formed, similar to that formed with gelator **3** (**Figure 1a**). Interestingly, although the turbid solution of **1** and the gel of **3** showed little fluorescence emission, upon the addition of fluoride to gelator **1**, the intensity

of the fluorescence emission increased dramatically (**Figure 1b**). This sol-to-gel transition induced by fluoride occurs as a result of the effective aggregation of gelators, which is made possible by the cleavage of a silyl ether group. This cleavage also results in a large enhancement of fluorescence as a result of ICT recovery. Another reaction-based gelator, **2,** behaved similarly, but was not as soluble as **1** in the same cosolvent system, and a higher concentration was necessary for gel formation.

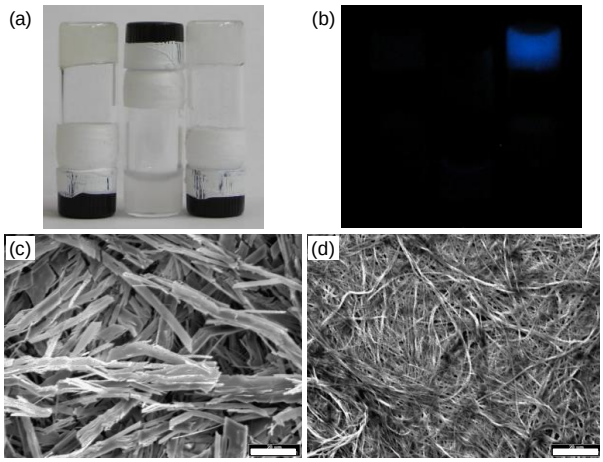

Figure 1. (a) Photograph and (b) fluorescence photograph of 3 (0.6 wt%), **1** (0.6 wt%), and **1** + F^- (0.6 wt% of **1**, 1.0 equiv. of NaF) in a 1:1 methanol/10 mM HEPES buffer (pH 7.4) solvent. Fluorescence emission was observed on excitation by UV irradiation (λ_{ex} = 365 nm). SEM images of (c) **3** and (d) **1** + F^- in the same cosolvent system. Scale bar = 20 μm.

SEM images of the xerogel of **3** and **1** + F^- exhibited bundles of fibrous structures of different sizes (**Figure 1c, d**). To examine differences in the self-assembled structures and fluorescence properties, we performed wide-angle X-ray scattering (WAXS) and ^{1}H NMR analysis. The ^{1}H NMR spectra of the xerogel of **1** + F^- indicated that the silyl ether protecting groups were not

completely cleaved by F^- (**Figure 2**). Residual signals representing **1** were still observed even after heating with F^-. This partial removal of the silyl ether protecting groups seemed to influence the fluorescence and gelation behaviors of **1** + F^-. When 1 was treated with 1.0 equivalent of NaF in a 1:1 mixture of methanol/water, non-fluorogenic **1** molecules (in which a TBDMS group remained intact) seemed to be intercalated between fluorogenic molecules formed by the removal of the silyl ethers on **1**. Therefore, the self-quenching effect, which arises from the complete aggregation of fluorescent coumarin moieties, was attenuated. This assumption was confirmed after investigating the self-assembled structures in a mixture of **1** and **3** in an appropriate ratio under the same gelation conditions. A 1:2 mixture of **1** and **3** formed gels that were fluorescent, but a 1:1 mixture of **1** and **3** did not form gels (**Figure 5**). In particular, gels derived from a 1:2 mixture of **1** and **3** at pH 9 demonstrated a stronger fluorescence emission than those formed at pH 7.4. Furthermore, gels formed after the complete removal of the TBDMS protecting groups on **1** by F^- showed relatively weak fluorescence, but the gels of **1** + F^- in which the TBDMS groups were not completely removed emitted a more intense fluorescence (**Figure 6**).

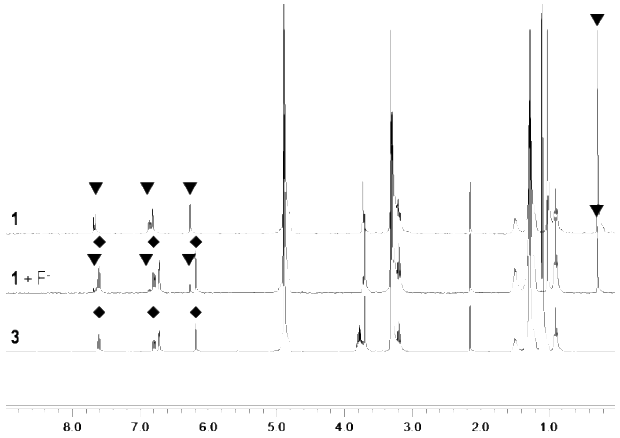

Figure 2. ^{1}H NMR spectra of **1**, **1** + F^- , and **3** in CD_3OD.

Since both of the self-assembled gels of **3** and **1** + F^- had similar X-ray scattering patterns, it was assumed that they had similar packing patterns (**Figure 7**). The alkyl chains of the gelators seemed to be fully intercalated with each other and the coumarin moieties interacted with each other via π–π interactions (**Figure 3**). **3** was extensively self-assembled and stacked up in an orderly way as a result of hydrogen bonding between amide groups and π-π interaction between coumarin units, which enabled the gelators to grow into large-sized fibers (**Figure 1c**). Similarly, in the case of **1** + F^-, **1** and deprotected **1** could exist in self-assembled fibrils. However, since the large silyl ether moieties on **1** remained partially intact and acted as obstacles to effective hydrogen bonding and π–π interactions between gelators, the fibers of **1** + F^- were relatively smaller than those of **3** (**Figure 1c, d**). Furthermore, the coumarin groups in the gels of **1** + F^- were not fully stacked because of the partially intact TBDMS groups, which prevented the regular stacking of the fluorescent 7-hydroxycoumarin groups and thus produced fluorescence in the gels of **1** + F^-.

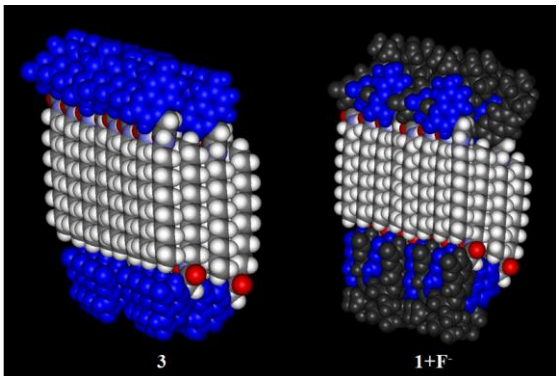

Figure 3. Proposed model of the self-assembled gelators **1** + F^- and **3**. Gelator **1** is shown in dark grey and gelator **3** is shown in blue. Gelators **1** and **3** alternate with each other and are arranged in an antiparallel fashion.

To confirm the selective response of **1** to fluoride anions, gelation behavior was investigated upon the addition of various other anions. In contrast to fluoride, Cl^-, Br^-, I^-, $H_2PO_4^-$, AcO^-, NO_3^-, ClO_4^- and N_3^- did not induce gelation or fluorescence enhancement using the same solvent conditions. These anions produced clear solution upon heating, but only yielded turbid solution after cooling. Only the fluoride anions induced both gelation and fluorescence enhancement (**Figure 4**). The other anions did not break the Si–O bond in the coumarin and, therefore, did not lead to gel formation or fluorescence emission.

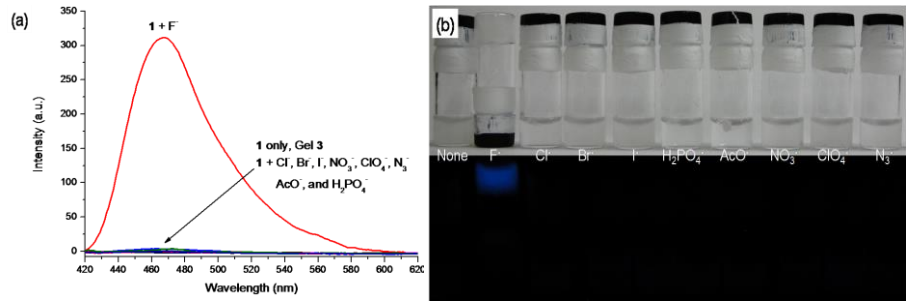

Figure 4. (a) Fluorescence spectra (λ_{ex} = 405 nm) and (b) photograph and fluorescence emission (λ_{ex} = 365 nm) of **1** (0.6 wt% in 1:1 MeOH/H_2O) in the presence of each anion (1 equivalent of NaX was used for the anion tests).

1.3. Conclusion

In conclusion, we developed reaction-based gelators which turn into fluorescent gels in aqueous solution when their silanol protecting groups are cleaved by fluoride anion. The above-mentioned system is highly selective to fluoride and exhibits both gelation and strong fluorescence as optical signals. This selectivity is a result of the affinity between fluoride and silanol

derivatives, which distinguishes this system from the amide-based fluoride-responsive gel systems previously reported.

1.4. Experimental

1.4.1. Instrumentation

^{1}H and ^{13}C NMR spectra were recorded using either a Bruker Advance DPX-300 or a Bruker Advance 500 spectrometer. Chemical shifts are given in parts per million using as internal reference the residual resonances of deuterated solvents (δ = in $CDCl_3$, CD_3OD and DMSO-d_6 (^{1}H NMR chemical shifts: δ = 7.27 ppm for $CDCl_3$, δ = 3.31 ppm for CD_3OD and δ = 2.50 ppm for $(CD_3)_2SO$). The XWINNMR program was used for the pulse program. Analytical thin-layer chromatography was performed using Kieselgel 60_F-254 plates from Merck. Column chromatography was carried out on Merck silica gel 60 (70 - 230 mesh). GC-MS was performed with a JEOL JMS-AX505WA and a HP 5890 Series II using the FAB method. UV/vis spectra were collected on a Beckman DU-800. Phosphorescence spectra were recorded on a Jasco FP-6500 spectrophotometer. Scanning electron microscope (SEM) images were observed with a JEOL-JSM 5410LV. Wide angle X-ray scattering (WAXS) analysis was performed with a Bruker GADDS.

1.4.2. Materials

All reagents were purchased from either sigma-aldrich or TCI and used without any further purification. Deuterated solvents were acquired from cambridge isotopic laboratories

1.4.3. Preparation of Gelators

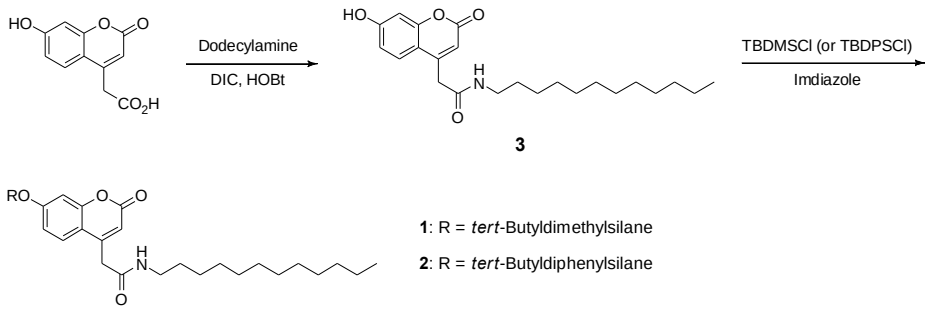

Scheme 2. Synthetic scheme for **1–3**.

7-Hydroxycoumarin-4-dodecylacetamide (3): To a solution of 7-hydroxycoumarin-4-acetic acid (619 mg, 2.81 mmol) and 1.0 equiv. of 1-hydroxybenzotriazole (382 mg, 2.83 mmol) in 20 mL THF, 1.1 equiv. of *N*,*N*′-diisopropylcarbodiimide (0.48 mL, 3.1 mmol) were added, followed by the addition of 1.0 equiv. of dodecylamine (530 mg, 2.86 mmol). After the yellowish reaction mixture was stirred at room temperature overnight, the mixture was concentrated. The residue was dissolved in ethyl acetate and washed with 1N HCl and brine. The solution was dried over Na_2SO_4 and concentrated *in vacuo*. Purification by silica-column chromatography (CH_2Cl_2 to CH_2Cl_2:MeOH = 50:1) was conducted to give **3** as white solid (553 mg, 41.2 % yield).

^{1}H NMR (300 MHz, DMSO-d_6): δ 0.85 (t, J = 6.90 Hz, 3H), 1.21–1.23 (m, 18H), 1.38 (t, 2H), 3.04 (q, J = 5.91 Hz, 2H), 3.59 (s, 2H), 6.09 (s, 1H), 6.64 (s, 1H), 6.71 (d, J = 8.64 Hz, 1H), 7.56 (d, J = 8.73 Hz, 1H), 8.16 (t, J = 5.34 Hz, 1H).

^{13}C NMR (75 MHz, DMSO-d_6): δ 13.92, 22.06, 23.26, 26.29, 28.68, 28.88, 28.94, 28.97, 29.01, 31.26, 38.67, 38.92, 39.77, 102.26, 111.38, 111.57, 112.81, 126.63, 151.28, 155.01, 160.22, 161.27, 167.35.

HR-MS (FAB+): *m*/*z* calculated. for $C_{23}H_{34}NO_4$ $[M + H]^+$: 388.2488, found: 388.2488.

7-*tert*-Butyldimethylsiloxycoumarin-4-dodceylacetamide (1): To a mixture of **3** (201 mg, 0.52 mmol) and imidazole (114 mg, 1.68 mmol) in 2 mL DMF, *tert*-butyldimethylchlorosilane (97 mg, 0.65 mmol) was added and the reaction mixture was stirred at r.t. for 6 hrs. A white turbid solution was formed after the addition of about 50 mL of water. The addition of ethyl acetate was followed by washing with a large volume of water several times to give a solution, which was dried over anhydrous Na_2SO_4 and concentrated. After silica-column chromatography (CH_2Cl_2 to CH_2Cl_2:MeOH = 100:1), the light yellowish solid **1** was obtained (191 mg, 73.4% yield).

^{1}H NMR (300 MHz, $CDCl_3$): δ 0.27 (s, 6H), 0.89 (t, J = 6.79 Hz, 3H), 1.00 (s, 9H), 1.23–1.31 (m, 18H), 1.45 (t, J = 6.17 Hz, 2H), 3.24 (q, J = 6.67 Hz, 2H), 3.66 (s, 2H), 5.56 (t, 1H), 6.24 (s, 1H), 6.79 (d, J = 2.35 Hz, 1H), 6.82 (s, 1H), 7.56 (d, J = 9.43 Hz, 1H).

^{13}C NMR (75 MHz, $CDCl_3$): δ 14.14, 18.26, 22.70, 25.55, 26.81, 29.22, 29.36, 29.52, 29.58, 29.64, 31.92, 40.03, 40.95, 107.89, 112.96, 113.66, 117.59, 126.02, 149.65, 155.28, 159.73, 160.95, 167.29.

HR-MS (FAB+): *m*/*z* calculated. for $C_{29}H_{48}NO_4Si$ $[M + H]^+$: 502.3353, found: 502.3342.

7-*tert*-Butyldiphenylsiloxycoumarin-4-dodecylacetamide (2): The synthetic procedure for the production of **2** was identical to that of **1**, except that *tert*-butyldiphenylchlorosilane was used instead of *tert*-butyldimethylchlorosilane, to give **2** as a yellow liquid (333 mg, 77.7% yield).

^{1}H NMR (300 MHz, $CDCl_3$): δ 0.89 (t, J = 6.70 Hz, 3H), 1.12 (s, 9H), 1.24–1.26 (m, 18H), 1.42 (t, J = 6.39 Hz, 2H), 3.21 (q, J = 6.64 Hz, 2H), 3.59 (s,

2H), 5.49 (t, 1H), 6.69 (s, 1H), 6.76 (d, J = 6.41 Hz, 1H), 7.38–7.47 (m, 7H), 7.71 (d, J = 7.12 Hz, 4H).

^{13}C NMR (125 MHz, $CDCl_3$): δ 14.16, 19.45, 22.71, 26.79, 29.20, 29.36, 29.52, 29.59, 29.65, 31.93, 40.00, 40.85, 107.86, 112.83, 113.63,117.35, 125.75, 128.05, 130.37, 131.60, 135.38, 149.49, 155.03, 159.47, 160.89, 167.20.

HR-MS (FAB+): m/z calculated. for $C_{39}H_{52}NO_4Si$ $[M+H]^+$: 626.3666, found: 626.3657.

1.4.4. Self-Assembling Process and Behaviors

Gelators in a 1:1 (v/v) mixture of MeOH and a 10 mM HEPES buffer solution (pH 7.4) were heated until the solutions were clear. The clear solutions turned immediately to turbid gels or precipitates when cooled to room temperature. For the anion tests, an appropriate amount of NaX dissolved in a buffer solution (10 mM HEPES buffer, pH 7.4) was added to a suspension of **1** in methanol.

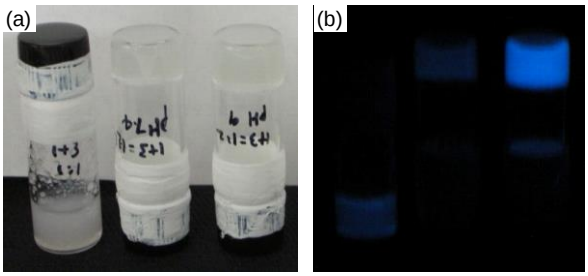

Figure 5. (a) Gelation behavior of 1:1 (pH 7.4), 1:2 (pH 7.4), and 1:2 (pH 9.0) mixture of **1** and **3**, and (b) corresponding fluorescence emission photograph (λ_{ex} = 365 nm) in 1:1 mixtures of MeOH and the corresponding buffer solution (10 mM HEPES buffer for pH 7.4; CHES buffer for pH 9.0).

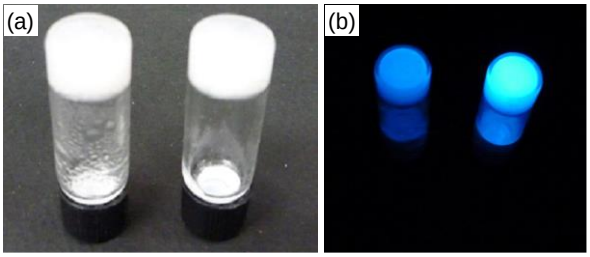

Figure 6. (a) Gelation behavior of **1** when the TBDMS protecting groups were completely removed by F^- (left) or were partially removed by F^- by the general gelation procedure (right), and (b) the corresponding fluorescence emission photographs (λ_{ex} = 365 nm).

1.4.5. Preparation Specimen for Electron Microscope Analysis

Gels were diluted with 500 μL of the cosolvent (MeOH:deionized water = 1:1, v/v). The diluted suspensions were dropped onto glass slides, and then dried in air. The prepared specimens were coated with Au.

1.4.6. Wide Angle X-ray Scattering Analysis

Gels were diluted with 500 μL of the cosolvent (MeOH:deionized water = 1:1, v/v) and the resulting suspensions were dried in air at room temperature and concentrated *in vacuo* to remove any remaining solvent. The diffraction step size was 0.02, and the scan speed was 1°/min. The wavelength of the X-rays was 1.5406 Å (generated at 40 kV, and 40 mA).

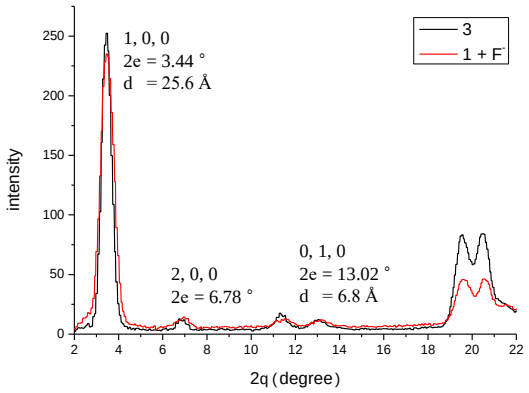

Figure 7. Wide-angle X-ray scattering (WAXS) patterns of **3** and **1** + F^-.

1.4.7. Preparation Sample for ^{1}H NMR Analysis

The gelation of **1** + F^- was carried out according to the general procedure described previously. N_2 gas was blown on the obtained gels to remove methanol. The concentrated gels were further dried using a freeze dryer (Labconco's Freeze Dryer-18 and Sin's FD5508). The obtained xerogel were dissolved in methylene chloride, and then washed twice with 1 N HCl to suppress any further reaction. The remaining organic phase was dried with Na_2SO_4, and then concentrated *in vacuo*. ^{1}H NMR analysis was performed using the resulting **1** + F^- sample in CD_3OD.

1.5. References and Notes

Miae Park, Donghak Jang, Soon Young Kim and Jong-In Hong, *New J. Chem.*, **2012**, *36*, 1145-1148.

1 (a) Venula, P. K.; Li, J.; John, G. *J. Am. Chem. Soc.* **2006**, *128*, 8932. (b) Wada, A.; Tamaru, S.; Ikeda, M.; Hamachi, I. *J. Am. Chem. Soc.* **2009**, *131*, 5321. (c) Jayawama, V.; Ali, M.; Jowitt, T. A.; Miler, A. E.; Saiani, A.;

Gough, J. E.; Jlijin, R. V. *Adv. Mater.* **2006**, *18*, 611.

2 (a) Lloyd, G. O.; Steed, J. W. *Nat. Chem.* **2009**, *1*, 437. (b) Maeda, H. *Chem. Eur. J.* **2008**, *14*, 11274. (c) Yamanaka, M.; Nakamura, T.; Nakagawa, T.; Itagaki, H. *Tetrahderon Lett.* **2007**, *48*, 8990. (d) Varghese, R.; George, S. J.; Ajayaghosh, A. *Chem. Commun.* **2005**, 593. (e) Piepenbrock, M.-O. M.; Lloyd, G. O.; Clarke, N.; Steed, J. W. *Chem. Commun.* **2008**, 2644.

3 (a) Sangeetha, N. M.; Maitra, U. *Chem. Soc. Rev.* **2005**, *34*, 821. (b) Hwang, I.; Jeon, W. S.; Kim, H.-J.; Kim, D.; Kim, H.; Selvapalam, N.; Fujita, N.; Shinkai, S.; Kim, K. *Angew. Chem., Int. Ed.* **2007**, *46*, 210. (c) Eastoe, J.; Sánchez-Dominguez, M.; Wyatt, P.; Heenan, R. K. *Chem. Commun.* **2004**, 2608. (d) Gao, J.; Wang, H.; Wang, L.; Wang, J.; Kong, D.; Yang, Z. *J. Am. Chem. Soc.* **2009**, *131*, 11286. (e) Wang, C.; Chen, Q.; Sun, F.; Zhang, D.; Zhang, G.; Huang, Y.; Zhao, R.; Zhu, D. *J. Am. Chem. Soc.* **2010**, *132*, 3092.

4 (a) Piepenbrock, M.-O. M.; Lloyd, G. O.; Clarke, N.; Steed, J. W. *Chem. Rev.* **2010**, *110*, 1960. (b) Piepenbrock, M.-O. M.; Lloyd, G. O.; Clarke, N.; Steed, J. W. *Chem. Commun.* **2008**, 2644. (c) Zhang, Y.-M.; Lin, Q.; Wei, T.-B.; Qin, X.-P.; Li, Y. *Chem. Commun.* **2009**, 6074.

5 (a) Kirk, K. L. *Biochemistry of the Halogens and Inorganic Halides*, Plenum Press, New York, **1991**, p.58. (b) Riggs, B. L. *Bone and Mineral Research, Annual 2*, Elsevier, Amsterdam, **1984**, pp.366-393.

6 Yang, H.; Yi, T.; Zhou, Z.; Zhou, Y.; Wu, J.; Xu, M.; Li, F.; Huang, C.; *Langmuir*, **2007**, *23*, 8224.

7 (a) Kim, T. H.; Choi, M. S.; Sohn, B.-H.; Lyoo, W. S.; Lee, T. S. *Chem. Commun.* **2008**, 2364. (b) Teng, M.; Kuang, G.; Jia, X.; Gao, M.; Li, Y.;

Wei, Y. *J. Mater. Chem.* **2009**, *19*, 5648. (c) Yamanaka, M.; Nakamura, T.; Nakagawa, T.; Itagaki, H. *Tetrahedron Lett.* **2007**, *48*, 8990.

8 Džolić, Z.; Cametti, M.; Cort, A. D.; Mandolini, L.; Žinić, M. *Chem. Commun.* **2007**, 3535.

9 Liu, J.-W.; Yang, Y.; Chen, C.-F.; Ma, J.-T. *Langmuir*, **2010**, *26*, 9040.

10 (a) Corey, E. J.; Snider, B. B. *J. Am. Chem. Soc.* **1972**, *94*, 2549. (b) Clarke, J. H. *Chem. Rev.* **1980**, *80*, 429; (c) Schmittling, E. A.; Sawyer, J. S. *Tetrahedron Lett.* **1991**, **32**, 7207.

11 Kim, S. Y.; Hong, J.-I. *Org. Lett.* **2007**, *9*, 3109.

12 Kim, S. Y.; Park, J.; Koh, M.; Park, S. B.; Hong, J.-I. *Chem. Commun.* **2009**, 4735.

13 See supporting information for details on the preparation and characterization of new compounds.

14 10 mM HEPES buffer (pH 7.4) was used.

Section 2.
Chemodosimetric Gelator Allows for the Visual Discriminating Homocysteine through Selective Fluorescent Gel Formation

2.1. Introduction

Biothiols, such as cysteine (Cys) and homocysteine (Hcy), are intriguing biologically active small molecules that are closely associated with several metabolic pathways.[1] Abnormal levels of Cys and Hcy induce changes in redox states, resulting in the development of various diseases. At high concentrations, products of Hcy auto-oxidation may damage endothelial cells by forming reactive oxygen intermediates.[2] The deficiency of Cys decreases the level of glutathione, which acts as a scavenger for reactive oxygen species, and results in liver damage.[3] Because Hcy and Cys have a wide range of effects on metabolic pathways, extensive research efforts are focused on the detection and discrimination of these two biothiols.

The majority of studies that sought to detect Hcy and Cys have failed in distinguishing these molecules because of their similar spatial arrangement and chemical reactivity.[4] Recently, several studies detected Cys by using

chemodosimetric probes through Michael-type reaction.[5] In contrast to Cys, a few methods enabled the selective discrimination of Hcy. They could detect Hcy over Cys through chemodosimetric[6], electrochemical[7] and self-assembling mechanism.[8] It is still necessary to develop a reliable strategy for distinguishing Hcy from Cys. The reports present method for the selective detection of Hcy by using a chemodosimetric gelator that self-assembles into a fluorescent gel upon the addition of Hcy.

Low molecular weight gelators are known to construct superstructures through the self-assembly of components in gelation systems.[9] In particular, target-responsive gelators have received much attention, because they have wide application and their structural changes can be easily detected. A self-assembling process can be controlled by external stimuli, such as introduction of additive,[10] induction of monomer structural changes,[11] and environmental changes.[12] The smallest change in the molecular structure of gelators may result in massive change in the self-assembling structures. We hypothesized that Hcy could be potentially distinguished from Cys if such strong and specific changes in the self-assembling process could be created. Herein, we report a novel strategy for discriminating Hcy based on chemodosimetric gelation system.

We recently synthesized a fluorescent probe for Hcy and Cys by using the condensation reaction between aldehyde and thiol.[13] The formyl moiety in the probe was changed into 5- and 6-membered cyclic thiaza-adducts as a result of the reaction with Cys and Hcy, respectively. Both adducts induced similar fluorescence changes, although they showed differences in interactions with themselves and solvent molecules, which suggested that they influenced the phase transition. Based on these differences, we designed

CHO-**1**, a chemodosimetric gelator that contained the formyl and *N*-dodecylacetamido moieties in the 7-hydroxycoumarin backbone (**Scheme 1**). The *N*-dodecylacetamido moiety in CHO-**1** adducts of Hcy and Cys initiated a self-assembling process through van der Waals and hydrogen bonding interactions. This self-assembling process was controlled by different hydrophilic head group in the CHO-**1** adduct. Through the phase transition that resulted from the controlled self-assembling process, we were able to differentiate between Hcy and Cys.

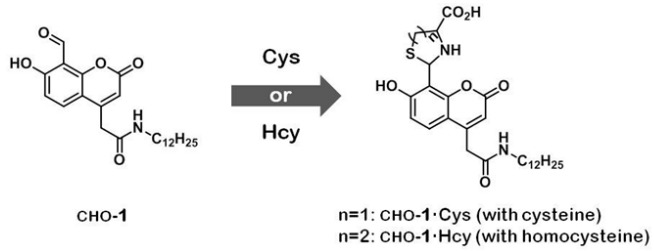

Scheme 1. Molecular structures of CHO-**1** and the adducts obtained as a result of condensation reaction with Hcy and Cys.

2.2. Results and Discussion

The chemodosimetric gelator CHO-**1** was synthesized from 7-hydroxycoumarin-4-acetic acid according to a previously described method.[14] First, we studied the self-assembling phenomena with and without Hcy and Cys. CHO-**1** itself did not dissolve in water even after heating to boiling temperature and adding a polar organic co-solvent such as ethanol. However, the addition of Cys (CHO-**1**•Cys) and Hcy (CHO-**1**•Hcy) induced changes in the solubility and self-assembling behavior. Heating a mixture of CHO-**1** and 2.0 equiv. Hcy in 1.0 M HEPES buffer and ethanol (1:2, v/v) produced a clear

solution. Interestingly, while the clear solution was allowed to cool to the ambient temperature, it turned cloudy and, finally, was transformed into a physical gel showing fluorescence (**Figure 1**). The sol-to-gel transition of CHO-**1**•Hcy occurred when the concentration of CHO-**1** was reduced to 2 mg/mL (5 mM) (**Figure 6**). As in the case with CHO-**1**•Hcy, we also observed the self-assembling behavior in the presence of Cys. However, the addition of Cys did not result in gelation, but only induced fluorescent precipitation. Thus, the chemodosimetric gelator, CHO-**1**, successfully discriminated Hcy from Cys through selective gelation of CHO-**1**•Hcy.

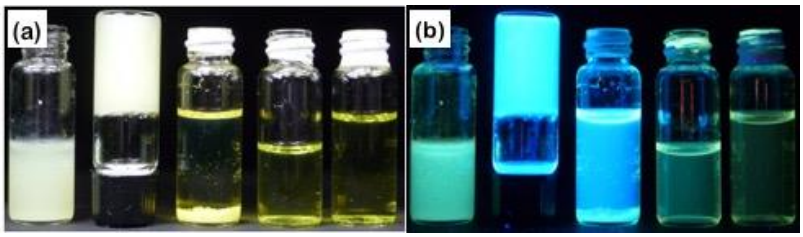

Figure 1. (a) Optical and (b) fluorescence image of the self-assembling behaviors of CHO-**1** (5 mg/mL, 12mM) with biothiols in HEPES buffer and ethanol (1:2 v/v). CHO-**1**, CHO-**1**•Hcy, CHO-**1**•Cys, CHO-**1**•GSH, and CHO-**1**•Met are indicated from left to right.

Fluorescence observed in the CHO-**1**•Hcy gel and CHO-**1**•Cys precipitate indicates that CHO-**1** formed 1,3-thiazinane and thiazolidine adducts with Hcy and Cys, respectively.[15] Their ^{1}H NMR spectra also confirmed the formation of thiaza cyclic adducts (**Figure 2**). Although these biothiols had similar chemical structures, the self-assembling process of CHO-**1**•Hcy was distinct from that of CHO-**1**•Cys. Scanning electron microscopy (SEM) images of xerogel and dry precipitates were analyzed to gain a better insight into differences between self-assembling behaviors of

CHO-**1**•Hcy and CHO-**1**•Cys. SEM images of CHO-**1**•Hcy and CHO-**1**•Cys revealed that both adducts self-assembled into fibrous microstructures (**Figure 3a, b**). It is noteworthy that the self-assembling fibers of CHO-**1**•Cys were thinner and thus, more tightly intertwined than those of CHO-**1**•Hcy, which resulted in the exclusion of solvent molecules from the networks of CHO-**1**•Cys fibers. This is why CHO-**1**•Cys precipitated. However, the self-assembling fibers of CHO-**1**•Hcy were thicker than those of CHO-**1**•Cys. In addition, CHO-**1**•Hcy fibers were intertwined, forming networks with relatively large cavities between fibers. Solvent molecules were stored within those cavities, possibly facilitating the transition of CHO-**1**•Hcy from sol to gel.

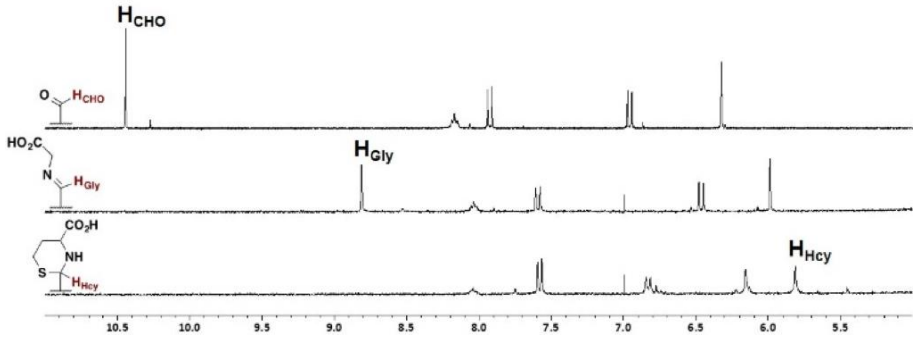

Figure 2. ^{1}H NMR spectrum of (top to bottom) CHO-**1**, CHO-**1**•Gly precipitate, and CHO-**1**•Hcy xerogel in DMSO-d_6, respectively.

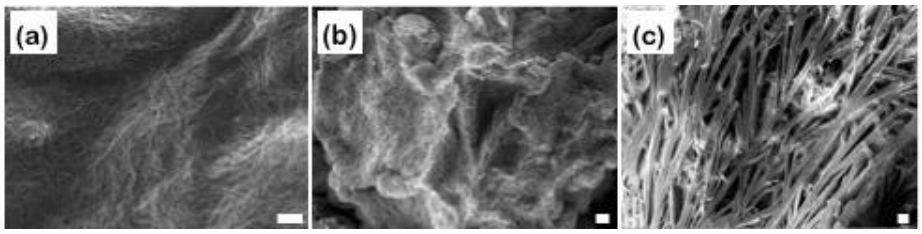

Figure 3. SEM images of (a) xerogel of CHO-**1**•Hcy (× 1000, scale bar = 20 μm), (b) dried precipitates of CHO-**1**•Cys (× 5000, scale bar = 2 μm), and (c)

CHO-**1**•Gly (scale bar = 20 μm).

Because biothiols and amino acids could react with the formyl moiety of CHO-**1**, we examined the effect of addition of biothiols and amino acids to CHO-**1** on the morphology of the resulting adducts. A mixture of glutathione (GSH) or methionine (Met) and CHO-**1** was dissolved in a mixture of HEPES buffer and ethanol (1:2, v/v) (**Figure 1a**) to give a yellow solution and a small amount of precipitate upon heating, which were not fluorescent (**Figure 1b**). Similar results were also observed after adding other amino acids. In particular, aspartic acid (Asp), glycine (Gly), lysine (Lys), serine (Ser), and glutamine (Gln) were selected as acidic, neutral, basic, nucleophilic, and amide species, respectively. The addition of these amino acids did not result in gelation or fluorescence emission. However, precipitation occurred upon the addition of Gly, Ser, or Lys (**Figure 4**).

Variations in the self-assembling behavior could be possibly attributed to the differences in adduct molecular structures. The complete reaction of other biothiols and amino acids with CHO-**1** resulted in the formation of imine intermediates, which was confirmed by the absence of fluorescence (**Figure 4b**) and characteristic ^{1}H NMR spectra (**Figure 7**). In contrast to the self-assembling behavior of CHO-**1**•Hcy cyclic thiaza adduct, the flexible non-cyclic imine adducts with other biothiols and amino acids are likely to self-assemble into well-stacked one-dimensional aggregates, and this was verified using SEM and wide-angle X-ray scattering (WAXS) analysis. SEM analysis of CHO-**1**•Gly revealed that the precipitates consisted of thick plate-like microstructures (**Figure 3c**), while the WAXS spectrum showed that CHO-**1**•Gly underwent self-assembly according to a lamellar pattern, which was

different from that observed in CHO-**1**•Hcy (**Figure 8**). Therefore, unlike CHO-**1**•Hcy, the imine-containing adducts were unable to self-assemble into physical gels.

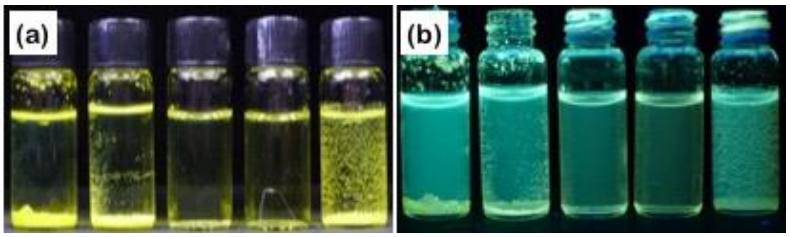

Figure 4. (a) Optical and (b) fluorescence image of the self-assembling behaviors of CHO-**1** (5 mg/mL, 12 mM) with amino acids (each 2.0 equiv. to gelator) in 1 M HEPES buffer and ethanol (1:2 v/v). CHO-**1**•Gly, CHO-**1**•Ser, CHO-**1**•Asp, CHO-**1**•Gln, and CHO-**1**•Lys are indicated from left to right.

2.3. Conclusion

In summary, we developed CHO-**1**, a chemodosimetric gelator, which selectively responded to Hcy through the formation of a thiaza cyclic adduct followed by self-assembly into a fluorescent gel. The use of other biothiols and amino acids did not result in gelation. Selective gelation feature of CHO-**1** was able to distinguish between Hcy and Cys, the molecules, which have a difference in only one carbon. This chemodosimetric gelation system could be thus used for differentiating a target analytes from other chemically and physically similar compounds.

2.4. Experimental

2.4.1. Instrumentation

The thin-layer chromatography for the reaction analysis was performed

with TLC silicagel 60 F_{254} plate from MERCK. The column chromatography for purification was performed with Merck silicagel 60 (70 – 230 mesh) from MERCK. ^{1}H and ^{13}C NMR spectra were measured on Bruker Advance 300 or 500 spectrometers. The XWINNMR program was used for the pulse program. GC-MS was performed with JEOL JMS-AX505WA and HP5890 Series II using the FAB method. SEM images were obtained using field-emission scanning electronic microscope (Carl Zeiss AURIGA).

2.4.2. Materials

All reagents were purchased from either sigma-aldrich or TCI and used without any further purification. Deuterated solvents were acquired from cambridge isotopic laboratories

2.4.3. Synthesis of CHO-1

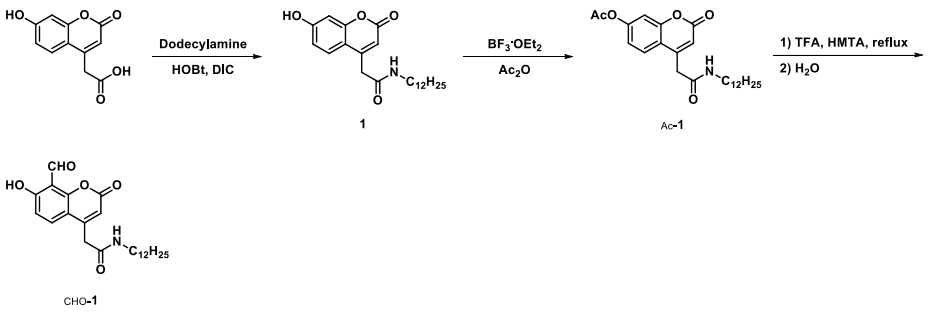

Scheme 2. Synthetic route of CHO-**1.**

7-Hydroxycoumarin-4-dodcylacetamide (1): To a solution of 7-hydroxycoumarin-4-acetic acid (619 mg, 2.81 mmol) and 1.0 equiv. of 1-hydroxybenzotriazole (382 mg, 2.83 mmol) in 20 mL THF, 1.1 equiv. of *N*,*N*′-diisopropylcarbodiimide (0.48 mL, 3.1 mmol) were added, followed by the addition of 1.0 equiv. of dodecylamine (530 mg, 2.86 mmol). After the

yellowish reaction mixture was stirred at room temperature overnight, the mixture was concentrated. The residue was dissolved in ethyl acetate and washed with 1 N HCl and brine. The solution was dried over Na_2SO_4 and concentrated *in vacuo*. Purification by silica-column chromatography (CH_2Cl_2 to CH_2Cl_2:MeOH = 50:1) was conducted to give **3** as white solid (553 mg, 41.2 % yield).

^{1}H NMR (300 MHz, DMSO-d_6): δ 0.85 (t, J = 6.90 Hz, 3H), 1.21–1.23 (m, 18H), 1.38 (t, 2H), 3.04 (q, J = 5.91 Hz, 2H), 3.59 (s, 2H), 6.09 (s, 1H), 6.64 (s, 1H), 6.71 (d, J = 8.64 Hz, 1H), 7.56 (d, J = 8.73 Hz, 1H), 8.16 (t, J = 5.34 Hz, 1H).

^{13}C NMR (75 MHz, DMSO-d_6): δ 13.92, 22.06, 23.26, 26.29, 28.68, 28.88, 28.94, 28.97, 29.01, 31.26, 38.67, 38.92, 39.77, 102.26, 111.38, 111.57, 112.81, 126.63, 151.28, 155.01, 160.22, 161.27, 167.35.

HR-MS (FAB+): *m*/*z* calculated. for $C_{23}H_{34}NO_4$ $[M + H]^+$: 388.2488, found: 388.2488.

7-Acetoxycoumarin-4-dodecylacetamide (Ac-1): $BF_3{\cdot}OEt_2$ (0.10 mL, catalytic amount) was added to a suspension of 7-hydroxycoumarin-4-dodceylacetamide (210 mg, 0.50 mmol) in acetic anhydride (5 mL). The resulting clear solution was stirred at room temperature for 3 hrs. Distilled water (10 mL) was carefully added, and then, the reaction mixture turned into suspension. The organic phase was washed successively with water and brine, dried with Na_2SO_4, and concentrated in vacuo. The residue was purified using SiO_2 column chromatography, eluting with CH_2Cl_2 and then 1 % methanol in CH_2Cl_2. Ac-**1** was further purified via recrystallization from methanol to give a white solid (210 mg, 90 % yield). ^{1}H NMR (400 MHz, $CDCl_3$): δ = 0.86 (3H, J = 6.8 Hz, t), 1.21-1.23 (18H, m), 2.32 (3H, s), 3.21 (2H, J = 6.4 Hz, q),

3.65 (2H, s), 5.53 (1H, bs), 6.34 (1H, s), 7.05 (1H, J = 2.4, 6.4 Hz, dd), 7.12 (1H, s), 7.68 (1H, J = 8.8 Hz, d).

^{13}C NMR (100 MHz, $CDCl_3$): δ = 14.1, 21.1, 22.7, 26.8, 29.2, 29.3, 29.4, 29.5, 29.6, 31.9, 40.1, 40.9, 110.7, 116.1, 116.6, 118.5, 125.9, 149.0, 153.5, 154.4, 160.0, 166.9, 168.6.

HR-MS (FAB+) *m/z*: calculated. for $C_{25}H_{36}NO_5$, 430.2593; found m/z, 430.2597.

8-Formyl-7-hydroxycoumarin-4-dodecylacetamide (CHO-**1):** 7-Acetoxycoumarin-4-dodecylacetamide (Ac-1, 210 mg, 0.5 mmol) and hexamethylenetetramine (HMTA, 300 mg, 2.2 mmol) were dissolved in 10 mL trifluoroacetic acid. The mixture was heated at reflux with stirring for 6 hrs, and then cooled to room temperature. The solvent was evaporated, and then H_2O (20 mL) was added. The resulting yellow suspension was stirred overnight. The suspension was filtered and washed with H_2O. The solid was recrystallized with MeOH, and then washed with ethylacetate and diethyl ether (70 mg, 34 % yield).

^{1}H NMR (400 MHz, $CDCl_3$): δ 0.86 (t, J = 6.8 Hz, 3H), 1.21-1.27 (m, 18H), 1.45 (m, 2H), 3.22 (q, J = 6.8 Hz, 2H), 3.62 (s, 2H), 5.54 (bs, 1H), 6.25 (s, 1H), 6.89 (d, J = 8.8 Hz, 1H), 7.81 (d, J = 9.2 Hz, 1H), 10.59 (s, 1H), 12.24 (s, 1H)

^{13}C NMR (100 MHz, $CDCl_3$): δ 14.08, 22.65, 26.80, 29.16, 29.30, 29.39, 29.49, 29.52, 29.58, 29.59, 30.91, 31.89, 40.13, 40.93, 108.71, 110.89, 113.45, 114.73, 133.43, 149.72, 158.80, 165.65, 166.64, 193.17.

HR-MS (FAB+): *m/z* calculated. for $C_{24}H_{34}NO_5$ 416.2437, found 416.2433

2.4.4. Self-assembling Behaviors

Chemodosimetric gelator CHO-**1** was suspended in ethanol. To the suspension, 2.0 equivalent cysteine and homocysteine in 1 M HEPES buffer (pH 7.40) was added in 2:1 volume ratio of EtOH and 1 M HEPES buffer. The mixture was heated until turning to clear solution. The clear solution was cooled to room temperature by standing on table. This solution was turned to gel or precipitate until cooling to room temperature. Self-assembled behavior of other biothiols and amino acids was confirmed in the same way as above.

Table 1. Self-assembling behavior of CHO-**1** with cysteine and homocysteine in various solvent systems.

Self-assembled condition		Phase
Gelator	**Biothiol**	
5 mg CHO-**1** in 530 uL MeOH	2.0 eq. Homocysteine in 270 uL H_2O[a]	Gel
5 mg CHO-**1** in 530 uL EtOH	2.0 eq. Homocysteine in 270 uL H_2O[a]	Gel
5 mg CHO-**1** in 530 uL PrOH	2.0 eq. Homocysteine in 270 uL H_2O[a]	Phase seperation
5 mg CHO-**1** in 530 uL MeOH	2.0 eq. Cysteine in 270 uL H_2O[a]	precipitate
5 mg CHO-**1** in 530 uL EtOH	2.0 eq. Cysteine in 270 uL H_2O[a]	precipitate

a) 1 M HEPES buffer (pH 7.40)

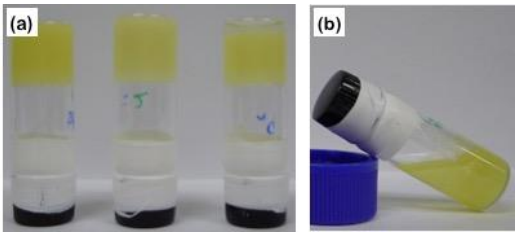

Figure 5. Optical images of self-assembling behavior of CHO-**1** with (a) homocysteine in 1 M HEPES buffer containing 50 vol % MeOH, EtOH, and n-PrOH, from left vials and (b) cysteine in 50 vol % MeOH.

The gelation concentration of CHO-**1**·Hcy was determined using the tube

inversion method. Volume of solvent mixture was increasingly added to the fixe d amount of CHO-**1** while maintaining a 2:1 volume ratio of EtOH and 1 M HEPES buffer**.**

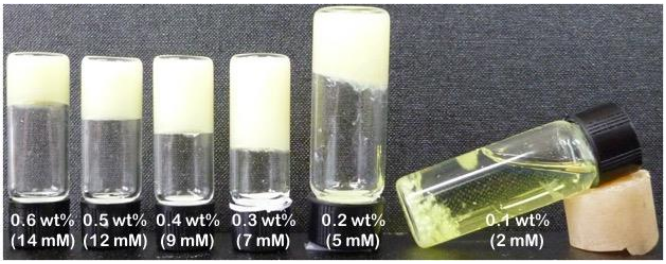

Figure 6. Gelation concentration of CHO-**1** with homocysteine (2 equiv.) in EtOH + 1 M HEPES buffer (pH 7.40).

2.4.5. NMR Analysis

A mixture of CHO-**1** and an analytes (homocysteine, cysteine, or glycine) were dried using a freeze dryer (Labconco`s Freeze Dryer-18 and Sin`s FD5508). NMR spectra were obtained for each mixture dissolved in DMSO-d_6.

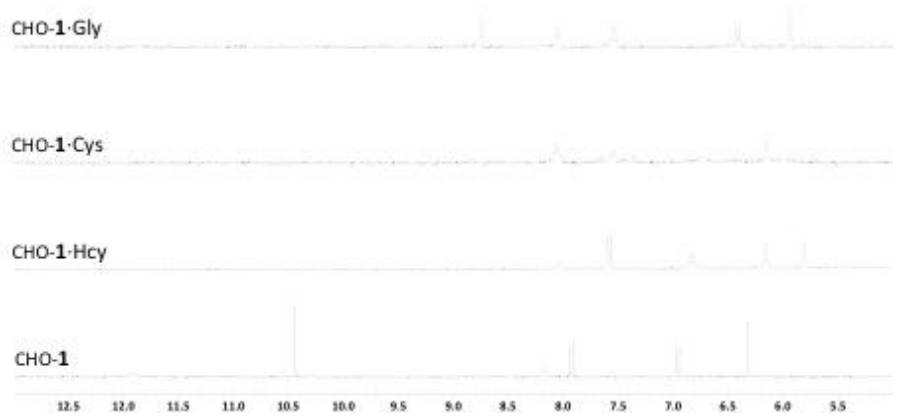

Figure 7. ^{1}H NMR spectra of xerogel or precipitate of CHO-**1**, CHO-**1**▪Gly, CHO-**1**▪Cys and CHO-**1**▪Hcy in DMSO-d_6.

2.4.6. Wide-angle X-ray scattering (WAXS) Analysis

Gels and precipitates were dried in air, and then further dried *in vacuo* to remove any remained solvent. The dried samples were analyzed with Bruker GADDS. The wavelength of X-ray is 1.5406 Å .

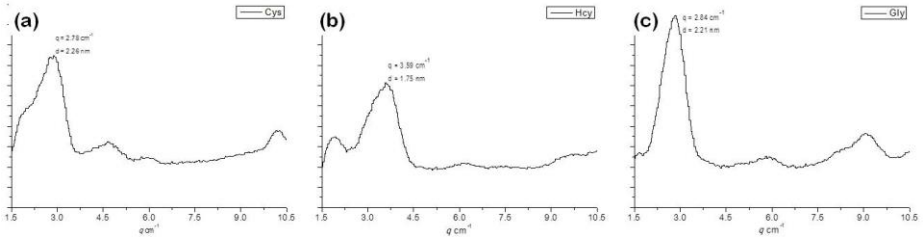

Figure 8. Wide-angle X-ray scattering spectrum of (a) CHO-**1**▪Cys, (b) CHO-**1**▪Hcy, and (c) CHO-**1**▪Gly.

2.5. References and Notes

Donghak Jang, Kyung-Sik Lee and Jong-In Hong, *manuscript* in preparation

1 (a) Wood, Z. A.; Schröder, E.; Harris, J. R.; Poole, L. B. *Trends Biochem. Sci.* **2003**, *28*, 32. (b) Schulz, J. B.; Lindenau, J.; Sevfried, J.; Dichgans, J. *Eur. J. Biochem.* **2000**, *267*, 4904. (c) Ball, R. O.; Courtney-Martin, G.; Pencharz, P. B. *J. Nutr.* **2006**, *136*, 1682S.

2 (a) Beije, B.; Arrhenius, E. *Chem.-biol. Interactions*, **1978**, *21*, 167. (b) Hidalgo, J.; Garvey, J. S.; Armario, A. *J. Pharmacol. Exp. Ther*. **1990**, *225*, 554. (c) Shahrokhians, S. *Anal. Chem.* **2001**, *73*, 5972. (d) Stipanuk, M. H.; Dominy Jr, J. E.; Lee, J.-I.; Coloso, R. M. *J. Nutr*. **2006**, *136*, 16525.

3 (a) McCully, K. S. *Ann. Clin. Lab. Sci.* **2009**, *39*, 219. (b) Zhang, C.; Cai, Y.; Adachi, M. T.; Oshiro, S.; Aso, T.; Kanufman, R. J.; Kitajima, S. *J. Biol. Chem.* **2001**, *276*, 35867. (c) McMahon, J. A.; Green, T. J.; Skeaff, C. M.; Knight, R. G.; Mann, J. I.; Williams, S. M. N. *N. Eng. J. Med.* **2006**, *354*, 2746.

4 (a) Rusin, O.; St. Luce, N. N.; Agbaria, R. A.; Escobedo, J. O.; Jiang, S.; Warner, I. M.; Dawan, F. B.; Lian, K.; Strongin, R. M. *J. Am. Chem. Soc.* **2004**, *126*, 438. (b) Chen, X.; Zhou, Y.; Peng, X.; Yoon, J. *Chem. Soc. Rev.* **2010**, *39*, 2120. (c) Yang, X.; Guo, Y.; Strongin, R. M. *Angew. Chem. Int. Ed.* **2011**, *50*, 10690. (d) Lim, S.-Y.; Yoon, D.-H.; Ha, D. Y.; Ahn, J.; Kim, D. I.; Kwon, H.; Ha, H.-J.; Kim, H.-J. *Sens. Actuator B Chem.* **2013**, *188*, 111. (e) Jung, H. S.; Pradhan, T.; Han, J. H.; Heo, K. J.; Lee, J. H.; Kang, C.; Kim, J. S. *Biomaterials*, **2012**, *33*, 8495. (f) Murale, D. P.; Kim, H.; Choi, W. S.; Churchill, D. G. *Org. Lett.* **2013**, *15*, 3630. (g) Yang, Y.-K.; Shin, S.; Tae, J. *Chem. Commun.* **2010**, *46*, 7766. (h) Ma, D. H.; Kim, D.; Seo, E.; Lee, S.-J.; Ahn, K. H. *Analyst*, **2015**, *140*, 422

5 (a) Yuan, L.; Lin, W.; Yang, Y. *Chem. Commun.* **2011**, *47*, 6275. (b) Zhou, X.; Jin, X.; Sun, G.; Wu, X. *Chem. Eur. J.* **2013**, *19*, 7817. (c) Wang, J.; Li, B.; Zhao, W.; Zhang, X.; Luo, X.; Corkins, M. E.; Cole, S. L.; Wang, C.; Xiao, Y.; Bi, X.; Pang, Y.; McElory, C. A.; Bird, A. J.; Dong, Y. *ACS Sens.* **2016**, *1*, 882.

6 (a) Wang, F.; Guo, Z.; Li, X.; Zhao, C. *Chem. Eur. J.* **2014**, *20*, 11471. (b) Wang, Y.-W.; Liu, S.-B.; Ling, W.-J.; Peng, Y. *Chem. Commun.* **2016**, *52*, 827. (c) Guo, F.; Tian, M.; Miao, F.; Zhang, W.; Song, G.; Liu, Y.; Yu, X.; Sun, J. Z.; Wong, W.-Y. *Org. Biomol. Chem.* **2013**, *11*, 7721. (d) Yue, Y.;

Huo, F.; Li, X.; Wen, Y.; Yi, T.; Salamanca, J.; Escobedo, J. O.; Strongin, R. M.; Yin, C. *Org. Lett.* **2017**, *19*, 82.

7 Wang, W.; Escobedo, J. O.; Lawrence, C. M.; Strongin, R. M. *J. Am. Chem. Soc.* **2004**, *126*, 3400.

8 (a) Lu, C.; Zu, Y. *Chem. Commun.* **2007**, 3871. (b) Lin, J.-H.; Chang, C.-W.; Tseng, W.-L. *Analyst*, **2010**, *135*, 104. (c) Sun, S.-K.; Wang, H.-F.; Yan, X.-P. *Chem. Commun.* **2011**, *47*, 3817.

9 (a) Estroff, L. A.; Hamilton, A. D. *Chem. Rev.* **2004**, *104*, 1201. (b) Sangeetha, N. M.; Maitra, U. *Chem. Soc. Rev.* **2005**, *34*, 821. (c) Jang, D.; Lee, H. Y.; Park, M.; Nam, S. R.; Hong, J.-I. *Chem. Eur. J.* **2010**, *16*, 4836.

10 (a) Piepenbrock, M.-O. M.; Lloyd, G. O.; Clarke, N.; Steed, J. W. *Chem. Rev.* **2010**, *110*, 1960. (b) Maeda, H. *Chem. Eur. J.* **2008**, *14*, 11274.

11 (a) Lee, H. Y.; Nam, S. R.; Hong, J.-I. *J. Am. Chem. Soc.* **2007**, *129*, 1040. (b) Duan, P.; Cao, H.; Liu, M. *Soft Matter*, **2014**, *10*, 5428. (c) Wang, C.; Chen, Q.; Sun, F.; Zhang D.; Zhang, G.; Huang, Y.; Zhao, R.; Zhu, D. *J. Am. Chem. Soc.* **2010**, *132*, 3092.

12 (a) Das, U. K.; Banerjee, S.; Dastidar, P. *Chem. Asian J.* **2014**, *9*, 2475. (b) Bai, S.; Debnath, S.; Javid, N.; Frederix, P. W. J. M.; Fleing, S.; Pappas, C.; Uljn, R. V. *Langmuir*, **2014**, *30*, 7576.

13 Lee, K.-S.; Kim, T.-K.; Lee, J. H.; Hong, J.-I. *Chem. Commun.* **2008**, 6173.

14 Park, M.; Jang, D.; Kim, S. Y.; Hong, J.-I. *New J. Chem.* **2012**, *36*, 11451.

국문 초록 (Abstract in Korean)

양친화성 화합물은 자기 조립 과정을 통해 다양한 형태의 나노 또는 마이크로 크기의 초분자 구조체를 형성할 수 있다. 양친화성 화합물의 자기 조립 과정은 분자 자체 또는 외부 환경 변화에 민감하게 반응하여 다른 방향으로 진행될 수 있다. 따라서 양친화성 화합물의 구조 변화 또는 외부 환경 제어를 통해 특정한 형태의 초분자 구조체를 얻을 수 있다. 이번 연구를 통해 양친화성 화합물의 자기 조립 과정을 이해하고, 이를 바탕으로 자기 조립 과정을 제어하여 다양한 형태의 초분자 구조체를 얻을 수 있었다. 더 나아가 자기 조립 과정 제어를 통해 단분자를 선택적으로 구분할 수 있는 기능성 화합물을 개발할 수 있었다.

Part I에서는, 양친화성 화합물의 화학 구조, 환경의 변화, 또는 첨가물에 의한 자기 조립 과정의 변화가 초분자 구조체의 형성에 끼치는 영향에 대해 연구하였다. 그리고 자기 조립 과정을 제어하여 여러 형태의 초분자 구조체를 얻을 수 있음을 확인하였다.

양친화성 화합물의 구조적 다양성을 유도하기 위해 terephthaloylbisalanine (TBA), dodecylamine (DA), 그리고 금속 양이온 (M^{2+})으로 구성된 three-component 시스템을 도입하였다. TBA와 DA 사이의 수소 결합에 의한 초분자 양친화성 화합물은 자기 조립 과정을 거쳐 나노 그리고 마이크로 크기의 초분자 구조체를 형성하였다. 실제 DA에 대한 TBA의 비율이 0.5 ~ 2.0으로 증가함에 따라 monoclinic, cloumn, 그리고 lamellar 형태의 자기 조립 과정을 거쳐 ribbon 형태의 구조에서 rod, tube 그리고 fiber 형태의 구조로

변화하였다. 또한 *rac*-$TBA_{1.0}DA_{2.0}$의 flat-ribbon 형태의 초분자 구조체는 *L*-$TBA_{1.0}DA_{2.0}$로의 카이랄성 변화를 통해 helical-ribbon 구조로 변화하였다. TBA_xDA_y에 다른 배위 결합 구조를 갖는 금속 양이온 Zn^{2+}, Cd^{2+} 그리고 Co^{2+}를 첨가함에 따라 cylindrical micelle, tube 그리고 bilayer 형태의 초분자 구조체로 얻을 수 있었다. 이번 연구를 통해 two- 혹은 three-component의 각 요소를 조절함으로써 다양한 형태의 자기 조립된 나노 또는 마이크로 크기의 초분자 구조체를 얻을 수 있었다.

양친화성 화합물의 화학 구조나 기하학적 구조가 변화하면 서로 다른 자기 조립 과정을 겪는다. 따라서 자기 조립 환경을 조절함으로써 원래와는 다른 초분자 구조체를 얻을 수 있을 것이다. 이를 위해 용매의 극성에 따라 기하학적 구조가 변화하는 양친화성 화합물, EG_nA을 합성하였다. 두개의 *N*-dodecylbenzamide을 다양한 길이의 ethylene glycol 중합체로 연결한 EG_nA는 아미드기 사이의 수소 결합을 통해 머리핀 형태의 구조를 갖게 된다. 비극성 용매 환경에서는 강한 수소 결합과 ethylene glycol 중합체의 입체 구조로 인해 친수성 부분과 소수성 부분의 부피 비율이 달라진다. 친수성 부분의 부피 비율이 더 큰 EG_4A와 EG_6A는 cylindrical micelle형태의 fiber를 형성하나, 부피 비율 차이가 없는 EG_5A는 bilayer형태의 ribbon 구조를 형성하게 된다. 반대로 극성 용매 환경에서는 약한 수소 결합력에 의해 ethylene glycol의 뒤틀림이 약해진다. 따라서 짧은 길이의 EG_4A만이 fiber 구조를 갖는 반면, EG_5A와 EG_6A는 ribbon 구조를 갖는다. 용매의 극성 변화에 의한 양친화성 화합물의 수소 결합력 조절은 cylindrical micelle 구조에서 bilayer 구조로의 변화를 유도할 수 있음을 알았다.

더 나아가 양친화성 화합물의 직접적인 화학 구조 변화가 아닌

둘 또는 그 이상의 양친화성 화합물 간 이종 자기 조립 (co-assembly) 과정을 통해 초분자 구조체의 형태를 제어할 수 있었다. 원뿔 형태의 입체 구조를 갖는 NDI•Car은 친수성 부분의 높은 부피 비율로 인해 자기 조립 과정을 거쳐 마이크로 크기의 micelle 구조를 형성하였다. 반면에 평평한 입체 구조를 갖는 NDI•OAc는 자기 조립 과정을 통해 나노 크기의 bilayer ribbon 구조를 형성하였다. 이 때 원뿔의 NDI•Car과 평평한 NDI•OAc를 일정 비율로 혼합하면 친수성 부분과 소수성 부분간의 부피비를 조절할 수 있을 것이다. 이러한 부피비를 제어를 통해 NDI•Car과 NDI•OAc의 이종 자기 조립 구조체의 형태를 제어할 수 있을 것이다. 실제로 NDI•OAc의 혼합 비율을 높임에 따라 NDI•Car의 micelle 구조는 NDI•OAc의 ribbon 구조로 변화함을 확인할 수 있었다. 특히, NDI•Car과 NDI•OAc의 비율이 1:1에서 1:9 사이일 경우 나노 크기의 tube 구조를 갖음을 알았다. 입체 구조가 다른 2개 또는 그 이상의 양친화성 화합물의 이종 자기 조립 과정을 통해 초분자 화합물의 구조 변화를 제어할 수 있었다.

Part II에서는, 자기 조립 과정을 통해 얻어진 초분자 구조체의 표면을 기능성 화합물로 치환하고자 하였다. 이를 통해 목적에 따라 서로 다른 기능성을 갖는 초분자 화합물을 개발하고자 하였다.

자기 조립 구조체의 표면을 기능성 화합물로 치환하기 위해 host-guest 결합력을 적용하였다. 자기 조립 구조체의 표면을 dpa-금속 복합체로 치환하면 기능성 phosphate 유도체와의 host-guest 결합을 통해 기능성 물질을 개발할 수 있을 것이다. 이를 위해 dpa가 포함된 양친화성 화합물 2-(dipicolylamino)ethyldodecanoyl amide, lipid-**1**,을 합성하였다. Lipid-**1**과 금속 양이온의 입체 구조 차이, 음이온 사이의 결합 강도의 변화를 통해 자기 조립체의 구조

변화를 유도하였다. Co(II)-**1** micelle은 pyrophosphate와의 결합에 의해 vesicle로 그 구조 변화하였으며, Cd(II)-**1** vesicle은 pyrophosphate에 의해 vesicle간 융합이 일어남을 TEM 분석을 통해 확인하였다. 하지만 입체 구조가 다른 인산염 그리고 결합 강도가 낮은 acetate 음이온의 첨가는 자기 조립체의 구조 변화를 유도할 수는 없었다. 이러한 결과를 바탕으로 인산염 유도체를 통해 자기 조립 구조체의 구조적 변화 없이 표면을 기능성 화합물로 치환할 수 있었다. 형광 인산염 유도체 FMN(=flavin mono-nucleotide)를 Zn(II)-**1** vesicle 혼탁액에 첨가하여 그 결과를 분석하였다. Zn(II)-**1**-FMN의 confocal 사진 분석을 통해 vesicle 표면이 FMN의 형광으로 염색되었음을 확인하였다. 이번 연구를 통해 dpa-Zn(II)와 인산염 사이의 host-guest 결합을 통해 구조체의 표면을 기능성 화합물로 치환할 수 있음을 알았다.

Part III에서는 자기 조립 과정의 제어를 통해 작은 분자를 탐지 혹은 구분하고자 하였다. 화학 반응에 의한 sol to gel 변환을 보여주는 두 개의 저분자 젤형성기(LMWG)를 설계하였고, 타켓 화합물을 선택적으로 구분할 수 있는지에 대해 확인하고자 하였다.

수소 결합에 의한 불소 음이온에 반응하는 LMWGs는 용매 환경과 낮은 음이온 선택성의 문제를 가지고 있다. 이를 극복하기 위해 불소 음이온과 선택적으로 반응하는 tert-butyldimethylsilyl (TBDMS)를 7-Hydroxycoumarin 유도체에 치환한 LMWG **1**을 합성하였다. 젤-형성 성질이 없는 LMWG **1**에 불소 음이온을 첨가하여 젤 형성을 관찰할 수 있었다. 특히, 불소 음이온에 의한 부분적 TBDMS 분해 반응을 통해 sol to gel 변환뿐만 아니라, 형광의 변화 또한 보여주었다. LMWG **1**은 할로겐 음이온을 포함한 다양한 음이온에 의한 젤-형성 반응을 보이지 않았다. 따라서 불소

음이온에 의한 TBDMS의 선택적 분해 반응을 통해 LMWG **1**이 불소 음이온에 대해 높은 선택성을 갖음을 보여주었다. 기존의 수소 결합을 바탕으로 하는 LMWG와는 달리, 화학 반응을 기반으로 하는 LMWG 시스템은 음이온에 대해 높은 선택성을 가지며, 높은 극성 용매 환경에서도 작동함을 확인할 수 있었다.

Hcy은 Cys와의 화학적/구조적 유사성으로 인해 Hcy만을 선택적으로 구분하는 것은 어렵다. 하지만 자기 조립 과정은 단위체의 작은 구조적 차이에도 민감하게 반응한다. 따라서 화학 반응 기반의 LMWG 시스템을 통해 Hcy를 선택적으로 구분하고자 하였다. 이를 위해 Hcy와 반응하여 부가물을 형성하는 알데히드를 치환한 7-hydroxycoumarin 기반의 LMWG CHO-1을 합성하였다. CHO-1과 Hcy 사이의 화학 반응을 통해 6각 고리의 부가물을 만들었다. 이러한 화학 반응은 CHO-1의 자기 조립 과정에 영향을 주어 젤-형성을 유도할 수 있었다. 하지만 5각 고리의 부가물을 형성하는 CHO-1•Cys는 젤-형성 반응을 보이지 않았다. Hcy와 Cys 부가물의 입체 구조 차이로 인해 자기 조립 fiber의 네트워크 크기에 영향을 주었으며, 이로 인해 서로 다른 젤-형성 반응을 보여주었다. Hcy에 대한 선택성을 확인하기 위해 다른 biothiol과 아미노산에 의한 젤-형성 반응 여부를 평가하였다. Cys 경우와 마찬가지로 다른 화합물의 첨가에 의한 젤-형성 반응은 나타나지 않았다. 우리는 CHO-1과 Hcy 사이의 선택적 젤-형성 반응을 통해 Hcy를 Cys으로부터 정확히 구분할 수 있었다. 그리고 이는 구조적, 화학적으로 유사한 다른 화합물들의 구분에 있어서도 효과적일 것으로 생각한다.

주요어: 자기조립, 3-요소 시스템, 저분자량 젤형성기 (LMWGs), 유기젤, 수화젤, Naphthalene diimide, Homocystein (Hcy), Cysteine (Cys), 불소 음이온, dipicolylamine-Zn(II), 표면 성질 개조, 키모도시미터, 솔-젤 변화.

학번: 2003-20495